Graduate School ETD Form 9
(Revised 12/07)

PURDUE UNIVERSITY
GRADUATE SCHOOL
Thesis/Dissertation Acceptance

This is to certify that the thesis/dissertation prepared

By Justin A. Williams

Entitled
BIOPHYSICAL STUDIES OF CHOLESTEROL IN UNSATURATED PHOSPHOLIPID MODEL MEMBRANES

For the degree of Doctor of Philosophy

Is approved by the final examining committee:

Stephen R. Wassall
Chair

Brian A. Todd

Ricardo S. Decca

Horia I. Petrache

Fangqiang Zhu

To the best of my knowledge and as understood by the student in the *Research Integrity and Copyright Disclaimer (Graduate School Form 20)*, this thesis/dissertation adheres to the provisions of Purdue University's "Policy on Integrity in Research" and the use of copyrighted material.

Approved by Major Professor(s): Stephen R. Wassall

Approved by: Ricardo S. Decca 11/08/2013
Head of the Graduate Program Date

BIOPHYSICAL STUDIES OF CHOLESTEROL IN UNSATURATED PHOSPHOLIPID MODEL MEMBRANES

A Dissertation

Submitted to the Faculty

of

Purdue University

by

Justin A. Williams

In Partial Fulfillment of the

Requirements for the Degree

of

Doctor of Philosophy

December 2013

Purdue University

West Lafayette, Indiana

For Ethan

ACKNOWLEDGEMENTS

I have many people I need to thank who helped make this possible. My amazing wife, Jacquelyn, for her love and reassurance, and for all the sacrifices that were tolerated along the way; my mom, Tina, and brother, Eric, who are always there for me; also my dad, aunts, in-laws, and grandparents who've supported me in this effort. I am indebted to my advisor, Dr. Stephen Wassall, for his patience, guidance, and encouragement to carry on. I truly would not have gone this far without him. I need to recognize my committee members Drs. Ricardo Decca, Horia Petrache, Fangqiang Zhu, and Brian Todd for their time and help in preparing this document. I am grateful for my interactions with the faculty at IUPUI, especially Drs. Marvin Kemple, AJ Rader, Gautum Vemuri, and Kathleen Marrs. Dr. William Stillwell was particularly influential in my work, generously sharing both his deep knowledge of biological membranes and use of the equipment in his lab. I am also appreciative of the opportunity Drs. Heiko Heerklotz and Alekos Tsamaloukas afforded in allowing me to spend time in their lab during the initial phase of our ITC experiments. It was a pleasure to collaborate with Dr. Saame Raz Shaikh, who added a biological perspective in our model membrane work. In the lab, Dr. Bruce Ray could always be counted on for advice and help with experimental setups and sample preparations. I must acknowledge the National Science Foundation GK-12 program and IUPUI Physics Department for financial support provided. Lastly, I would like to thank my high school Physics teacher, Dr. Duane Nickell, whose enthusiasm for the subject was contagious and who instilled in me the confidence to pursue this path.

TABLE OF CONTENTS

Page

Page

LIST OF TABLES

Appendix Table Page

LIST OF FIGURES

Figure Page

Figure Page

Figure Page

Figure Page

Appendix Figure Page

Appendix Figure Page

LIST OF ABBREVIATIONS

AFM	Atomic Force Microscopy
B_0	Static Applied Magnetic Field
BHT	Butylated Hydroxytoluene
BSA	Bovine Serum Albumin
^{14}C	Carbon-14
C-C	Carbon-Carbon Bond
C=C	Carbon-Carbon Double Bond
cal	calorie
chlstn	3β-doxyl-5α-cholestane
chol	Cholesterol
CL	Cardiolipin
CTL	Cholestatrienol
$-d_{\#}$	# of Deuterium Labels
DHA	Docosahexaenoic Acid
DOPC	1,2-dioleoyl-sn-glycero-3-phosphocholine
DPA	Docosapentaenoic Acid
DPPC	1,2-dipalmitoyl-sn-glycero-3-phosphocholine

DRM	Detergent-Resistant Membrane
DSC	Differential Scanning Calorimetry
DSM	Detergent-Soluble Membrane
DSPC	1,2-distearoyl-*sn*-glycero-3-phosphocholine
EFG	Electric Field Gradient
EPA	Eicosapentaenoic Acid
EPR	Electron Paramagnetic Resonance
FID	Free Induction Decay
FFT	Fast Fourier Transform
FT	Fourier Transform
g	Gauche
GPCR	G Protein-Coupled Receptor
$\hbar$	Reduced Planck's Constant
^{2}H or D	Deuterium
^{3}H	Tritium
ΔH	Enthalpy Change
I	Nuclear Spin Moment
IR	Infrared
ITC	Isothermal Titration Calorimetry
K_x	Equilibrium Partition Coefficient
K_B^A	Partition Coefficient Ratio

L_α	Liquid Crystalline
l_d	Liquid Disordered
l_o	Liquid Ordered
LUV	Large Unilamellar Vesicles
M	Magnetization
M_1	First Moment
μ	Dipole Magnetic Moment
MAS	Magic Angle Spinning
mβCD	Methyl-β-Cyclodextrin
MD	Molecular Dynamics
mol	Mole
n-3 or ω-3	Omega-3
NMR	Nuclear Magnetic Resonance
NSOM	Near-Field Scanning Optical Microscopy
OA	Oleic Acid
P_2	Second Order Legendre Polynomial
PAS	Principal Axis System
PAPC	1-palmitoyl-2-arachidonoyl-*sn*-glycero-3-phosphocholine
PC	Phosphatidylcholine
PDPC	1-palmitoyl-2-docosahexaenoyl-*sn*-glycero-3-phosphocholine
PE	Phosphatidylethanolamine

PEPC	1-palmitoyl-2-eicosanpentaenoyl-*sn*-glycero-3-phosphocholine
PG	Phosphatidylglycerol
PI	Phosphatidylinositol
PLPC	1-palmitoyl-2-linoleoyl-*sn*-glycero-3-phosphocholine
POPC	1-palmitoyl-2-oleoyl-*sn*-glycero-3-phosphocholine
PS	Phosphatidylserine
PUFA	Polyunsaturated Fatty Acid
RF	Radio Frequency
S_{CD}	Carbon-Deuterium Order Parameter
SDPC	1-stearoyl-2-docosahexaenoyl-*sn*-glycero-3-phosphocholine
s_o	Solid Ordered
SOPC	1-stearoyl-2-oleoyl-*sn*-glycero-3-phosphocholine
SM	Sphingomyelin
sn	Stereospecific Numbering
SUV	Small Unilamellar Vesicles
t	Trans
T	Tesla
ν_0	Lamor Frequency
χ_Q	Quadrupolar Coupling Constant

ABSTRACT

Williams, Justin A. Ph.D., Purdue University, December 2013. Biophysical Studies of Cholesterol in Unsaturated Phospholipid Model Membranes. Major Professor: Stephen R. Wassall.

Cellular membranes contain a staggering diversity of lipids. The lipids are heterogeneously distributed to create regions, or domains, whose physical properties differ from the bulk membrane and play an essential role in modulating the function of resident proteins. Many basic questions pertaining to the formation of these lateral assemblies remain. This research employs model membranes of well-defined composition to focus on the potential role of polyunsaturated fatty acids (PUFAs) and their interaction with cholesterol (chol) in restructuring the membrane environment. Omega-3 (n-3) PUFAs are the main bioactive components of fish oil, whose consumption alleviates a variety of health problems by a molecular mechanism that is unclear. We hypothesize that the incorporation of PUFAs into membrane lipids and the effect they have on molecular organization may be, in part, responsible. Chol is a major constituent in the plasma membrane of mammals. It determines the arrangement and collective properties of neighboring lipids, driving the formation of domains via differential affinity for different lipids.

The molecular organization of 1-[$^2H_{31}$]palmitoyl-2-eicosapentaenoylphosphatidylcholine (PEPC-d_{31}) and 1-[$^2H_{31}$]palmitoyl-2-docosahexaenoylphosphatidylcholine (PDPC-d_{31}) in membranes with sphingomyelin (SM) and chol (1:1:1 mol) was compared by solid-state ^2H NMR spectroscopy. Eicosapentaenoic (EPA) and docosahexaenoic (DHA) acids are the two major n-3 PUFAs found in fish oil, while PEPC-d_{31} and PDPC-d_{31} are phospholipids containing the respective PUFAs at the sn-2 position and a perdeuterated palmitic acid at the sn-1 position. Analysis of spectra recorded as a function of temperature indicates that in both cases, formation of PUFA-rich (less ordered) and SM-rich (more ordered) domains occurred. A surprisingly substantial proportion of PUFA was found to infiltrate the more ordered domain. There was almost twice as much DHA (65%) as EPA (30%). The implication is that n-3 PUFAs can incorporate into lipid rafts, which are domains enriched in SM and chol in the plasma membrane, and potentially disrupt the activity

of signaling proteins that reside therein. DHA, furthermore, may be the more potent component of fish oil.

PUFA-chol interactions were also examined through affinity measurements. A novel method utilizing electron paramagnetic resonance (EPR) was developed, to monitor the partitioning of a spin-labeled analog of chol, 3β-doxyl-5α-cholestane (chlstn), between large unilamellar vesicles (LUVs) and methyl-β-cyclodextrin (mβCD). The EPR spectra for chlstn in the two environments are distinguishable due to the substantial differences in tumbling rates, allowing the population distribution ratio to be determined by spectral simulation. Advantages of this approach include speed of implementation and avoidance of potential artifacts associated with physical separation of LUV and mβCD. Additionally, in a check of the method, the relative partition coefficients between lipids measured for the spin label analog agree with values obtained for chol by isothermal titration calorimetry (ITC). Results from LUV with different composition confirmed a hierarchy of decreased sterol affinity for phospholipids with increasing acyl chain unsaturation, PDPC possessing half the affinity of the corresponding monounsaturated phospholipid.

Taken together, the results of these studies on model membranes demonstrate the potential for PUFA-driven alteration of the architecture of biomembranes, a mechanism through which human health may be impacted.

CHAPTER 1: MEMBRANE ORGANIZATION AND THE INFLUENCE OF CHOLESTEROL AND POLYUNSATURATED LIPIDS

1.1 Cellular Membranes

Cellular membranes are chemically complex, dynamic structures across which the flow of molecules is regulated. They constitute the boundary which defines the cell and the organelles within, and are essential to life. A basic feature that is common to all membranes is that of a semipermeable barrier to ions and polar molecules. In this role as chemical insulator, they allow for compartmentalization of the cell and isolation of chemical events. The influence of biomembranes on cellular activity is not limited to this simple but crucial role. Membranes are involved in the majority if not all critical activities of the cell. They provide the fluid environment necessary for the function of embedded proteins and a substrate for peripheral proteins; the chemical and electric gradients maintained by the membrane provide a source of energy for the cell; and, of course, signaling between cells must take place at, or pass through, the membrane.

The biomechanical processes underlying physiologically significant functions of the membrane are governed by the physiochemical properties of constituent molecules and of their collective arrangement in a two dimensional fluid. An accurate, quantitative description of membrane structure is of paramount importance as it relates to function of the membrane and of the cell as a whole. Study of this system has proven to be a difficult undertaking owing to the chemical complexity (a great diversity of lipids and proteins), dynamic nature (fluctuations occurring on time scales ranging from picoseconds to seconds) and size (angstrom to micron dimensions) of the system; consequently many details remain unresolved. Much of our present understanding is the product of technological advancements from the last 70 years (Stillwell 2013). Many competing models have been cast aside in favor of the currently, most widely accepted view, the fluid mosaic model (Fig. 1.1) of Singer and Nicolson, which has survived with only slight modification (Vereb et al. 2003) since its conception in 1972.

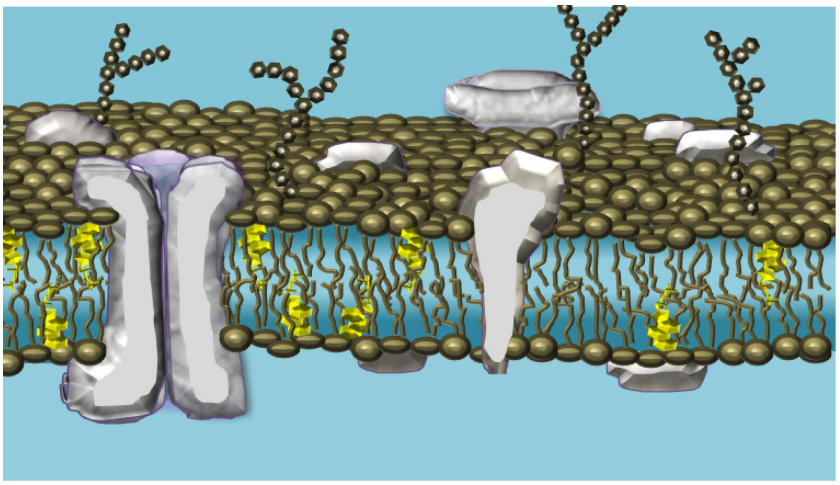

Figure 1.1 Cross section depiction of the fluid mosaic model. Globular structures represent protein, spheres and attached wiggly lines correspond to lipid headgroups and acyl chains respectively, cholesterol is shown in yellow and the branches on the membrane surface are carbohydrates. Lipids are ordered and oriented forming a sheet ~5 nm thick: the lipid bilayer. Proteins are embedded in this two dimensional viscous solution. A modern view admits restricted diffusion of components, local population density fluctuations of individual molecular varieties and high protein-lipid ratios. Cytoskeleton not included in depiction.

Biomembranes exhibit a wide variety of distinct topographies and functions, but the fundamental underlying structural scheme is conserved as captured by the fluid mosaic model. In this model, the central component of the membrane is the lipid bilayer (Gorter and Grendel 1925, Bloom et al. 1991), a 3-6 nm thick sheet, within which membrane molecules are organized such that their hydrophobic components are located inside the bilayer and hydrophilic components are presented outwards towards the two aqueous environments. Biological membranes consist of lipids, proteins and a small amount of carbohydrates (~10% by weight covalently bonded to protein and lipid in plasma membranes (Hauser 2005)). Protein is bound to the surface or partially solvated by the lipid bilayer. The plasma membrane, which delineates the eukaryote cell from its surroundings, is supported by a cytoskeleton substructure. External to the cell a glycocalyx carbohydrate network extends into the surrounding medium and is responsible for cell to cell recognition and binding and repelling of substrates. Membrane composition varies cell to cell, organelle to organelle, even between opposing monolayers or leaflets of a bilayer and laterally within leaflets. The fluid mosaic model is often depicted having a uniform sea of lipids, but fluidity should not be confused with randomness (Mouritsen and Jørgensen 1994; Engelman 2005). Singer and Nicolson acknowledged the possibility of short

range order and heterogeneities in lipid and protein composition which experimental evidence has since been found to support (Karnovsky et al. 1982; Simons and Ikonen 1997, Spira et al. 2012). The lipid to protein ratio varies greatly from membrane to membrane just as function does. On opposite ends of the spectrum, the multilayered myelin membrane that electrically insulates the axon of neurons has a dry weight, protein to lipid ratio of only 1:4; whereas the mitochondrial inner membrane, where ATP synthesis occurs, has been found to have a ratio of 3:1 (Guidotti 1972). This high ratio is possible because not all protein is solvated by lipid, but may be peripherally associated with the membrane either through surface electrostatic interactions, covalently linked lipid components, binding of membrane lipid or exist in protein-protein complexes.

There is still much to learn about the system, for example the interplay between lipids and proteins is one avenue that is just beginning to open up. To simplify the task of studying the elusive properties of dynamic biological membranes containing a large variety of molecules a divide and conquer method is often employed; focusing on specific components of model systems with defined compositions and a limited number of lipid species. This approach is still challenging due to inherent extreme length scales and fluctuation rates, and care has to be taken when extending relevance of uniformly prepared systems to nonequilibrium biological ones.

1.2 The Lipid Bilayer

Lipids have exceedingly low solubility in water and spontaneously self-assemble (Marrink et al. 2001) to form ordered structures when hydrated. The lipid bilayer is a smectic liquid crystal and the basic structural unit of biological membranes. Within the bilayer, lipids are oriented due to their amphiphillic nature with their long molecular axis on average coinciding with the bilayer normal. Nonpolar lipid hydrocarbon moieties are sequestered within the bilayer and polar, or charged, lipid headgroups are presented at the aqueous interface of the two leaflets.

1.2.1 The Hydrophobic Effect

The hydrophobic effect is the dominant organizing force responsible for formation and stabilization of the bilayer (Tanford 1980). This effect is not the result of mutual attraction

between lipids or a repulsive force between water and lipid, but is attributed to the strong attraction between water molecules. Liquid water forms a highly structured isotropic network of hydrogen bonds, with each water molecule capable of accepting four and on average 3.4 hydrogen bonds with nearest neighbor molecules (Kumar et al. 2007). These bonds are constantly being broken and reformed at a rate of 10^{11} positional changes per second (Luckey 2008). Nonpolar molecules are incapable of hydrogen bonding and their insertion in water creates defects in the isotropic hydrogen bond network. There is an energetically unfavorable decrease in entropy as water molecules reorient to form a structured cage around nonpolar molecules. Water molecules comprising the cage have a reduced degree of motional freedom and their hydrogen bonds between water molecules are more stable than surrounding bulk water. Hydrophobic lipid components will aggregate, minimizing surface area exposed, while hydrophilic headgroups are drawn to the surface and shield nonpolar components from exposure to water. In this regard the membrane bilayer is self-sealing. The lipids are anchored to the aqueous interface by electrostatic forces acting on their headgroups, and the liquid hydrocarbon core is weakly stabilized through van der Waals interactions. These factors contributing to condensation are opposed by steric effects, electrostatic repulsive forces between headgroups, and the entropic cost of ordering the hydrocarbon core. The lipid bilayer is only one of the structures that can result when lipids spontaneously assemble in water; the types of lipids present in the mixture will dictate the morphology of the extended form.

1.2.2 Lipids

In recognition of the widespread physiological influence lipids have, that extends beyond their membrane structural and functional role (they also act as signaling and energy storage molecules) and in anticipation of a coming advancements in lipodomics, a coordinated effort has been made to catalog and classify the tremendous diversity of chemically distinct lipid species (Fahy et al. 2005). Amphiphilic lipids form the basic structural unit of membranes, with a hydrophilic headgroup and hydrophobic hydrocarbon tail group. Within this unifying motif there are many possible variations. Eukaryotic cells support a lipid diversity that can exceed 1000 distinct lipid types, although a complete account of a cell's lipidome is not currently possible (Wenk 2010). The major membrane lipids belong to three categories: glycerolphospholipids, sphingolipids, and sterols. Glycerolphospholipids and sphingolipids account for more than 50%

of membrane lipid and share a similar general structure with a polar or charged headgroup and usually two fatty acyl chains (Fig. 1.2). Headgroups can vary by size and ability to hydrogen bond and will either be zwitterionic or anionic, rarely cationic. Acyl chains will have an even number of carbon segments from synthesis and will vary in total length (between 12 and 24 carbons long) and by location and level of unsaturation, having up to six double bonds almost always in the cis conformation.

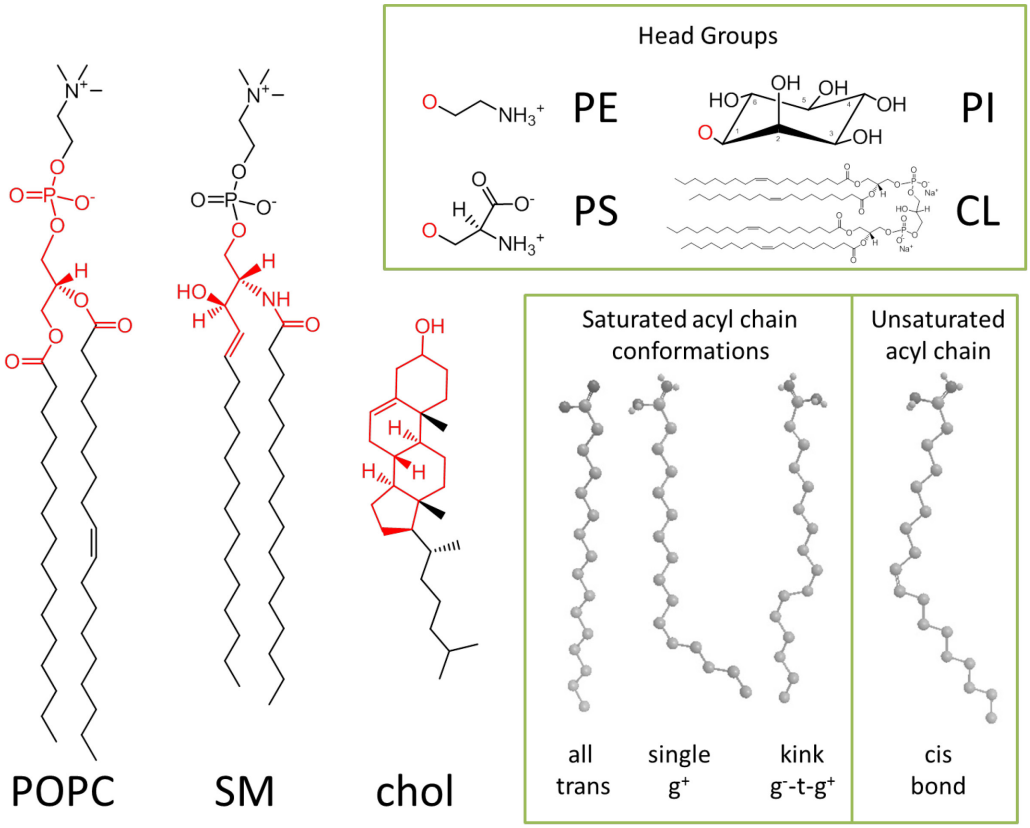

Figure 1.2 General structure of membrane lipids, headgroups and acyl chains. POPC, SM and cholesterol are representative of the three most important membrane lipid classes: glycerolphospholipids, sphingolipids and sterols, respectively. Structure in red is common to lipid class. Upper insert displays common phospholipid headgroup variations. Lower insert shows examples of acyl chain bond conformations. In the gel phase acyl chains adopt an all trans (t) conformation. Increasing temperature causes rotation isomerization between trans and gauche conformations ($g^{\pm}$). Chains with solitary gauche bonds do not pack well; accordingly kink (g-t-g) or jog (g-t-t-g) sequences are more prevalent. Double bonds introduce a rigid kink in unsaturated chains while decreasing the energy barrier to rotation of adjacent C-C bonds.

1.2.2.1 Glycerolphospholipids

Glycerolphospholipids are more ubiquitous than sphingolipids. In eukaryotes glycerolphospholipid structures include a phosphorylated alcohol esterified to the sn-3 hydroxyl

group of glycerol and fatty acid chains ester-linked at the sn-1 and sn-2 positions. The sn (stereospecific numbering) notation is the convention used for glycerophospholipids (Hirschmann 1960). The headgroup is modified by attachment of an alcohol to the phosphate group, and serves as a basis to subdivide the glycerophospholipid class. Common headgroups include phosphatidylcholine (PC), phosphatidylethanolamine (PE), phosphatidylserine (PS), phosphatidylinositol (PI), and cardiolipin (CL) (Fig. 1.2). Glycerolphospholipids are often specified using a short hand notation which includes acyl chain length, number and location of unsaturated bonds, and headgroup type. For example palmitoyloleylphosphatidylcholine (POPC), having a saturated 16 carbon sn-1 chain and an 18 carbon monounsaturated sn-2 chain, is denoted 16:0-18:1Δ9 PC. The Δ9 signifies the location of the double bond as the ninth bond from the terminal methyl.

In mammals 80-90% of glycerophospholipids are zwitterionic (PC or PE) and of the remaining 10-20% that bear a net charge, PS has the greatest abundance (Hauser 2005). On the inner leaflet of the plasma membrane PE and PS lipids are more concentrated. PS lipids act as an anchor point for the cytoskeleton network through interactions with the cytoskeleton protein spectrin (Maksymiw et al. 1987). While PC and PE are found across all cellular membranes some lipid types are restricted to specific organelles. The low concentration of anionic PI lipid is tightly regulated as it is an important substrate for protein binding both due to its charge and shape (Lemmon 2008). The structural outlier of glycerolphospholipids is CL, a symmetric molecule having not two, but four acyl chains connected through two phosphoglycerols joined via a third glycerol group. Many proteins have positively charged domains which will bind to anionic lipid regions in membranes. CL carries two negative charges and its cellular function and location lies in the protein dense mitochondrial inner membrane.

The immense variety of glycerophospholipids comes from the number of unique combinations of headgroups and hydrophilic hydrocarbon chains possible. In nature most lipids have two acyl chains: one saturated in the sn-1 position (usually palmitoyl or stearoyl) and unsaturated in the sn-2 position. One exception is the disaturated dipalmitoylphosphatidylcholine (DPPC or 16:0-16:0 PC) which lines the air-water interface of the lungs where unsaturated lipids would be readily oxidized. Despite the fact that disaturated lipids are only a minor constituent in most

biological membranes they are among the most widely studied in biophysical experiments. Saturated chains have methylene segments connected either through gauche or trans sigma bonds (Fig. 1.2).

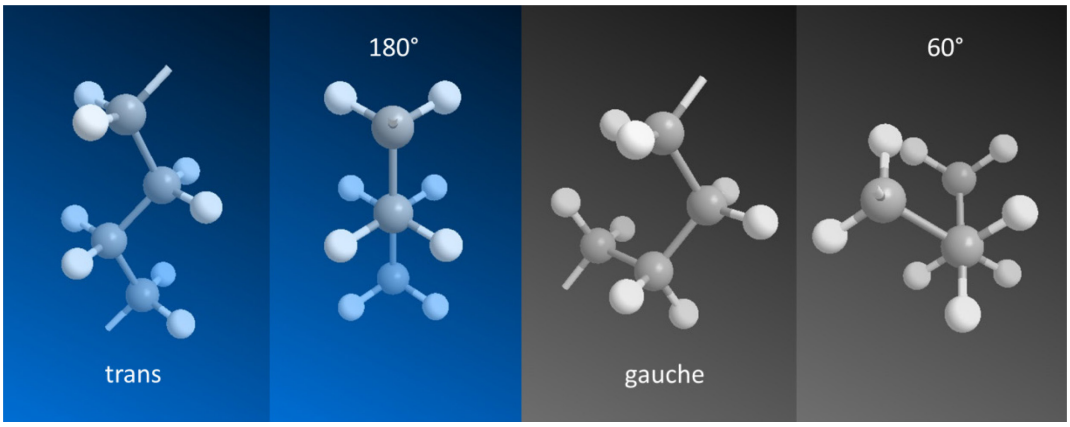

Figure 1.3 Profile and torsion angle views for trans and gauche bonds. Torsion angle is defined by three adjacent C-C bonds: the angle between the first and third bond in the sequence as viewed along the axis of the second.

For a saturated acyl chain there are three rotational conformations about C-C bonds for which there are energy minima: the 180° trans and ±60° gauche conformations (Fig. 1.3). The trans conformation is more stable having potential energy 0.5-0.9 kcal/mol below that of the gauche and there is a 3-4 kcal/mol barrier to rotation between the two (Feller 2008). At low temperatures saturated acyl chains will be in a fully extended all trans conformation, aligned parallel or slightly tilted relative to the bilayer normal. Increasing thermal energy of the system melts acyl chains, which is signified by the onset of rapid isomerization between trans and gauche conformations at a rate of 10 to 20 jumps per nanosecond (Venable et al. 1993). Gauche bonds introduce kinks in acyl chains that increase the disorder of the bilayer. Not all trans–gauche chain sequences are allowed. The upper portion of the acyl chain is motional restricted and isomerization is limited, additionally, some sequential gauche combinations are sterically hindered. Furthermore, isomerizations are not independent; on average gauche bonds tend to occur in pairs which pack more easily in the bilayer (Fig. 1.2) (Schindler and Seelig 1975).

Unsaturated chains have one or more C=C double bonds. Double bonds are rigid, fixed in the cis conformation with a 30° torsion angle. Trans double bond conformations (180° torsion angle)

are rare in nature, but can be found in the fats of processed food due to manipulations like partial hydrogenation meant to lengthen shelf life of the product. Unlike the linear defect of a trans double bond, cis double bonds create a rigid kink that interferes with tight packing of chains. Surprisingly, inclusion of this rigid kink imparts greater flexibility to the chain overall as adjacent bonds have a reduced barrier to rotation (approximately 1/3 that of the saturated chain) and broader energy minima (Feller 2008). Isomerization of these bonds occurs on the order of picoseconds. The effect is a more disordered lipid chain that rapidly reorients. The tremendous mobility of the sn-2, docosahexaenoic (DHA) chain of SDPC (18:0-22:6PC) is an example of the dynamism that accompanies polyunsaturation. DHA, with 22 carbons and 6 double bonds, is the most unsaturated lipid acyl chain in nature and, remarkably, explores its full conformational space in tens of nanoseconds (Soubias and Gawrisch 2007). How these fluctuation and entropy relate to the properties of the extended structure will be discussed later.

1.2.2.2 Sphingolipids

Sphingolipids as a class include some important signaling and membrane structural molecules. They have a motif similar to glycerophospholipids, but with a sphingoid base structurally replacing the glycerol backbone and sn-1 chain (Holthuis et al. 2001). Sphingomyelin (SM) is the most common form of sphingolipid in mammal membranes and the second most common phospholipid in the plasma membrane (Slotte 2013). As shown in Figure 1.2, SM has a PC headgroup connected to a sphingosine backbone containing a trans double bond and an amide linked fatty acid chain which is typically long and saturated. The hydroxyl group on the amide allows for hydrogen bonding with other membrane lipids, which facilitates clustering of certain membrane components. Both glycerolphospholipids and sphingolipids can be modified with sugar attachments on their headgroups.

1.2.2.3 Sterols

Sterols are a third important class of membrane lipids. Their shared structure includes four fused hydrocarbon rings and a short branched tail group. Cholesterol is the main sterol found in eukaryotes (Dufourc 2008) and is especially concentrated in plasma membranes of human erythrocytes where it can constitute up to 50 mol% of lipids. Cholesterol cannot form a fluid

bilayer on its own, having only a hydroxyl for a polar group. The cholesterol nucleus is a planar structure with rings fused in trans junctions. The ring system of other sterols will vary in number and location of double bonds along with substituent functional groups.

Research on model systems is typically conducted with synthetic lipids. Utilizing molecular probes intramolecular properties of specific lipids can be studied, as well properties of the aggregate. Both the organization and dynamics of lipids determine the properties of the collective; the control of which is essential for proper functioning of the membrane.

1.2.3 Collective Properties

In the study of membrane properties, models are often used which retain some fundamental aspects of biomembranes, but with reduced complexity. These can be constructed to expose particular properties or interactions of interest. The self-assembly of lipid mixtures is manipulated to form model systems best suited to the requirements specified by a method of investigation. A variety of structures are possible including multilamellar liposomes, unilamellar vesicles, micelles, bicelles, monolayers, and supported or painted bilayers (Chan and Boxer 2007). The chemical make-up of the model can range from having a single lipid component to something that approaches a more physiological representative composition via reconstitution of an isolated biological membrane.

Membrane processes and interactions occur over many length and time scales making complete characterization of the membrane by a single biophysical technique unfeasible. Accordingly, a multifaceted approach is required to untangle all the weak, noncovalent interactions, dynamic and sometimes transient properties of the membrane (Table 1.1).

Table 1.1 Partial list of common biophysical techniques used in the investigation of model membrane systems including examples of properties measured.

Categories	Methods	Examples of Properties Measured
Spectroscopy	Solid State NMR	Membrane Organization and Dynamics
	EPR	Membrane Order and Dynamics
	IR	Trans and Gauche Bond Populations
Scattering Techniques	X-Ray	Bilayer Thickness
	Neutron	Transbilayer Profiles
	Raman	Vibration Modes of Bonds
Calorimetry	DSC	Phase Transition Temperatures
	ITC	Interaction Energies and Binding
Microscopy	Fluorescence	Diffusion and Molecular Associations
	AFM	Supported Bilayer Topology
	Electron	Fixed Membrane Topology
	NSOM	Spatiotemporal Organization of Membrane Components
Computer Simulations	All Atom	Dynamics of Individual Lipids Including Flip Flop Rates
	Course Grained	Large Scale Membrane Associated Events
Electrophysiology	Painted Bilayer-Ion Channel	Ion Conductance and Lifetime of Membrane Pore Formation

Computer simulations are sometimes used to tie together and interpret experimental results; simulations which can currently deliver up to a millisecond (but typically only nano- to microseconds) of atomically resolved lipid trajectories. This rich detail can be mined to extract many physical properties of the system, but simulations are only as good as the force fields and parameters applied; input which is informed by experiment and refined to match observed phenomena. As computational costs decrease, simulations will be able to capture biological processes that occur on longer time scales and in greater detail. Through combined efforts and a steady accumulation of data, the field of membrane biophysics has matured to the point where many questions of lipid behavior in basic model systems have been answered and focus is increasingly turning toward more biologically relevant systems and molecules.

1.2.3.1 Bilayer Dynamics

Many bilayer properties are interrelated and can be linked to basic motions (Fig. 1.4) of the constituent lipids. A superposition of movements, with associated characteristic time scales ranging from femtoseconds to hours (Table 1.2), underlie the motion of individual lipids.

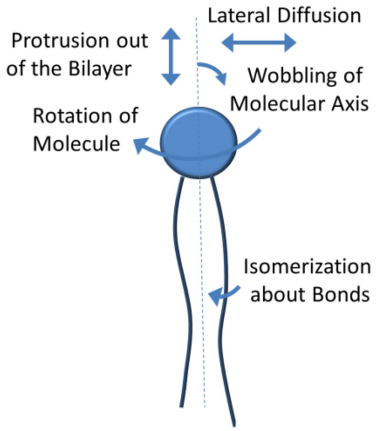

Figure 1.4 Motions of phospholipids within monolayer contributing to collective motion of bilayer.

Lipids at physiological temperatures will undergo rotational and translational diffusion. Polar lipid headgroups are confined (but possess a high degree of flexibility) to the aqueous interface, anchoring acyl chains to the surface. For glycerolphospholipids, the chains are weakly ordered in the bilayer interior with considerable entanglement, but experience increasing order approaching the motionally restricted glycerol backbone from the unbound terminal methyl. Chains exhibit rapid anisotropic motion about an axis parallel with the bilayer normal, reorientation the result of isomerization about C-C bonds and of small fluctuations in bond length and angle.

Table 1.2 Characteristic time scale of model bilayer dynamics. Values collected from Gawrisch 2005.

Length Scale	Motion	Time Scale
Intramolecular Motions	Bond Vibrations	ps
	Isomerization	1 - 100 ps
Molecular Motions	Protrusion	ns
	FlipFlop	ms - hrs
	Rotation	1 - 10 ns
	Wobble	0.1 - 1 ns
	Lateral Diffusion	50 – 100 ns
Collective Motions	Undulations	100 ns – s

In model systems the lateral diffusion of lipids has been observed at rates characterized by $D \cong$ 3-20 $\mu m^2/s$, the typical value is closer to the lower end of this range which corresponds to the viscosity of olive oil (Edidin 2003). At these rates an individual lipid could circumnavigate a human erythrocyte (a disk-like cell with diameter ~7µm and thickness ~2µm) on the order of

seconds. In biological membranes diffusion rates are observed to be 1-2 orders of magnitude slower than in artificial membranes. This discrepancy is attributed to compartmentalization of the bilayer due to three factors: interactions of the cytoskeleton and glycocalyx with transmembrane proteins, and specie specific lipid immiscibility within differentiated regions of the membrane (Murase 2004). At low observation rates (33 ms resolution) lipid diffusion appears to be a Brownian random walk, but upon increased time resolution (0.11 ms) lipids are observed to exhibit hop diffusion between lateral domains, residing within a confined region for a period of time before hopping to the next.

The passive transfer of lipid between leaflets is called flip-flop. This action provides accommodation for the volume changes that accompany membrane deforming events and protein conformation changes. Compared to chol, whose leaflet lifetime limit may be on the order of milliseconds (Jo et al. 2010), the flip-flop of phospholipids with bulky hydrophilic headgroups is a rare event. In biomembranes asymmetry between leaflets is setup by membrane trafficking and is actively maintained by flippase proteins. Breakdown of this asymmetry is known to correspond to the onset of apoptosis, programmed cell death.

The softness of the membrane is such that at physiological temperatures large deformations are possible due to thermal energy alone (Boal 2002). As a deformable fluid, the bilayer is charged with the complex task of maintaining a barrier while its surface undulates and thickness fluctuates. The extended two dimensional structure of model membranes can support stretching and bending forces, but not shearing (a hallmark of fluids). Biomembranes do possess a shear modulus (albeit miniscule), but this is attributed to the influence of the cytoskeleton (Nelson et al. 2004).

1.2.3.2 Physical Properties

Many environmental factors have bearing on the physical properties of the bilayer including temperature, pH, hydration, pressure and ion concentration; as do the membrane components themselves. In particular the inclusion of cholesterol, unsaturated lipids, proteins, and charged or hydrogen bond accepting headgroups can drastically alter the landscape.

Lipid volume is a reliably measured observable that can be used to carefully convert between area per lipid and bilayer thickness (Nagle and Tristram-Nagle 2000). The average area per lipid of phospholipids typically falls in the range of 50 to 80 $Å^2$ (Petrache et al. 2000), and functionally decreases with increasing cholesterol concentration, increasing chain length, or decreasing level of chain unsaturation. Longer, saturated chains have more stable van der Waals interactions between them and consequently contract within a smaller lateral area as projected on the surface of the bilayer. This results in a thickening of the bilayer, an increase in order and decrease in permeability. Thickness can be measured by x-ray and neutron scattering techniques (Wiener and White 1992). Neutron scattering affords greater resolution than x-ray and position specific probes can be used that establish depth within the bilayer profile (e.g. Marquardt et al. 2013).

The molecular organization of lipids within the hydrophobic portion of the membrane is described by order parameters, which will be discussed in greater detail in Chapter 2. Generally there exists a chain flexibility gradient linked with rapidly decreasing order towards the bilayer center. Order parameters are a measure of conformational freedom related to the orientational fluctuations of molecular segments, and can be measured by solid state deuterium NMR with great precision (Seelig and Seelig 1974). Increased disorder corresponds to the accumulation of gauche bonds. Chain packing determines or is tied to many bilayer properties including permeability, fluidity, rigidity, lateral pressure, curvature and, as previously mentioned, area per lipid and bilayer thickness.

In biomembranes curvature, both global and local, can be induced by lipid asymmetry between leaflets of the bilayer and the inclusion of nonlamellar lipid species. Nonspherical shapes are also permitted by interactions with the cytoskeleton. An aqueous solution of lipids will spontaneously assembly into structures whose form will vary depending on the molecular shape of the constituent lipids. Mixed chain or saturated PC lipids have a cylindrical geometry with a headgroup cross sectional area roughly equal to that of their acyl chains. These lipids will form lamellar bilayer structures. Lipids with disproportionate headgroup and acyl chain areas affect the membrane lateral pressure profile and are capable of forming different structures in model

systems such as hexagonal and cubic structures which are not observed in biomembranes (Gruner 2005).

1.2.3.3 Phase Behavior

The phase behavior exhibited by model membranes varies depending on its components. Cooperative transitions between lamellar phases are a possibility as well as complex behavior like phase coexistence or transitions between lamellar and nonlamellar structures. As a function of increasing temperature, the main lamellar transition between gel and liquid crystalline phases can be observed by DSC or ^{2}H NMR, respectively as a discontinuity in enthalpy or an abrupt reduction in average order. This transition is characterized by the onset of fast axial rotation and acyl chain melting coinciding with a decrease in bilayer thickness. In the gel phase lipid chains are packed tightly and limited isomerization occurs. Increasing thermal energy, the system transforms to a fluid state with lipids diffusing laterally and acyl chains rapidly reorienting. Small differences in lipid structure and changes in membrane composition can have a substantial impact on phase behavior. For example, a single double bond variation is responsible for the disparity in melting temperatures between the fully saturated lipid DSPC (di18:0 PC) at 55 °C and the monounsaturated lipid SOPC (18:0-18:1 PC) at 6 °C; further still, the transition temperature for DOPC (di18:1 PC), with two monounsaturated chains, is all the way down at -17 °C. Chain length also matters as longer chain lipids tend to be solid at room temperature whereas shorter chain lipids are fluid. Ternary systems composed of one high melting and one low melting lipid along with the sterol cholesterol are a popular model for the plasma membrane outer leaflet of eukaryotes and their phase behavior has been heavily studied. In the next section the way in which cholesterol interacts with these lipids to modulate membrane structure will be discussed.

1.3 Cholesterol

A considerable amount of research has been devoted to cholesterol, both for its role in atherosclerosis and as an essential component required for the growth and viability of mammalian cells. Cholesterol levels, supported by de novo synthesis and dietary absorption, are highly regulated in membranes (Brown and Goldstein 1999). Model PC bilayers can incorporate cholesterol up to 66 mol% of total lipid before it precipitates out of the membrane as cholesterol monohydrate crystal (Huang et al. 1999). In eukaryotic cells a cholesterol

concentration gradient exists between organelle membranes and across the Golgi, where cholesterol represents almost half of the total lipid content of the plasma membrane and the ER membrane, the site of cholesterol synthesis, paradoxically only contains a few mole percent of the sterol (Ikonen 2008).

From membrane trafficking and organization to cell signaling, cholesterol has an acute effect on many physical properties and functions of biomembranes. For reviews on cholesterol's membrane behavior see Yeagle (1985), Ohvo-Rekilä et al. (2002), and Mouritsen and Zuckermann (2004). Cholesterol's unique qualities allow it to modulate the membrane environment in ways that cannot be completely replicated by other sterols (Henricksen et al. 2006). A fused tetracyclic ring makes up the nucleus of the molecule. The ring system is rigid and planar with two distinct faces. Ring methyls project from one side, the β-face, leaving the α-face relatively smoother (Fig. 1.5).

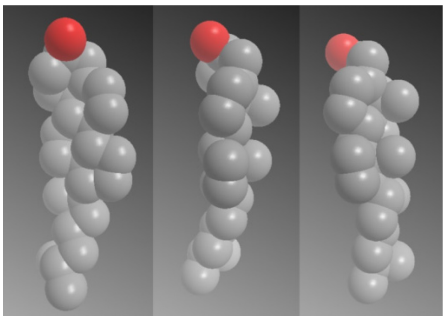

Figure 1.5 Planar nature of cholesterol structure. A space filling display of cholesterol's smooth α-face, end view and rough β-face with protruding methyls.

Cholesterol's native orientation is upright, parallel to the bilayer normal (Scheidt et al. 2003), with one interesting exception which will be discussed later. The isooctyl side chain that extends towards the center of the bilayer is stiff (Dufourc et al. 1984). With limited flexibility, the predominate modes of motions entail wobbling of and rotation about the molecular axis. The whole molecule has a length approximately equivalent to 17 hydrocarbon chain links. In its upright orientation the rigid steroid nucleus is placed in close proximity with the upper portion of adjacent lipid acyl chains, impeding isomerization between trans and gauche conformations of C-C bonds. Restriction of acyl chain motion by cholesterol leads to retraction of phospholipid methyl groups away from the water-bilayer interface increasing packing, elastic rigidity and

thickness of the membrane (Mihailescu et al. 2011). Membrane permeability is also decreased as cholesterol reduces the occurrence of membrane defects through increased ordering of acyl chains (Yeagle 1985). In monolayers an overall reduction in average area per lipid accompanies cholesterol incorporation (what is known as the condensing effect) except in monolayers composed of dipolyunsaturated lipids (Demel et al. 1972, Pan et al. 2008).

The hydrophilic portion of cholesterol is small, being only comprised of hydroxyl group at the 3β carbon position (Fig. 1.2). This hydroxyl is buried in the membrane near the carbonyls of adjacent phospholipid. The umbrella model (Huang and Feigenson 1999) posits that this positioning below the aqueous interface is a consequence of the hydrophobic cross section of the mostly nonpolar cholesterol not being fully covered by its hydroxyl group, thus requiring additional shielding by the headgroups of surrounding lipids from unfavorable contact with water. This necessity for cover makes in-leaflet cholesterol-cholesterol interactions unfavorable and the ordered arrangement of cholesterol within a 2-D lattice favorable. The reduced affinity for PE lipids shown by cholesterol relative to PC lipids (van Dijck et al. 1976) is in agreement with the umbrella model as the PE head group is smaller and less capable of shielding the nonpolar area of cholesterol.

1.4 Functional Lipid Diversity and Domains

It is advantageous for organisms to synthesize and support a varied collection of lipids. The staggering number of unique possible headgroup and acyl chain combinations allows for the fine-tuned adjustment of membrane properties through variations in a membrane's lipid profile.

Biomembranes must be in a fluid state in order to resist rupture, but not so fluid that they become excessively permeable. As a compromise between these opposing pressures some have argued (McMullen et al. 2004) that plasma membrane exist in a mostly liquid ordered (l_o) phase that is an intermediate of gel (solid ordered, s_o) and disordered liquid crystalline phases. In this phase lipids undergo rapid axial rotation and fluid lateral diffusion akin to lipids in the liquid disordered (l_d) phase, but have restricted chain isomerization as they would in the s_o phase. Modification of lipid fatty acid content (i.e. increasing or decreasing unsaturation levels or chain length) is a way in which some organisms can maintain membrane fluidity in the face of environmental stressors; alternatively this delicate balance can be upheld by the presence of

cholesterol, which acts as a kind of buffer to membrane phase (Sinensky 1974, Hazel and Williams 1990, Blom et al. 2001).

For eukaryotic membranes the l_o phase is exclusively induced by the presence of cholesterol. The inclusion of cholesterol in lipid mixtures broadens and suppresses the thermotropic transition between s_o and l_d phases; at low temperature cholesterol disrupts orderly packing and decreases the tilt angle of lipids in the s_o phase, while at high temperatures chain reorientation is hampered and order is increased in what would be the l_d phase (Vist and Davis 1990). For lipids with strong cholesterol associations the s_o to l_d phase transition can be completely obliterated by high concentrations of the sterol. Due to varying cholesterol-lipid affinities cholesterol may become more concentrated in regions of mixed or biological membranes, because of cholesterol's special ordering activity these regions will have different properties than the surrounding membrane.

Lipid diversity enables the formation of specialized functional environments through which resident protein activity can be modulated. Domains are regions of membrane having properties that differ from the immediate surroundings due local variations in membrane composition. Demixing can lead to liquid-liquid and liquid-gel phase separation in model systems, but only liquid-liquid phase coexistence is likely in biological systems. Domain formation is a somewhat mysterious, or at least not well characterized phenomenon. Many questions remain about their basic nature; like what their size, duration and prevalence is, as well as what are the dominant assembly promoters. In model systems domains can form spontaneously as a consequence of thermodynamics and unequal lipid-lipid affinities, but in nonequilibrium biomembranes, interactions with the cytoskeleton and proteins are also a factor.

Domains have been readily observable in model systems, but remain elusive in biological systems. There is currently no consensus model which describes how domains form, their stability, or the extent of their structure in biomembranes. Studies on model membranes of ternary system composed of a high and low melting lipid along with cholesterol, designed to mimic the plasma membrane, provide clues, but may be so far removed from the nonequilibrium biological conditions as to be inapplicable. Whether detection of domains in

biomembranes is a verifiable result or an artifact of the method of investigation has been a matter of debate (Munro 2003). An excellent review article containing select evidence for domain existence in biomembranes is provided by Jacobson et al. (2007). Currently membrane models are limited in their ability to replicate the high density of membrane protein, the influence of the cytoskeleton, protein-protein oligimerization, lipid asymmetry, or the rapid rate of lipid turnover of biomembranes.

By far the most widely studied domain type is the SM and cholesterol rich lipid raft (Simons and Ikonen 1997, Edidin 2003). The origin of the term “raft” relates to the appearance of the domain, which is raised relative to the surrounding sea of lipids. The structure of cholesterol is compatible with being in close proximity to the long saturated chains of sphingomyelin, allowing for strong van der Waals interactions. This association is further stabilized through hydrogen bonding between the hydroxyl group of cholesterol and the amide on the sphingosine backbone (Ohvo-Rekilä et al. 2002). Due to their increased affinity for one another relative to other lipid species present, microdomains form with elevated cholesterol and sphingomyelin levels. These rafts are liquid ordered and exist in biological systems bordered by more disordered regions of unsaturated glycerophospholipids and lower cholesterol content. The current view is that these assemblies are small (nanoscale), dynamic and transient.

Domains may occur over a range of length scales: a shell of lipids or annulus surrounding protein, clusters of a few molecules, to nano and microscale domains. The membrane surface maybe mostly a mosaic patchwork of domains (Kusumi et al. 2005) where nondifferentiated inclusions are the exception. These domains are sure to be imperfect; rich or poor in constituents relative to the surrounding, but not pure. Domains on the order of micrometers have been produced in GUVs of reconstituted membranes, whereas evidence in biomembranes point towards submicron average dimensions with the potential to coalesce into larger domains.

In a MD simulation of rhodopsin incorporated in a 18:0-22:6PC, 18:0-22:6PE membrane with cholesterol, the DHA (22:6) chains were shown to preferentially associate with the face of rhodopsin and penetrate the crevices of its surface while cholesterol avoided contact with the protein (Pittman et al. 2006). The implications are that rhodopsin, in its native membrane, may

seek out or stimulate the formation of domains rich in unsaturated lipids and devoid of cholesterol. Rhodopsin has seven transmembrane α-helices, with lateral area per helix ~1 nm^2. The concentration of rhodopsin in the rod outer segment membrane (30,000 per μm^2, 20-25% of surface area) leaves only enough room for a thin shell of lipids (2-3 rings) around each protein (~50 lipids per protein, ~14 makeup the protein boundary) (Jacobson et al. 2007).

At this point proposals of raft function are somewhat speculative. In contrast to globular proteins, membrane proteins have to function in an anisotropic environment and are subject to fluctuations in membrane properties. Domains may act as a platform for binding certain peripheral proteins or clustering of transmembrane proteins (e.g. GPI-anchored proteins) consequently controlling protein trafficking, diffusion and oligimerization. Domains compartmentalize and modify reactions that occur on the membrane through alteration of the rates of interaction of membrane components, but also by providing an environment that influences the function of resident proteins contained therein through matching or mismatching the hydrophobic profile of embedded proteins. Domains are prospective targets for drug therapies, as they are known sites of virus infiltration and their disruption interrupts signal persistence (Schmitz and Grandl 2008).

The mattress model of Mouritsen and Bloom (1984) describes how the lipid bilayer will deform in the region around an embedded protein to prevent the unfavorable contact of water with either of the hydrophobic portions of protein or bilayer. The bilayer is more capable of deforming and adapts the hydrophobic profile of the rigid protein. When hydrophobic mismatch is extreme the force exerted on the protein will stretch transmembrane segments, providing energy which can potentially inhibit or promote conformational changes thereby modulating the activity of the protein (Kaiser et al. 2011). The tilt orientation of protein in the bilayer can also be regulated by hydrophobic mismatch. Cholesterol increases the energy penalty of hydrophobic mismatch, as it stiffens the membrane and hinders acyl chain rearrangement necessary to accommodate the protein's profile. Mismatch avoidance may be a driving factor in lateral sorting and protein clustering in the membrane. Cholesterol in particular could play a central role in sorting of proteins and lipids by hydrophobic length along the membrane trafficking pathway.

There is still much uncharted territory to be explored in the field of membrane biophysics. Significant holes exist in our understanding of membrane organization and of fundamental molecular interactions that occur there. The next and final section will discuss the properties of polyunsaturated lipids, their steric incompatibility with cholesterol and a hypothetical liquid disordered domain concentrated in these unique lipids.

1.5 Unsaturated Lipids

Unsaturated lipids are found in most membranes, notably in the inner leaflet of the plasma membrane, but there are select tissues in which polyunsaturated fatty acids (PUFAs), possessing two or more unsaturated bonds, account for 50 mol% of membrane lipid acyl chains. These include the specialized membranes of sperm, neural and retinal tissues. The motional behavior of PUFA chains varies depending the number and location of unsaturated bonds in its sequence, the repeat unit -C=C-C-C=C- is a common structural motif for PUFA. Two examples of PUFA bond sequences appear in Figure 1.6.

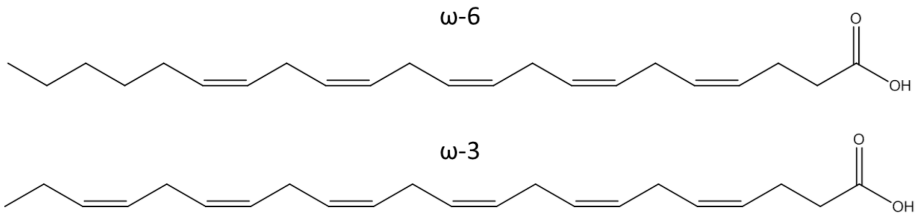

Figure 1.6 Structure of the polyunsaturated fatty acids (PUFAs) docosapentaenoic acid (22:5n6, top) and docosahexaenoic acid (22:6n3, bottom).

Docosapentaenoic acid (DPA, 22:5) and DHA (22:6) are representative of the ω-6 and ω-3 (or n-6 and n-3) PUFA classes having six and three, respectively, consecutive saturated bonds linked to the terminal methyl. These chains have the same overall carbon length but, as we have already stated with regards to phase transition temperatures, a single double bond addition can impact membrane organization and physiological function.

Humans cannot convert between ω-6 and ω-3 PUFA. Long chain ω-3 PUFA are considered essential fatty acids in that they are inefficiently produced in situ, through modification and elongation of short chain ω-3 PUFA, and should be supplemented by diet to avoid deleterious physiological effects. Current dietary recommendations call for a balance between ω-3 and ω-6

PUFA consumption (Simopoulos 2002). The western diet is deficient in ω-3 PUFA, with ω-6 PUFA typically being consumed 15:1 over ω-3 PUFA. Increased cold-water fish consumption or fish oil supplementation is advised to boost ω-3 levels. Fish oil supplements are increasingly being used to alleviate symptoms or prevent the onset of a number of varied, seemingly unrelated diseases and ailments. The list includes some of the more prevalent afflictions in western society: dementia, arthritis, depression, asthma, cancer and heart disease (Wassall and Stillwell 2009). Some of these health claims are in dispute, others have gained acceptance and ω-3 PUFA are routinely prescribed (e.g. Lovaza). It is unclear what molecular mode of action is behind the numerous associated health benefits of ω-3 PUFA consumption. There are likely multiple avenues through which ω-3 PUFA act to alter physiological responses. Modulation of eicosanoid activity, for one, has been widely reported (Calder 2009). It is their less examined role in determining membrane organization and dynamics which we hypothesize may have a significant contribution to some of the ascribed health benefits.

1.5.1 Unique Properties of PUFA

Because of the reduced barrier to rotation about double bond adjacent, C-C bonds, PUFA chains have short reorientational correlation times and rapidly explore large conformational spaces; compared to lipids with saturated acyl chains of equal length, PUFA containing lipids will have a larger average area per lipid. PUFA chains are highly disordered, capable of snorkeling up to the membrane surface due to their increased flexibility and polarity relative to saturated chains. PUFA containing membranes are thin. A decrease in average chain order corresponds to a shortening of projected acyl chain length along the bilayer normal. PUFA chains interact weakly, so membranes composed of lipids possessing them tend to have low transition temperatures. Beyond these generalizations it is a mistake to assume that all PUFAs, or even PUFAs with the same length, number of unsaturated bonds, or belonging to the same ω-3 or ω-6 class, will have equivalent effects on membrane organization (Williams et al. 2012) and fill the same physiological role.

Eldho et al. (2003) showed that mixed chain PC lipids having stearic (18:0) sn-1 chains and DPA (22:5n-6) or DHA (22:6n-3) (Fig. 1.6) sn-2 chains exhibit remarkable differences in chain distribution, but in many ways their membranes are otherwise indistinguishable. The DHA chain

density increases near the membrane surface where the DPA chain has a more even distribution throughout the membrane. This could have profound biological implications. Brain and retina membranes will substitute DPA for DHA when ω-3 PUFAs are unavailable (Salem et al. 2001), but this does not occur without some loss of function (Niu et al. 2004). The impact on transmembrane proteins, from the change in membrane lateral pressure density profile corresponding to the two distinct chain distributions, may be the root of functional impairment.

1.5.2 PUFA-Cholesterol Interactions

For a mixed chain lipid bilayer (18:0-22:6 PC), cholesterol has been shown by MD simulation (Pittman et al. 2004) to exhibit higher affinity for saturated chains, meaning that on average within the shell of lipids immediately surrounding cholesterol (which is constantly exchanging members with the bulk lipid) lipids are oriented with their saturated chains in contact with cholesterol. The smooth α-face of cholesterol in particular has a pronounced tendency for preferential association with saturated chains.

Within the hydrophobic core of the bilayer, acyl chain concentration is nearly constant. For bilayers composed of a mixed chain lipid 18:0-22:6 PC, the density of the DHA chain in the region near the hydrophobic-hydrophilic interface is greater than that of the saturated counterpart in the sn-1 position (Eldho et al. 2003). The increased conformational fluctuations of the PUFA chain in the transverse direction push cholesterol away. Neutron scattering on aligned multilayers of dipolyunsaturate lipid (di20:4 PC) has revealed that cholesterol, in this highly disordered environment, is displaced from its canonical upright position and sequestered in the center of the bilayer (Harroun et al. 2008). The result agrees well with the observation that cholesterol has limited to no condensing effect on membranes of polyunsaturated homoacid lipids (Demel et al. 1972, Pan et al. 2008). Doping the dipolyunsaturate-cholesterol membrane with 50 mol% of mixed chain 16:0-18:1PC or 5 mol% of fully saturated di14:0PC restores cholesterol's erect status (Kučerka et al. 2010). Rather than adopt a non-upright orientation to accommodate their fluctuations the rigid cholesterol molecule is displaced away from the highly disordered PUFA chain and associates with the saturated chains which pack more readily. In biological systems cholesterol would likely be driven out of regions or leaflets having elevated PUFA concentration and take refuge in more ordered domains. This aversion could be explained

either by a steric compatibility with more ordered saturated chains, or, in line with the concept of the umbrella model, by a preference for the shelter provided by saturated lipids whose molecular shape is more cylindrical compared to PUFA containing lipids. Aversion for PUFA chains could be a mechanism that generates lateral segregation of the membrane, i.e. the formation of PUFA-rich/cholesterol-poor domains. Figure 1.7 provides an illustration of this concept.

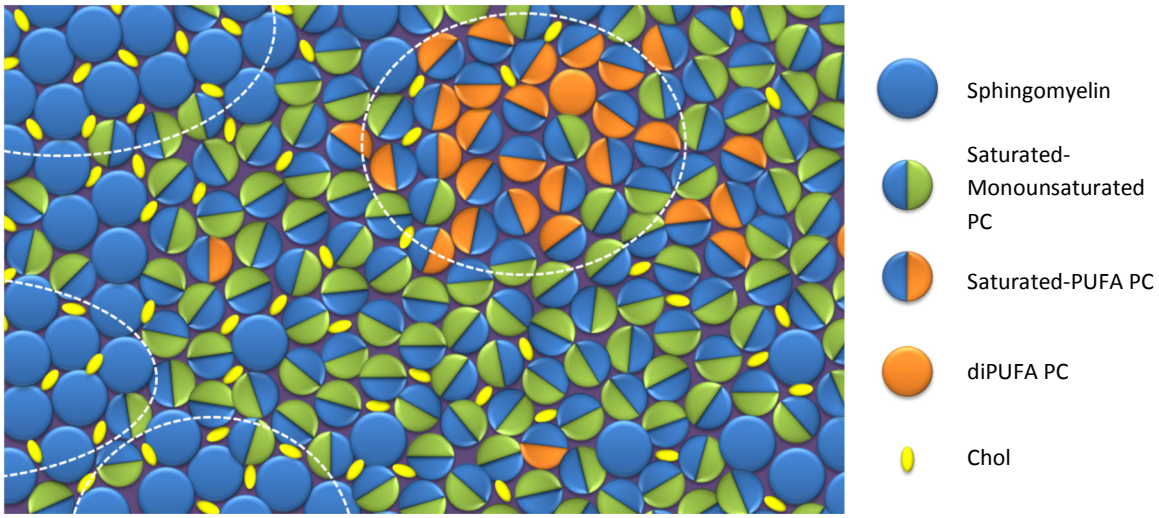

Figure 1.7 A cartoon of a model membrane surface, aqueous view, showing the nonrandom distribution of SM, PC, and cholesterol in PUFA-rich/cholesterol-poor liquid disordered and SM-/cholesterol-rich raft-like domains (indicated by dashed enclosures). Heterogeneities spontaneously develop in the membrane where clusters of ten to twenty similar lipid species emerge from the sea of bulk lipid. Nanoscale domains would encompass hundreds to thousands of lipids. These clusters potentially can gather to form larger microdomains. The planar α- and β-face of cholesterol is predominately solvated by saturated chains (in blue), a driving factor in segregation of lipids. Cholesterol's reduced affinity for PUFA and increased affinity for SM, respectively, leads to depleted levels of cholesterol in the liquid disordered domain and enrichment of cholesterol in raft domains. Cholesterol and mixed chain lipids decrease the line tension at domain boundaries. Domains are not pure; clustering as a consequence of lipid-lipid affinity is opposed by the entropic cost of demixing. In model systems domains often appear circular. Domains in biomembranes have irregular shapes and are transient assemblies. These domains represent distinct environments within the membrane, whose different physical properties can modulate the activity of resident proteins.

The steric incompatibility of cholesterol and PUFA has been measured indirectly in a number of ways. The solubility of cholesterol in dipolyunsaturated-PC was observed by x-ray diffraction to be reduced by more than half when compared to mixed chain- or saturated-PC lipids (Brzustowicz et al. 2002). In ternary systems composed of a high melting lipid (often SM), low

melting PUFA-containing lipid and cholesterol, differential lipid-lipid affinity can drive phase separation. By ^{2}H NMR cholesterol was shown to order the sn-1 palmitoyl chain of 16:0-18:1PE to a greater extent than that of 16:0-22:6PE in PE/SM/cholesterol mixtures, the smaller effect implying that the PUFA containing PE was driven out of SM-/sterol-rich domains more so than the monounsaturate containing PE (Wassall et al. 2004). In monolayers of these mixtures, the size of ordered domains in the PUFA containing sample, as measured by AFM (Shaikh et al. 2004), was shown to increase relative to the monounsaturated-PE sample, suggesting that the DHA containing lipid elicited a larger phase segregation response due to PUFA-cholesterol aversion. From the same group (Shaikh et al. 2002), a DSC heating scan of 16:0-22:6PE with SM revealed two transition peaks: a high temperature transition for SM and a low melting transition for 16:0-22:6PE. Upon addition of cholesterol (0.005 mol fraction) the SM peak was obliterated while the low melting peak remained unchanged. This data was presented in contrast to a 16:0-18:1PE/SM mixture in which only a single peak was detected, subsequently diminished at equivalent cholesterol levels. The two peaks detected in the PUFA containing sample, but not in the monounsaturated sample, indicate phase separation. Furthermore, analogous to the ^{2}H NMR data (Wassall et al. 2004), the observed suppression of the SM peak reflects the preferential incorporation of cholesterol into the ordered SM domain. Taken together the sum of this model work point towards the potential for the formation of PUFA-rich/cholesterol-poor l_d domains in driven not by PUFA-PUFA interactions, but by a reduced cholesterol affinity for PUFA. In Chapter 4, a more in depth look at cholesterol-lipid affinity will be presented along with a novel method of measuring it (Williams et al. 2013).

1.5.3 PUFA-Protein Interaction

Finally before this chapter concludes, I would like to provide a brief example of lipid-protein interactions. While lipids are deserving of much more attention than they are typically afforded in cell biology texts, their importance, outside of their basic barrier forming function, is still tied in large part to their interactions with proteins. Understanding protein-lipid interactions is of vital importance, as an estimated 60% of all drug targets are membrane associated. Class A of G protein-coupled receptors (GPCRs) in particular accounts for over a quarter of all human-genome-derived protein targets for FDA approved drugs (Overington et al. 2006). The GPCR family encompasses a large array of transmembrane proteins that respond to a variety of

different stimuli and are involved in diverse range of physiological processes. The GPCR A class includes rhodopsin, which is found in the outer segment disk membrane of photoreceptor rod cells. Few crystal structures of proteins in this class are known, which is what makes rhodopsin, whose structure was solved in 2000 (Palczewski et al.), an attractive model for protein-lipid interactions.

The rod outer segment is composed of a stack of disk membranes whose cholesterol content decreases as the disk ages and moves further away from the main body of the rod. These membranes are rich in the ω-3 PUFA, DHA (Albert et al. 1998). Cholesterol and PUFA are essential in balancing the activity of rhodopsin. In cholesterol-rich membranes, rhodopsin is protected from denaturing but its function is impaired, being predominately locked in a conformational state unresponsive to light stimulus (Burger et al. 2000). Polozova and Litman (2000) showed that for a mixed system containing disaturated-PC, dipolyunsaturated-PC and cholesterol, rhodopsin clusters in PUFA rich domains where the PUFA chain compressibility, among other factors (Soubias and Gawrisch 2012), allows for conformational changes and proper functioning of the protein. The compartmentalization of the disk membrane into PUFA-rich/cholesterol-poor and cholesterol-rich/PUFA-poor regions would satisfy both the need for mechanical stability and cohesion of the disk membrane, and the requirement a PUFA environment to lower the free energy of activation for rhodopsin. It seems the cholesterol gradient of the rod disk stack may exist to provide protection of rhodopsin until its resident disk is displaced to the outer reaches of the rod where it becomes photoactive in PUFA-rich domains. These rhodopsin findings have implications for regulation of GPCR signaling, widespread in other physiological processes, via membrane heterogeneity, and are suggestive of the potential for targeted dietary fat management in medicine.

1.6 Concluding Remarks

In an attempt to add to this story, our work has focused on examining the interplay between polyunsaturated lipids and cholesterol and the role of PUFA-cholesterol interactions in domain formation. In Chapter 3 we examine the differential membrane organizing effect of the ω-3 PUFAs, eicosahexaenoic acid and docosahexaenoic acid, in model membranes containing cholesterol and SM. We've found evidence of liquid ordered-liquid disordered phase

coexistence, and were able to provide a rough estimate of the size of the domains induced by the ω-3 PUFAs. Additionally, we detected a surprisingly substantial amount of ω-3 PUFA infiltration in the ordered, raft-like domain, given the earlier described results, which could potentially disrupt native protein signaling if this were to occur in vivo. The observed differences between these structurally similar ω-3 PUFAs were significant enough to support the notion that there is a need of greater specificity in membrane models, and to avoid over simplification and generalization of lipid traits. Chapter 2 serves as a theoretical primer for the main method of investigation, solid state ^{2}H NMR, implemented in Chapter 3. In Chapter 4 a novel EPR method of measuring cholesterol affinity as a function of lipid acyl chain unsaturation is presented. Our findings confirm reduced affinity for increasing levels of unsaturated and agree with relative values measured by other biophysical approaches including our own independent Isothermal Titration Calorimetry measurements. Finally, Chapter 5 will summarize findings and suggest future directions.

1.9 References

Albert AD, Young JE, Paw Z (1998) Phospholipid fatty acyl spatial distribution in bovine rod outer segment disk membranes. Biochim Biophys Acta 1368:52-60

Blom TS, Koivusalo M, et al. (2001) Mass spectrometric analysis reveals an increase in plasma membrane polyunsaturated phospholipid species upon cellular cholesterol loading. Biochem 40:14635-14644

Bloom M, Evans E, Mouritsen OG (1991) Physical properties of the fluid lipid-bilayer component of cell membranes: a perspective. Quart Rev Biophys 24:293-397

Boal D (2002) Mechanics of the cell. Cambridge University Press

Brown MS, Golstein JL (1999) A proteolytic pathway that controls the cholesterol content of membranes, cells, and blood. Proc Natl Acad Sci USA 96:11041-11048

Brzustowicz MR, Cherezov V, et al. (2002) Controlling membrane cholesterol content. A role for polyunsaturated (docosahexaenoate) phospholipids. Biochem 41:12509-12519

Burger K, Gimpl G, Fahrenholz F (2000) Regulation of receptor function by cholesterol. Cellular and molecular life sciences 57:1577-1592

Calder PC (2009) Polyunsaturated fatty acids and inflammatory processes: new twists in an old tale. Biochimie 91:791-795

Chan YHM, Boxer SG (2007) Model membrane systems and their applications. Curr Opin Chem Biol 11:1-7

Demel RA, van Kessel WSMG, van Deenen LLM (1972) The properties of the polyunsaturated lecithins in monolayers and liposomes and the interactions of these lecithins with cholesterol. Biochim Biophy Acta 266:26-40

Dufourc EJ, Parish EJ, Chitrakorn S, Smith ICP (1984) Structural and dynamical details of cholesterol-lipid interaction as revealed by deuterium NMR. Biochemistry 23:6062-6071

Dufourc EJ (2008) Sterols and membrane dynamics. J Chem Biol 1:63-77

Edidin M (2003) Lipids on the frontier: a century of cell-membrane bilayers. Nat Rev Mol Cell Biol 4:14-418

Edidin M (2003) The state of lipid rafts: from model membranes to cells. Annu Rev Biophys Biomol Struct 32:257-283

Eldho NV, Feller SE, Tristram-Nagle S, Polozov IV, Gawrisch K (2003) Polyunsaturated docosahexaenoic vs docosapentaenoic acid-differences in lipid matrix properties from the loss of one double bond. J Am Chem Soc 125:6409-6421

Engelman DM (2005) Membranes are more mosaic than fluid. Nature 438:578-580

Fahy E, Subramaniam S, et al. (2005) A comprehensive classification system for lipids. J Lipid Res 46:839-861

Feller SE (2008) Acyl chain conformations in phospholipid bilayers: a comparative study of docosahexaenoic acid and saturated fatty acids. Chem Phys Lipids 153:76-80

Gawrisch K (2005) The dynamics of membrane lipids, In Yeagle PL (ed) The structure of biological membranes. CRC Press, Boca Raton FL

Gorter E, Grendel F (1925) On bimolecular layers of lipoids on the chromocytes of the blood. J Exp Med 41:439-443

Gruner SM (2005) Nonlamellar lipid phases, In Yeagle PL (ed) The structure of biological membranes. CRC Press, Boca Raton FL

Guidotti G (1972) Membrane Proteins. Ann Rev Biochem 41:731-752

Harroun TA, Katsaras J, Wassall SR (2008) Cholesterol is found to reside in the center of a polyunsaturated lipid membrane. Biochem 47:7090-7096

Hauser H, Poipart G (2005) Lipid structure, In Yeagle PL (ed) The structure of biological membranes. CRC Press, Boca Raton FL

Hazel JR, Williams EE (1990) The role of alterations in membrane lipid composition in enabling physiological adaptation of organisms to their physical environment. Prog Lipid Res 29:167-227

Hirschmann H (1960) The nature of substrate asymmetry in stereoselective reactions. J Biol Chem 235:2762-2767

Holthuis JCM, Pomorski T, Raggers RJ, Sprong H, van Meer G (2001) The organizing potential of sphingolipids in intracellular membrane transport. Physiol Rev 81: 1689-1723

Huang J, Buboltz JT, Feigenson GW (1999) Maximum solubility of cholesterol in phosphatidylcholine and phosphatidylethanolamine bilayers. Biochim Biophys Acta 1417:89-100

Huang J, Feigenson GW (1999) A microscopic model of maximum solubility of cholesterol in lipid bilayers. Biophys J 76:2142-2157

Ikonen E, (2008) Cellular cholesterol trafficking and compartmentalization. Nat Rev Mol Cell Bio 9:125-138

Jacobson K, Mouritsen OG, Anderson RGW (2007) Lipid rafts: at a crossroad between cell biology and physics. Nat Cell Biol 9:7-14

Jo S, Rui H, Lim JB, Klauda JB, Im W (2010) Cholesterol flip-flop: insights from free energy simulation studies. J Phys Chem B 114:13342-13348

Kaiser HJ, Orlowski A, et al. (2011) Lateral sorting in model membranes by cholesterol-mediated hydrophobic matching. Proc Nat Acad Sci 108:16628-16633

Karnovsky MJ, Kleinfeld AM, Hoover RL, Klausner RD (1982) The concept of lipid domains in membranes. J Cell Biol 94:1-6

Kučerka N, Marquardt D, et al. (2010) Cholesterol in bilayers with PUFA chains: Doping with DMPC or POPC results in sterol reorientation and membrane-domain formation. Biochem 49:7485-7493

Kumar R, Schmidt JR, Skinner JL (2007) Hydrogen bonding definitions and dynamics in liquid water. J Chem Phys 126:204107

Kusumi A, Nakada C, et al. (2005) Paradigm shift of the plasma membrane concept from the two-dimesional continuum fluid to the partitioned fluid: high-speed single-molecule tracking of membrane molecules. Ann Rev Biophys Biomol Struct 34:351-378

Luckey M (2008) Membrane structural biology with biochemical and biophysical foundations. Cambridge University Press New York, NY

Maksymiw R, Fang Sui S, Gaub H, Sackmann E (1987) Electrostatic coupling of spectrin dimers to phosphatidylserine-containing lipid lamellae. Biochem 26:2983-2990

Marquardt D, Williams JA, et al. (2013) Tocopherol activity correlates with its location in a membrane: a new perspective on the antioxidant Vitamin E. J Am Chem Soc 135:7523-7533

Marrink SJ, Lindahl E, Edholm O, Mark AE (2001) Simulation of the spontaneous aggregation of phospholipids into bilayers. J Am Chem Soc 123:8638-8639

McMullen TPW, Lewis RNAH, McElhaney RN (2004) Cholesterol-phospholipid interactions, the liquid-ordered phase and lipid rafts in model and biological membranes. Curr Opin Colloid In 8:459-468

Mihailescu M, Vaswani RG, et al. (2011) Acyl-chain methyl distributions of liquid-ordered and –disordered membranes. Biophys J 100:1455-1462

Mouritsen OG, Bloom M (1984) Mattress model of lipid-protein interactions in membranes. Biophys J 46:141-153

Mouritsen OG, Jørgensen K (1994) Dynamical order and disorder in lipid bilayers. Chem Phys Lipids 73:3-25

Mouritsen OG, Zuckermann MJ (2004) What's so special about cholesterol? Lipids 39:1101-1113

Munro S (2003) Lipid rafts: elusive or illusive? Cell 115:377-388

Murase K, Fujiwara T, et al. (2004) Ultrafine membrane compartments for molecular diffusion as revealed by single molecule techniques. Biophys J 86:4075-4093

Nagle JF, Tristram-Nagle S (2000) Structure of lipid bilayers. Biochim Biophys Acta 1469:159-195

Nelson D (2004) Statistical mechanics of membranes and surfaces. World Scientific

Niu SL, Mitchell DC, et al. (2004) Reduced G protein-coupled signaling efficiency in retinal rod outer segments in response to n-3 fatty acid deficiency. J Biol Chem 279:31098-31104

Ohvo-Rekilä H, Ramstedt B, Leppimäki P, Slotte JP (2002) Cholesterol interactions with phospholipids in membranes. Prog Lipid Res 41:66-97

Pan J, Mills TT, Tristram-Nagle S, Nagle JF (2008) Cholesterol perturbs lipid bilayers nonuniversally. Phys Rev Lett 100:19803-19806

Petrache HI, Dodd SW, Brown MF (2000) Area per lipid and acyl length distributions in fluid phosphatidylcholines determined by ^{2}H NMR spectroscopy. Biophys J 79:3172-3192

Pittman MC, Suits F, MacKerell AD, Feller SE (2004) Molecular-level organization of saturated and polyunsaturated fatty acids in a phosphatidylcholine bilayer containing cholesterol. Biochem 43:15318-15328

Pittman MC, Grossfield A, Suits F, Feller SE (2006) Role of cholesterol and polyunsaturated chains in lipid-protein interactions: molecular dynamics simulation of rhodopsin in a realistic membrane environment. J Amer Chem Soc 127:4576-4577

Polozova A, Litman BJ (2000) Cholesterol dependent recruitment of di22:6-PC by a G protein receptor in lateral domains. Biophys J 79:2632-2643

Salem N, Litman B, Kim HY, Gawrisch K (2001) Mechanisms of action of docosahexaenoic acid in the nervous system. Lipids 39:945-959

Schindler H, Seelig J (1975) Deuterium order parameters in relation to thermodynamic properties of a phospholipid bilayer. A statistical mechanical interpretation. Biochem 14:2283-2287

Schmitz G and Grandl M (2008) Update on lipid membrane microdomains. Curr Opin Clin Nutr 11:106-112

Seelig A, Seelig J (1974) The dynamic structure of fatty acyl chains in a phospholipid bilayer measured by deuterium magnetic resonance. Biochem 13:4839-4845

Shaikh SR, Brzustowicz MR, et al. (2002) Monounsaturated PE does not phase-separate from lipid raft molecules sphingomyelin and cholesterol: a role for polyunsaturation? Biochem 41:10593-10602

Shaikh SR, Dumaual AC, et al. (2004) Oleic and docosahexaenoic acid differentially phase separate from lipid raft molecules: A comparative NMR, DSC, AFM, and detergent extraction study. Biophys J 87:1752-1766

Simons K, Ikonen E (1997) Functional rafts in cell membranes. Nature 387:569–372

Simopoulos AP (2002) The importance of the ratio of omega-6/omega-3 essential fatty acids. Niomed Pharmacother 56:365-379

Sinensky M (1974) Homoviscous adaptation – a homeostatic process that regulates viscosity of membrane lipids in Escherichia coli. Proc Nat Acad Sci USA 71:522-525

Singer SL, Nicoholson GL (1972) The fluid mosaic model of the structure of cell membranes. Science 175:720-731

Slotte JP (2013) Biological functions of sphingomyelins. J Lipid Res 52:424-437

Soubias O, Gawrisch K (2007) Docosahexaenoyl chains isomerize on the sub-nanosecond time scale. J Am Chem Soc 129:6678-6679

Soubias O, Gawrisch K (2012) The role of the lipid matrix for structure and function of the GPCR rhodopsin. Biochim Biophys Acta 1818:234-240

Spira F, Mueller NS, von Olshausen P, Beig J, Wedlich-Sldner R (2012) Patchwork organization of the yeast plasma membrane into numerous coexisting domains. Nat Cell Biol 14:640-648

Stillwell W (2013) An introduction to biological membranes: from bilayers to rafts. Elsevier

Tanford C (1980) The hydrophobic effect formation of micelles and biological membranes, 2nd edn. Wiley. New York.

van Dijck PWM, de Kruijff B, van Deenen LLM, de Gier J, Demel RA (1976) The preference of cholesterol for phosphatidylcholine in mixed phosphatidylcholine-phosphatidylethanolamine bilayers. Biochim Biophys Acta 455:576-587

Vereb G, Szöllõsi J, et al. (2003) Dynamic, yet structured: the cell membrane three decades after the Singer-Nicolson model. P Natl Acad Sci USA 100:8053-8058

Venable RM, Zhang Y, Hardy BJ, Pastor RW (1993) Molecular dynamics simulations of a lipid bilayer and of hexadecane: an investigation of membrane fluidity. Science 262:223-226

Vist MR, Davis JH (1990) Phase equilibria of cholesterol/dipalmitoylphosphatidylcholine mixtures: 2H nuclear magnetic resonance and differential scanning calorimetry. Biochem 29:451-464

Wassall SR, Brzustowicz MR, et al. (2004) Order from disorder, corralling cholesterol with chaotic lipids: the role of polyunsaturated lipids in membrane raft formation.

Wassall SR, Stillwell W (2009) Polyunsaturated fatty acid-cholesterol interactions: domain formation in membranes. Biochim Biophys Acta 1788:24-32

Wenk MR (2010) Lipidomics: new tools and applications. Cell 143: 888-895

Wiener MC, White SH (1992) Structure of a fluid dioleoylphosphatidylcholine bilayer determined by joint refinement of x-ray and neutron diffraction data. III. Complete structure Biophys J 61:434-447

Williams JA, Batten SE, et al. (2012) Docosahexaenoic and eicosapentaenoic acids segregate differently between raft and nonraft domains. Biophys J 103:228-237

Williams JA, Wassall CD, Kemple MD, Wassall SR (2013) An EPR method for measuring the affinity of a spin labeled analog of cholesterol for phospholipids. J Mem Biol 246:689-696

Yeagle PL (1985) Cholesterol and the cell membrane. Biochim Biophys Acta 822:267-287

CHAPTER 2: SOLID STATE ^{2}H NMR OF MODEL MEMBRANES

2.1 Introduction

Nuclear Magnetic Resonance (NMR) Spectroscopy is a widely used technique in physical, chemical, biological, and medical sciences which is capable of uncovering structural and dynamical information of molecules and assemblies of molecules at an atomic level. Spectroscopy is the study of the interaction of matter and electromagnetic radiation, and with this method it is the nuclear excitation response to radio frequency (RF) photon absorption that is measured. Only nuclei possessing an intrinsic property known as spin (which is restricted to integer or half integer values) are observed in NMR experiments. Modern NMR experiments take place in the static field of a magnet (commonly superconducting) which is used to orient nuclear spins. Resonance in this instance refers to the tuning of the RF radiation to the natural frequency of the nuclei of interest so that the stimulation of excitation phenomena is maximized; because nuclei are quantum objects, only certain frequencies of radiation will trigger an excitation response.

NMR can be performed on gas, liquid, and solid state systems. Of the three, solution NMR of spin ½ molecules is the most prevalent. In contrast to the high resolution spectra of solution NMR, solid state spectral lines are broad and interactions of interest can be obscured. Advances in pulse NMR since the 1970s and the advent of magic angle spinning (MAS) spectrometry have led to increases in spectral resolution that have made solid state spectroscopy analysis more tractable. While the specific techniques and interpretations can differ, the fundamental experimental premise is essentially the same. Nuclei possessing nuclear spin are immersed in a magnetic field and irradiated with a RF pulse which is absorbed by some of the nuclei inducing a transition to a higher energy state. As these nuclei return to the lower energy state they emit photons. The photon emission signal after RF pulse is Fourier transformed to produce a NMR

spectrum whose features can be interpreted to obtain atomic interactions and structural and dynamical information about the system at a nuclear level.

The first application of solid state ^{2}H NMR to examine hydrocarbon chain mobility within a membrane system was reported in 1971 by Oldfield, Chapman and Derbyshire, and has since proven to be a versatile tool for biophysists in the study of the extend structures of lipid assemblies. The selective isotopic substitution of deuterium for hydrogen on a lipid acyl chain is a minimally invasive way of probing motional freedom inside the bilayer, as well as nonlamellar structures. Deuterium is a stable isotope of hydrogen with low natural abundance. There is considerable overlap between phenomena that can be measured by ^{2}H NMR and EPR techniques. Deuterium has the advantage over EPR nitroxide labels however, in that there is no difference sterically between deuterium-labeled and unlabeled chains and the probe has negligible impact on acyl chain motion; thus greatly reducing experimental error of the method relative to EPR (Seelig and Niederberger 1974). A slight perturbation from native behavior is expected though, in the form of a 3-4 °C drop in transition temperature for a lipid with fully deuterated (perdueterated) chains compared to protiated lipid (e.g. Davis 1979). Model membranes of controlled composition are most often used in ^{2}H NMR studies, but biological systems can be investigated as well. The findings of Stockton et al. (1977) confirmed the conduct of lipids in model systems is analogous to that in biomembranes.

The fluid dynamic nature of the membrane is the result of superimposed motions occurring over a range of time scales, from picosecond bond vibrations to large scale structure undulations evolving over seconds. ^{2}H NMR captures the motions occurring on the order of 100 kHz, or the 10 μs time scale, a range sensitive to the anisotropic motions of acyl chains in the hydrophobic core of the bilayer. Motions occurring at higher frequencies are time averaged over the course of the experiment, while slower motions appear as a frozen, population weighted superposition. The information obtained at the atomic level is gathered over a discrete amount of time and so the resulting picture is not a snapshot of molecular organization, but rather a statistical description of the average structure (Nagle and Tristram-Nagle 2000).

In this chapter an account of solid state ^{2}H NMR theory will be given and extended to liquid crystalline model membrane systems with the goal of elucidating the basis of the ^{2}H spectrum and what information can be extracted from it. For authoritative text on fundamental NMR theory see Haeberlen 1976, Abragam 1983, and Slichter 1990; Seelig 1977, Davis 1983, Bloom et al. 1992, and Brown 1996 are excellent resources on the subject solid state NMR as applied to membrane systems; and for practical aspects of NMR methodology the reader can refer to Pochapsky and Pochapsky 2007, and Polozov and Gawrisch 2007.

2.2 Solid State ^{2}H NMR Theory

The deuterium (^{2}H or D) nucleus, composed of a proton and neutron, possesses a spin nuclear moment ($I = 1$) with three degenerate spin states (magnetic quantum number $m = -1, 0, 1$). In the presence of an external magnetic field ($\hat{B}$) or an electric field gradient (EFG) the degeneracy is broken. Chemical shift anisotropy and magnetic dipole-dipole coupling also perturb energy levels, but for deuterium the quadrupolar interaction is orders of magnitude greater and obscures these two effects.

The splitting of nuclear spin energy levels due to the influence of an external magnetic field is a phenomenon known as the Zeeman Splitting. The interaction energy of the nucleus with the applied field is given by $-\hat{\mu} \cdot \hat{B}$ ($\hat{\mu}$ being the magnetic moment of the nucleus) with a corresponding Hamiltonian:

$$\hat{\mathcal{H}}_Z = -\gamma \hbar B_0 \hat{I}_z \tag{1}$$

where γ is a constant scalar property of the nucleus known as the gyromagnetic ratio, the ratio being the magnetic dipole moment to the angular momentum of the nucleus; $\hbar$ is Planck's constant in units of energy divided by angular frequency; B_0 is the magnitude of the applied field, taken to be entirely along the z-axis ($\hat{B} = \langle 0,0,B_0 \rangle$); and I_z is the z-component of the nuclear spin operator. Applied to the spin state $|I, m\rangle$,

$$\hat{I}_z |I, m\rangle = m |I, m\rangle \tag{2}$$

so that the energy eigenvalues of the Zeeman Hamiltonian are

$$E_Z = -\gamma \hbar B_0 m \tag{3}$$

yielding an energy level difference of magnitude

$$|\Delta E_Z| = \gamma \hbar B_0 \tag{4}$$

between adjacent states ($|\Delta m| = 1$). As a result of Zeeman splitting we have three equally spaced energy levels (Fig. 2.1), whose difference is proportional to the strength of the applied field. The lowest energy level corresponds to $m = 1$, which is the case when the projection of the magnetic moment on the z-axis is positive, aligned with the applied field.

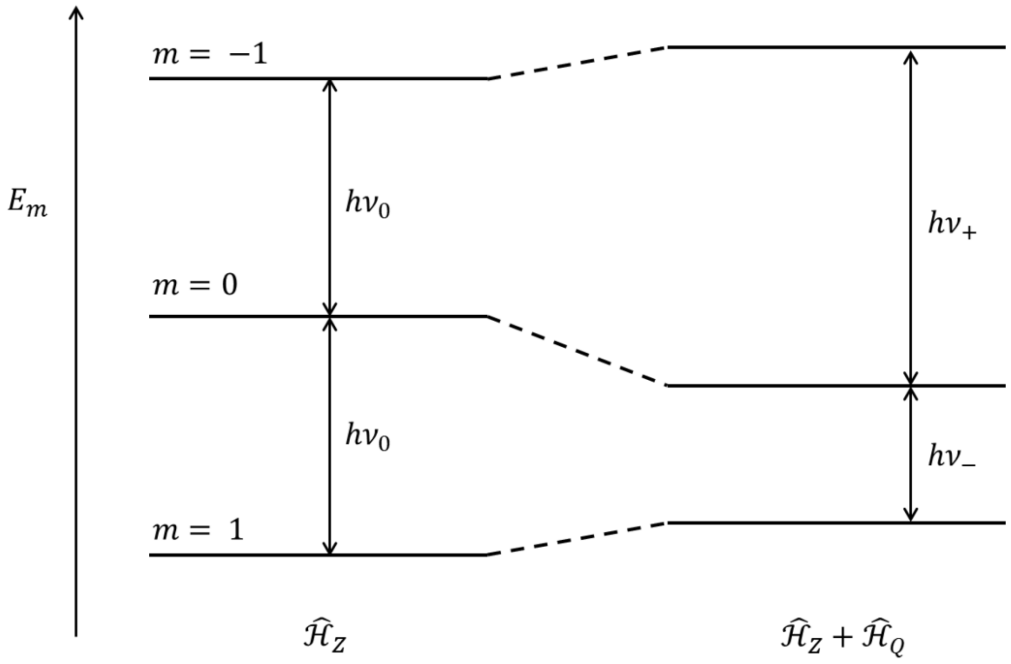

Figure 2.1 Energy levels of deuterium nucleus in spin state $|1, m\rangle$. Zeeman interaction breaks degeneracy of spin state energy levels. Quadrupolar coupling of nucleus with EFG perturbs levels so that the transition gap between adjacent states ($1 \leftrightarrow 0$ and $0 \leftrightarrow -1$) are inequivalent. ν_0 is the Larmor frequency and $\nu_\pm$ are the resonance frequencies required for transition between adjacent levels.

The energy levels are modified further through the quadrupolar coupling interaction of the deuterium nucleus with the EFG in which it is located. The nucleus has a nonspherical charge distribution and therefore an electric quadrupole moment, $\hat{Q}$, which is a measure of how far the ellipsoid nucleus deviates from having spherical symmetry. $\hat{Q}$ is a traceless second rank tensor dependent on the quantum mechanical charge distribution which is nuclear state specific property (Jackson 1999). The equilibrium position of the nucleus will be located where the electric field is zero, but there is an orientation dependent energy associated with the coupling of the quadrupole moment with a nonspherically symmetric EFG (Figure 2.2).

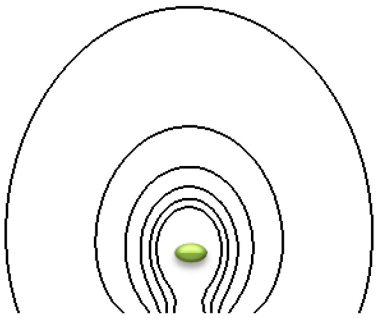

Figure 2.2 While electric field located at deuteron is zero, the EFG is not. The figure shows a hypothetical 2-D projection of equipotential shells surrounding a nucleus with a quadrupole moment, the interaction energy of the electric quadrupolar moment with the EFG corresponding to the equipotential lines shown will be different for nuclear orientations. The EFG is due to the electron distribution associated with the deuterium bond.

The EFG is an intramolecular property. Where $\mathcal{H}_Z$ is considered an external Hamiltonian, as $\hat{B}$ is under control of the experimenter, the quadrupolar Hamiltonian shares a form common to internal Hamiltonians, i.e. the dipole coupling and chemical shift Hamiltonians (Haeberlen 1976). The electron distribution about deuterium chemical bonds are the source of the directional variation in the EFG, as deuterium has a largely spherical 1s electron orbital that symmetrically contributes to the EFG at the deuteron. The EFG is a symmetrical rank 2 tensor with zero trace. A molecule fixed, principal axis system (PAS) can be chosen such that the EFG matrix is diagonalized, with $|V_{zz}| \geq |V_{xx}| \geq |V_{yy}|$, where the EFG component V_{ij} is the second (i,j) derivative of the electrostatic potential at the site of the nucleus. The EFG can therefore be described with two parameters $eq = V_{zz}$ and $\eta = \frac{V_{xx}-V_{yy}}{V_{zz}}$. For a $(C\text{-}D_2)_n$ chain, V_{zz} is along the axis of the C-D bond and the asymmetry parameter, η, is approximately zero (Caspary et al. 1969). In matrix form

$$V^{PAS} = eq\begin{pmatrix} -1/2 & 0 & 0 \\ 0 & -1/2 & 0 \\ 0 & 0 & 1 \end{pmatrix}. \tag{5}$$

Treating the quadrupolar interaction as a first order perturbation of the Zeeman effect ($\hbar\mathcal{H}_Z \gg \hbar\mathcal{H}_Q$) and with $\eta \cong 0$, the quadrupolar Hamiltonian, $\widehat{\mathcal{H}}_Q$, can be expressed as

$$\widehat{\mathcal{H}}_Q = \frac{e^2qQ}{4\hbar}\left(3\hat{I}_Z^2 - \hat{\boldsymbol{I}}^2\right)P_2(cos\theta') \tag{6}$$

where

$$P_2(cos\theta') = \frac{1}{2}(3cos^2\theta' - 1) \tag{7}$$

is a second order Legendre polynomial that rotates the system from the PAS (C-D bond axis) to lab frame (axis of the applied magnetic field), θ' is the angle between the two axes (Fig. 2.3), Q is the scalar quadrupole moment of deuterium ($2.8 \times 10^{-27}\mathrm{cm}^2$) (Caspary et al. 1969) and e is the elementary charge. Note that when the lab frame coincides with the PAS $P_2(cos\theta') = 1$ as no rotation is required. For a treatment of deuterium quadrupolar interactions with $\eta \neq 0$ see Brown (1996).

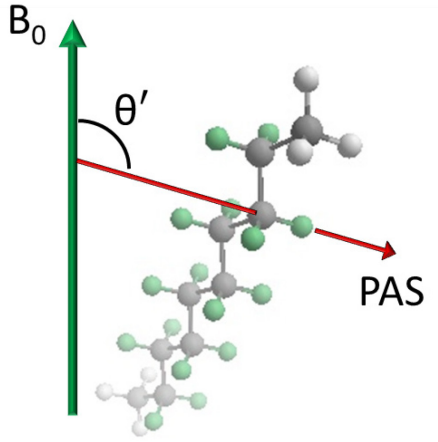

Figure 2.3 Static orientation of deuteron EFG PAS with respect to the applied magnetic field, B_0. PAS coincides with the C-D bond axis.

The total Hamiltonian for the system will then be the combination of Zeeman and quadrupolar coupling Hamiltonians, in frequency units

$$\hat{\mathcal{H}} = \hat{\mathcal{H}}_Z + \hat{\mathcal{H}}_Q = -\gamma B_0 \hat{I}_z + \frac{e^2qQ}{4\hbar}\left(3\hat{I}_z^2 - \hat{I}^2\right)P_2(cos\theta'). \tag{8}$$

So now for our three spin states $|I,m\rangle = |1,1\rangle, |1,0\rangle, |1,-1\rangle$, the energy eigenvalues, E_m, of $\hat{\mathcal{H}}$ will be given by

$$\hbar\hat{\mathcal{H}}|I,m\rangle = E_m|I,m\rangle \tag{9}$$

Applying

$$\hat{I}^2|I,m\rangle = I(I+1)|I,m\rangle \tag{10}$$

and Eqn. 2 the E_m are

$$E_{-1} = \gamma\hbar B_0 + \frac{e^2qQ}{4}P_2(cos\theta') \tag{11}$$

$$E_0 = -\frac{e^2qQ}{2}P_2(cos\theta') \tag{12}$$

$$E_1 = -\gamma\hbar B_0 + \frac{e^2qQ}{4}P_2(cos\theta') \tag{13}$$

so the quadrupolar perturbation breaks the equivalency of the two allowed transitions ($|\Delta m| = 1$) as shown in Fig. 2.1. The anti-aligned state maintains the highest energy level, and the levels are shifted depending on the angle between the PAS and lab frame, the $m = 0$ state being shifted opposite to that of $m = 1, -1$. Transition between adjacent levels can be stimulated by the absorption or emission of a photon whose frequency, ν, satisfies the condition

$$|\Delta E| = h\nu, \tag{14}$$

where h is Planck's constant. These resonance frequencies as depicted in Fig. 2.1 are

$$\nu_+ = \frac{E_{-1} - E_0}{h} = \frac{\gamma B_0}{2\pi} + \frac{3e^2qQ}{4h} P_2(cos\theta') \tag{15}$$

$$\nu_- = \frac{E_0 - E_1}{h} = \frac{\gamma B_0}{2\pi} - \frac{3e^2qQ}{4h} P_2(cos\theta') \tag{16}$$

The emission spectrum for a given crystal orientation will have two peaks centered around the Larmor frequency ($\nu_0 = \frac{\gamma B_0}{2\pi}$) with a quadrupolar splitting

$$\Delta\nu_Q \equiv \nu_+ - \nu_- = \frac{3}{2}\chi_Q \left(\frac{3cos^2\theta' - 1}{2}\right) \tag{17}$$

where χ_Q is the electrostatic quadrupolar coupling constant defined as

$$\chi_Q \equiv \frac{e^2qQ}{h} \tag{18}$$

which has been measured for solid C_6D_{14} to be approximately 168 kHz (Burnett and Muller 1971). The two transitions are essentially equally probable as the quadrupolar perturbation of the levels is small with respect to k_BT, so the intensity of the peaks will be the same. Figure 2.4 shows spectral doublets for three θ' values of interest to get a better feel for the effect rotating the crystal C-D bond axis within the external field has on spectral shape.

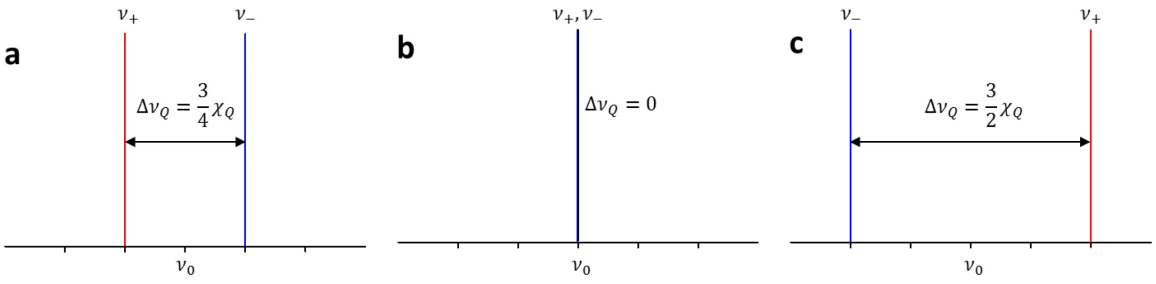

Figure 2.4 Doublets associated with the rotation of the crystal PAS by angle θ with respect to the external magnetic field. Quadrupolar splittings, $\Delta\nu_Q$, shown are for $\theta' = 90°$ (a), the $magic\ angle$ $54.7°$ (b), and $0°$ (c). Doublets are centered on υ_0, the Larmor frequency. At the magic angle the quadrupolar effect vanishes as transition gaps are equivalent. As a function of θ', υ_+ is shifted down from υ_0 at 90°, unperturbed at 54.7°, and greater than υ_0 at 0°.

The splitting factor $P_2(cos\theta')$ varies from $1 \rightarrow -½$ for $\theta' = 0° \rightarrow 90°$. At $\theta' = 54.7°$, the magic angle, $P_2(cos\theta')$ goes to zero so that only a single peak, representative of both transitions ($\Delta\nu_Q = 0$), is observed at the location of the Larmor frequency. This fact is exploited in MAS NMR where spinning a polycrystalline sample at the magic angle relative to the magnetic field partially averages the quadrupolar interaction increasing resolution of spectra. For $\theta' < 54.7°$, $\upsilon_+ > \upsilon_-$ and for $\theta' > 54.7°$ the relationship is reversed, which corresponds to the gap for the $m = 1 \leftrightarrow 0$ transition becoming larger than that of the $m = 0 \leftrightarrow -1$. The magnitude of the quadrupolar splitting at $\theta = 0°$ is twice as wide as for the $90°$ orientation, $\left|\Delta\nu_Q(0°)\right| = 2\left|\Delta\nu_Q(90°)\right| = \frac{3}{2}\chi_Q$. The quadrupolar perturbation is the greatest when the PAS axis (V_{zz}) is aligned with the external magnetic field. The deuteron magnetic resonance theory developed so far is applicable to homogeneously aligned system of deuterium bond vectors in the absence of molecular motion; we now turn our attention to NMR of selectively labeled lipids in randomly oriented liquid crystalline membrane structures.

2.3 ^{2}H NMR of Labeled Membranes

Membranes can be macroscopically aligned with their bilayer normals parallel, either through physical preparation on a glass coverslip (Katsaras 1997) or magnetically in the case of bicelles (Marcotte and Auger 2005), so that their orientation is fixed with respect to the applied field. The bilayer normal is the axis of symmetry for motion of lipid hydrocarbon chains in the liquid crystalline phase. Anisotropic motion occurring on the time scale $\lesssim \chi_Q^{-1}$ will result in the incomplete averaging of the static quadrupolar tensor, and the splitting observed for the same static crystal orientation will be reduced. For an aligned sample with the bilayer normal parallel to the magnetic field, the residual quadrupolar splitting is

$$\Delta\nu_r = \frac{3}{2}\chi_Q S_{CD} \tag{19}$$

with carbon deuterium order parameter,

$$S_{CD} = \frac{1}{2}\langle 3cos^2\beta - 1\rangle \tag{20}$$

describing the angular fluctuations of the C-D bond with respect to the bilayer normal as it rapidly rotates about the long molecular axis of the lipid and that axis wobbles about the bilayer normal director. The angular brackets indicate a time average and β is the time dependent angle measured between the bilayer normal and the C-D bond vector. S_{CD} could be positive or

negative, but only its magnitude is measurable. S_{CD} can be calculated through closure as the product of two independent order parameters, one describing C-D bond fluctuations around the molecular axis and the other corresponding to fluctuations of the molecular axis about the bilayer normal (Vermeer et al. 2007, e.g. Brzustowicz et al. 2002). Structural and dynamical information is contained in its value. For completely isotropic motion $\Delta\nu_r$ will go to zero. Alternatively, for a perfectly ordered all-trans chain rapidly rotating about the bilayer normal $|S_{CD}| = 0.5$.

For nonaligned samples, a powder pattern spectrum will be produced with a continuum of quadrupolar splittings now being described by

$$\Delta\nu_r = \frac{3}{2}\chi_Q S_{CD}\left(\frac{3cos^2\theta-1}{2}\right). \quad (21)$$

The last term is the second order Legendre polynomial as a function of $\cos\theta$, and accounts for the random distribution of bilayer orientations, θ being the angle between a particular bilayer normal and external field (Fig. 2.5). A time average is not taken for this term as the orientation of the bilayer with respect to the magnetic field is static on the time scale of the experiment. Taken together, the term $S_{CD}P_2(\cos\theta)$ accounts for the sequential rotations required to transform from the principal quadrupole interaction axis to the lab frame.

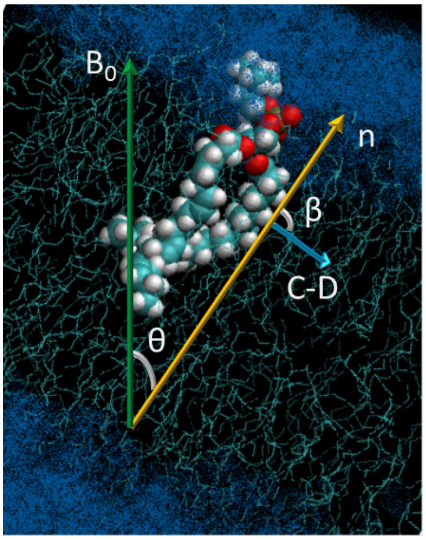

Figure 2.5 Angles relating C-D bond axis of deuterated position on phospholipid chain to applied magnetic field, B_0, within membrane bilayer. The bilayer normal is represented by $\hat{n}$, and the angle β factors in the calculation of S_{CD}. For nonaligned samples the probability distribution of θ scales as $\sin\theta$.

All bilayer orientations contribute to the spectra, but in spherical coordinates orientations perpendicular to the magnetic field are more numerous and are represented with greater intensity. The splitting contribution from perpendicular orientations will have half the width of parallel orientations,

$$\frac{\langle \Delta \nu_Q^{\pm} \rangle_{\parallel}}{\langle \Delta \nu_Q^{\pm} \rangle_{\perp}} = 2\,. \tag{22}$$

A Pake doublet is the characteristic spectral shape of an axially symmetric powder pattern produced for spin $I = 1$ systems (Pake 1948). Its line shape can be simulated in the following manner.

Assuming a spherical symmetry to the distribution of bilayer normal vectors (all orientations equally probable), the fraction of bilayers having an orientation between θ and $\theta + d\theta$, dN/N, would be equal to the fraction of the total surface of a sphere bound by those angles

$$\frac{dN}{N} = \frac{2\pi r^2 \sin\theta d\theta}{4\pi r^2}\,. \tag{23}$$

The probability distribution of the orientation can be identified as

$$p(\theta) = \frac{1}{2}\sin\theta, \tag{24}$$

such that

$$\int_0^{\pi} p(\theta) d\theta = 1. \tag{25}$$

Moving away from the pole ($\theta = 0°$), contributions to spectral line shape increase such that splittings corresponding to bilayers perpendicular to the external field will have the greatest intensity, as that orientation angle is most probable (Fig 2.6 a, b). Splittings are dependent on the quadrupolar component of $\nu_{\pm}$; we can introduce a dimensionless reduced resonance frequency proportional to this component:

$$\nu_Q \propto \left(\frac{3\cos^2\theta - 1}{2}\right) \equiv \xi \tag{26}$$

where

$$-\frac{1}{2} \leq \xi \leq 1 \tag{27}$$

and the probability for the frequency, $p(\xi)$, can be related to $p(\theta)$ by

$$p(\theta)d\theta = p(\xi)d\xi \tag{28}$$

and arranged as

$$p(\xi) = \frac{1}{2}\sin\theta\frac{d\theta}{d\xi} = -\frac{1}{2}\frac{d\cos\theta}{d\xi} \tag{29}$$

where, from Eqn. 26,

$$\cos\theta = \sqrt{\frac{2\xi+1}{3}}\,. \tag{30}$$

Keeping in mind that we have both ν_+ and ν_- contributions to the spectrum the probability for the reduced frequency can be solved as

$$p(\xi_\pm) \propto (\pm 2\xi + 1)^{-1/2}\,. \tag{31}$$

The spectral intensity scale is arbitrary, but will be proportional to the sum of these probabilities,

$$I \propto p(\xi_+) + p(\xi_-)\,. \tag{32}$$

Resonance lines are broadened by a number of mechanisms. Uncertainty in energy levels leads to line broadening of spectra, i.e. the "natural" linewidth; other effects dominate in practice. Figure 2.6 shows a simulated powder pattern spectral line shape for motionally and orientationally equivalent deuterated positions, based on Eqn. 32, after convolution with a Gaussian line broadening function (Dietrich and Trahms 1987). A choice can be made whether to apply Gaussian or Lorentzian line broadening, or a weighted mixture of the two. Gaussian has been found to be appropriate at low temperatures where line broadening is primarily attributed to dipolar coupling; Lorentzian broadening tends to provide better fits in the L_α state where these interactions are averaged more completely (i.e. motional narrowing).

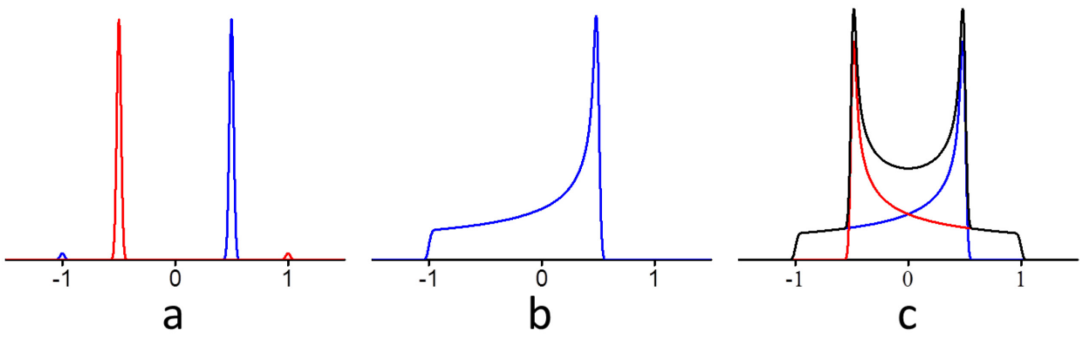

Figure 2.6 Simulation of powder pattern spectrum with Gaussian line broadening. Scaled relative doublet intensities of $\theta = 0°, 90°$ bilayer orientation contributions to overall Pake doublet line shape (a). Line shape representing one of two possible transitions with contributions from all bilayer orientations (b). Simulation of powder pattern line shape as $p(\xi_+) + p(\xi_-)$ (c). Separation of peaks will be proportional to S_{CD} of the deuterated position.

Figure 2.6 demonstrates how for a deuterated position characterized by S_{CD} we'll get a spectrum with a continuum of splittings between $\frac{3}{2}\chi_Q S_{CD}$ and $-\frac{3}{4}\chi_Q S_{CD}$; the negative splitting meaning that the energy gap between the m = 1 and 0 state becomes less than the gap between the m = 0 and -1. Figure 2.6c shows how the spectrum is a composite of emission from the two transitions. The predominant peaks are attributed to the 90° orientation and their splitting is half that of the 0° orientation which corresponds to the less intense outside edges of the spectrum. For samples with molecules deuterated at multiple motionally inequivalent sites, their spectrum will have multiple peaks resulting from a superposition of powder pattern spectra of different widths.

At this point, we have fleshed out the physical basis for the solid state ^{2}H NMR spectrum of a labeled membrane system. In the next section, we explain how the NMR signal is detected employing a semi-classical description of spin ensemble dynamics and provide examples and analysis of spectra associated with probes of model membranes.

2.4 The Solid State ^{2}H NMR Experiment

In the previous section, we established, in the absence of a magnetic field, the three ^{2}H nuclear spin states are degenerate and, therefore, equally probable. This equivalence is broken by the application of a static field (B_0) and the lowest energy state becomes the most occupied following a Boltzmann distribution. The effect is small, but the slight imbalance of the spin state population distribution is responsible for producing a macroscopic net magnetization (M); with roughly only 5 in 1,000,000 nuclear spins contributing to M of a spin ensemble placed in a 7T magnetic field at room temperature. NMR experiments can be thought of, semi-classically, as the detection of the dynamic reorientation of the ensemble's macroscopic magnetization in response to a perturbation, in the form of electromagnetic radiation pulses, away from an equilibrium alignment with a static field.

2.4.1 Manipulation of Spin System by Alternating Magnetic Pulse

The deuterium nucleus has a dipole magnetic moment associated with its nuclear spin angular momentum,

$$\boldsymbol{\mu} = \gamma \boldsymbol{I} \tag{33}$$

which when placed in a magnetic field will experience a torque,

$$\boldsymbol{\tau} = \boldsymbol{\mu} \times \boldsymbol{B} \tag{34}$$

causing it to precess about the axis of the field (Fig. 2.7). The energy of this interaction (Eqn. 3) is orientation dependent and quantized such that only certain angles of nuclear precession are permitted. The equation of motion for the magnetic moment

$$\boldsymbol{\tau} = \frac{d\boldsymbol{I}}{dt} = \gamma \boldsymbol{I} \times \boldsymbol{B} \tag{35}$$

can be solved by employing a rotating frame of reference to show that the frequency of precession happens to be identical to the Larmor frequency (Slichter 1990).

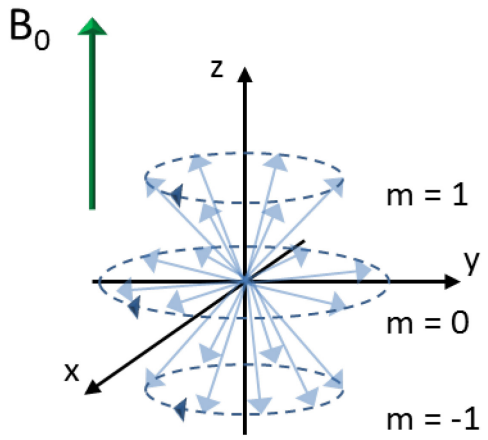

Figure 2.7 Quantized angular precession about axis of applied magnetic field. At thermal equilibrium, a slight preponderance of spin nuclei in the $m = 1$ state creates a macroscopic net magnetization in the z direction. For noncoherent ensemble precession there is no transverse component of the net magnetization in the x-y plane. Precession is clockwise about z axis and the cone angle of $m = 1, -1$ spin precession is 45°.

The net magnetization will coincide with the direction of the applied field for an equilibrated sample, z in the lab frame (Fig. 2.7). If nuclei are stimulated into transitioning to a nonaligned higher energy spin state, M will diminish along z. Experimentally this is achieved by applying a short EM pulse at the frequency of precession, whose oscillating magnetic field rotates M away from the z axis; the quantum equivalent of bombarding the system with photons of energy that satisfy the condition for transition.

An inductor coil, within which the sample is situated, is responsible for producing this oscillating pulse field that will be directed along its long axis. A linearly polarized oscillating field can be formed by the vector sum of a pair of circularly polarized rotating fields (Fig. 2.8).

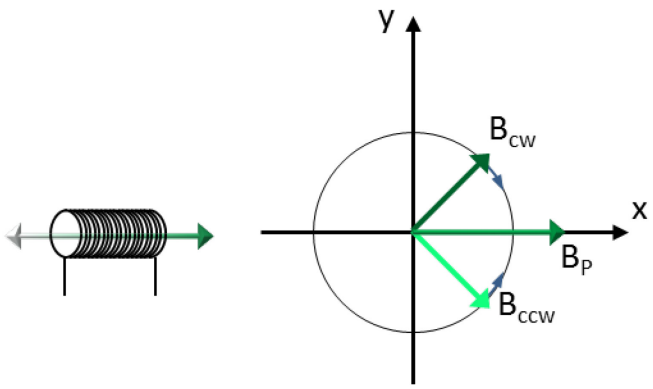

Figure 2.8 The oscillating magnetic field created along the sample coil axis taken to be the x axis in the lab frame. This field can be thought of as the sum of two field vectors rotating in phase with the same angular frequency, clockwise and counterclockwise about the z axis (viewed from above the coil).

In a reference frame rotating at the Larmor frequency following the precession of the nuclei spin, the clockwise component of the pulse field will appear frozen while the counterclockwise component will be rotating at twice the Larmor frequency. Only the component which rotates in sync with the precession of the spin will have a non-zero average effect. This static field will operate on M, causing it to rotate by

$$\vartheta = \gamma B_1 t_1 \tag{36}$$

away from z, where we are renaming the clockwise component B_1 and t_1 is the length of time the pulse is applied. Figure 2.9 shows a 90° deflection of M from z to the x-y plane in the lab and rotating frame.

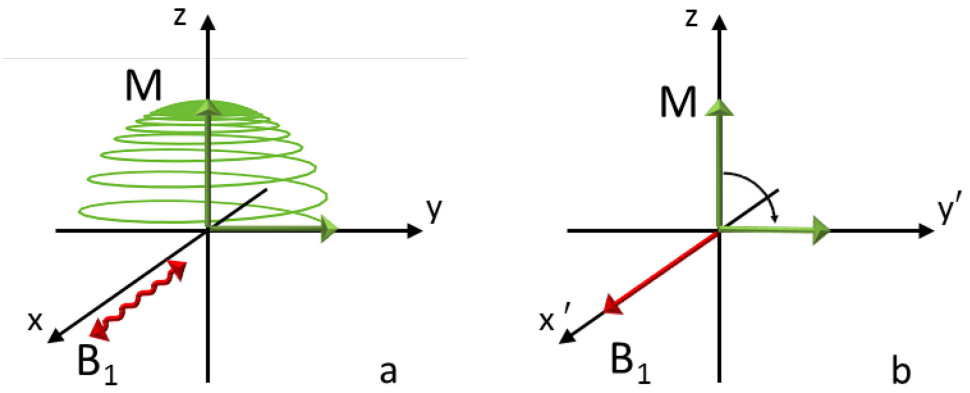

Figure 2.9 Rotation of macroscopic net magnetization vector (M) by a $90°$ pulse. In the lab frame (a), as the pulse field oscillates along the x-axis, M completes many revolutions about z before being brought completely to the x-y plane. In the rotating frame the pulse magnetic field appears static and M is rotated away from the z to y' axis. The precession of M in the x-y plane is the source of the NMR signal.

2.4.2 Signal Detection

By rotating M to the x-y plane, a net transverse magnetization is generated, which precesses about the B_0 in response to the torque of the applied and pulsed fields on the individual nuclear dipoles. After the pulse is terminated the spin nuclei precess coherently in phase. This signal decays as the net magnetization returns to the longitudinal direction and coherence is lost. This initial phase coherence is lost as there is a distribution of nuclear precession rates present. This results in the decay of the transverse signal, characterized by the transverse relaxation time T_2. Also contributing to this decay is the realignment of M with z in the absence of additional stimulus, a process known as longitudinal relaxation with associated decay time T_1. This oscillatory behavior of M induces a signal in the receiver coil, the same coil in which the sample is located, called a free induction decay (Fig. 2.10). The coil, part of a LC circuit that makes up the NMR probe (Barnaal and Lowe 1966), is tuned to the resonance frequency where system stimulation and detection of precession is most efficient. This is crucial as the FID signal is weak.

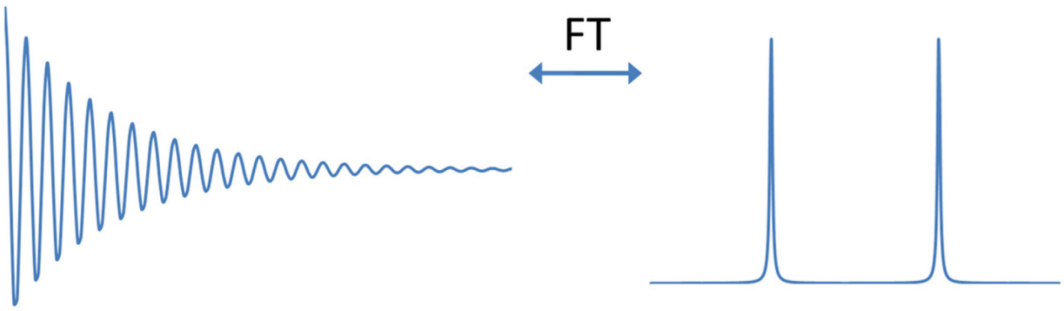

Figure 2.10 Cartoon of FID response to RF pulse. FID results from the free precession of M following a RF pulse, and diminishes in time due to relaxation processes. Here the FID line shape is portrayed as a single frequency cosine function with amplitude that decays exponentially in time. Actual experimental FID will be the result of the sum of signals from many satellites emitting different frequencies producing beat pattern with an exponential envelope. Fourier transform of the FID yields the frequency domain spectrum.

The free induction decay (FID) signal has the form of a sinusoidal function with an exponential decay envelope defined by the rate constant $1/T_2$, the transverse relaxation time being shorter than the longitudinal (a large collection processes contribute to transverse relaxation, or dephasing, whereas longitudinal relaxation requires nuclear transitions to lower energy states). The FID contains real and imaginary components corresponding to the x' and y' rotating frame axes, respectively, and has the form of a decaying spiral in complex space with time along the z axis. The phase of the pulse is adjusted so that the real component has a cosine form. The FID reaches zero when the precession of spins dephases, which occurs prior to relaxation of the spin lattice back into thermal equilibrium following a pulse induced elevation in spin system temperature. Fourier transformation (FT) is performed on the FID to uncover what frequencies of waves are contained in the signal. The result is the frequency domain NMR spectrum.

A wide range of frequencies will be present in any solid state spectrum. Simultaneous stimulation of the entire spectrum is achieved with a square wave pulse (e.g. Fig. 2.11). The amplitude of the FID induced depends on the pulse width. The maximum response is achieved by a 90° square pulse (Eqn. 36) which rotates M completely into the x-y plane. The pulse width required to generate a 90° pulse is inversely proportional to the strength of the field produced by the coil. In practice, the magnitude of B_1 is fixed and the angle of the rotation is controlled by varying the length of time B_1 is applied (the pulse width).

The RF pulse is a square wave in time and sinc function of frequency, it is therefore necessary to have a narrow pulse width so that the pulse intensity of the frequency range corresponding to the central 100 kHz is nearly constant. A square wave, in time, is a convolution of step and cosine functions. The line shape of the pulse in the frequency domain can be calculated as a sinc function via Fourier transform of the square wave. The pulse maximum is centered on the Larmor frequency, and the pulse width determines the bandwidth of frequencies excited. A 90° pulse width of less than 5 μs is required for homogenous excitation. For larger pulse widths a correction factor can be applied to account for intensity drop-off (Spiess 1983). Pulse width can be reduced for spectrometers capable of delivering higher power to the coil. With increasing bandwidth comes a decrease in signal to noise so there is a balance to be struck.

2.4.3 Echo Sequence

Rapid decay in the free induction signal occurs as a result of relaxation through spin-lattice interactions and destructive interference of a plurality of spectral components. After RF pulse there is a receiver dead time (10's μs) associated primarily with the magneto-acoustic ringing of the coil and body of the probe which will obscure the beginning of the FID signal, where for broad solid state spectra much information is contained. The oscillating M of the ensemble in the transverse plane produces a signal on the order of mW's as detected by the sample coil. To avoid bleed through of the high power (~100W) pulse into the acquired signal, a pulse sequence is utilized (Fig. 2.11), which refocuses the transverse magnetization after a delay creating an echo. The $90°_x$ - τ - $90°_y$ "Solid Echo" pulse sequence shifts the response signal away from the last pulse of the sequence (Fig. 2.11) and beyond the dead time of the receiver, through refocusing of static dipolar and quadrupolar couplings, so that the FID maximum can be detected, 2τ after the sequence is initiated and no distortion occurs during FT (Powles and Strange 1963). The two pulses are 90° out of phase out, hence the x and y subscripts. A quantum mechanical treatment of pulse interaction with spin system is given by (Vega and Luz 1986).

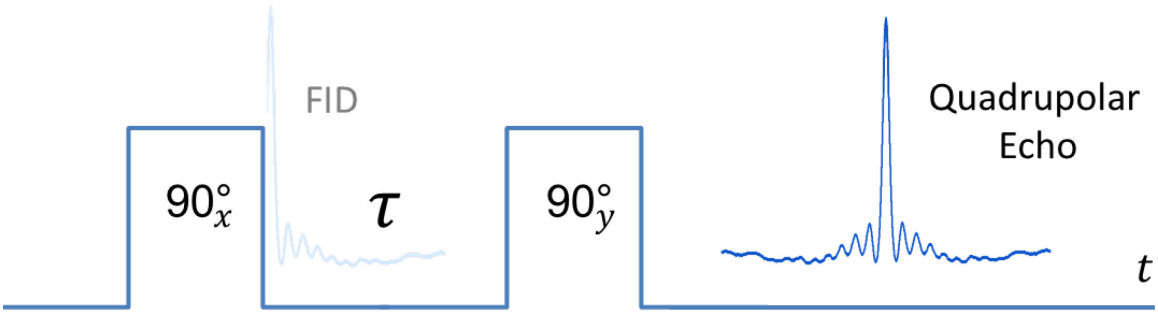

Figure 2.11 The quad echo sequence is used to shift the system response away from the RF pulse in time for probes which use the same induction coil for both excitation and detection of FID. For a short period of time after a high power pulse, ringing occurs in the coil which distorts any acquired signal. This pulse sequence delays the start of acquisition beyond the dead time of the coil so pulse bleed through does not occur. The two 90° pulses are 90° out of phase with each other in the rotating frame. The duration of the pulse is short compared to decay time of the coherent signal (not portrayed to scale). The maximum of the echo is located a time τ after the second pulse and is the point where the FT is performed. The echo is slightly attenuated relative to the FID.

The first demonstration of a spin echo was by Hahn (1950). With a 90°_x - τ - 180°_x pulse sequence he was able refocus spin procession in a liquid system of coupled spin ½ nuclei where inhomogeneties in magnetic field and chemical shift anisotropy primarily contribute to spin dephasing. This approach was modified and later applied to EFG coupled spin 1 system (Solomon 1958), where, in solids, spin dephasing is caused by the distribution of EFG and dipolar interactions and can be refocused by a 90°_x - τ - 90°_y pulse sequence. This solid echo sequence has been shown to faithfully reproduce the FID line shape for $t > 2\tau$ both in theory (Boden and Levine 1978) and experimentally (Powles and Strange 1963, Davis et al. 1976), with only a slight diminution in amplitude relative to the FID corresponding to a single 90° pulse. The degree to which the echo is reduced is proportional to the time τ between pulses.

The FID is built up over many acquisitions and phase cycling of the pulses is applied to eliminate some of the artifacts associated with defects of the circuitry. The signal is mixed and amplified through quadrature to produce real cosine and imaginary sine components. Conversion from time to the frequency domain is achieved via FT applied at the echo maximum. In practice, FT of the large data set amassed by thousands of acquisitions is handled by a computer algorithm employing fast Fourier transform. The FID can be processed prior to FT to improve signal to noise resolution. The resulting spectral peak shape depends on the extent of signal processing

and is often Gaussian as opposed to the Lorentzian line shape anticipated for the FT of an exponential decay curve. In the following section, examples and analysis of spectra from deuterated lipids in model membranes will be discussed.

2.5 Analysis of ^{2}H NMR Model Membrane Spectra

Rather than having to build up a picture from multiple experiments involving lipids selectively deuterated at individual sites, the dynamics and orientation of the entire acyl chain can be investigated through use of lipids with perdeuterated acyl chains. The two approaches have been shown to produce equivalent results, but much less work is involved in the latter. Each deuterated position contributes a powder pattern spectrum (for nonoriented samples) possessing a unique splitting set by the segment's order parameter. These quadrupolar splittings stem from a dynamic equilibrium between various chain conformational states (Seelig and Seelig 1980). Figure 2.12 presents a typical powder pattern spectrum of a perdeuterated palmitoyl chain (isotopic substitution of ^{2}H for ^{1}H at 31 sites) belonging to the lipid 1-palmitoyl-2-oleoyl-sn-glycero-3-phosphocholine (POPC-d_{31}).

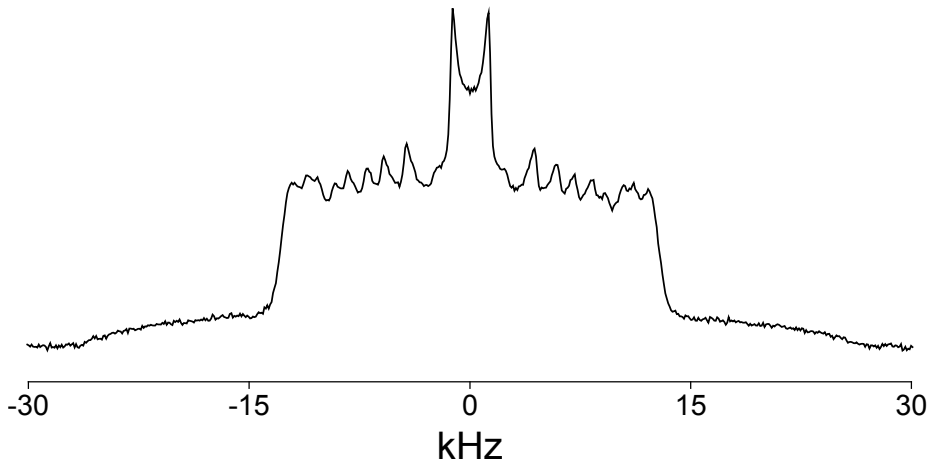

Figure 2.12 Experimental accumulated Fourier transform spectrum of POPC-d_{31} at 30 °C in the liquid crystalline state. Spectrum the result of relaxation of nonequilibrium ensemble prepared by quadrupolar echo pulse sequence. Resonance peaks correspond to methyl and methylene deuterons of bilayers oriented at 90° with respect to the external magnetic field.

The Larmor frequency is dependent on the magnitude of the applied field, while quadrupolar splittings, being an intramolecular property, are consistent regardless of the magnet being used.

It is for this reason that spectral frequencies are reported relative to a carrier frequency adjusted to the Larmor frequency.

Phospholipid chains in the liquid crystalline phase (L_α) execute rapid axially symmetric reorientations. Incomplete motional averaging within the bilayer produces reduced quadrupolar splittings. For equivalent average orientations splittings will be narrower for positions that undergo greater fluctuations. The terminal methyl of the acyl chain acts as a rigid rotor whereas chain methylenes rotate between two stable molecular conformations: trans and gauche. The quadrupole splitting is therefore decreased more for the freely rotating methyl group, which is represented by the two intense central peaks whose increased area corresponds to three deuterons where the methylenes only have two. The powder pattern spectrum contains contributions from all bilayer orientations, the weak outer shoulders belong to the $\theta = 0°$ orientation. The spectrum presented here is characteristic of a homogeneous sample; as we will see in Chapter 3, samples containing multiple distinct motional regimes may have additional spectral features present (Veatch et al. 2004).

A spectrum representative of a single membrane normal orientation can be extracted from the powder pattern through a numerical inversion process known as dePaking (McCabe and Wassall 1995, Bloom et al. 1981). The resulting dePaked spectrum, analogous to that of an aligned sample spectrum with bilayer normal parallel to B_0 ($\theta = 0°$), has increased spectral resolution which makes analysis requiring peak picking more straightforward (Fig. 2.13).

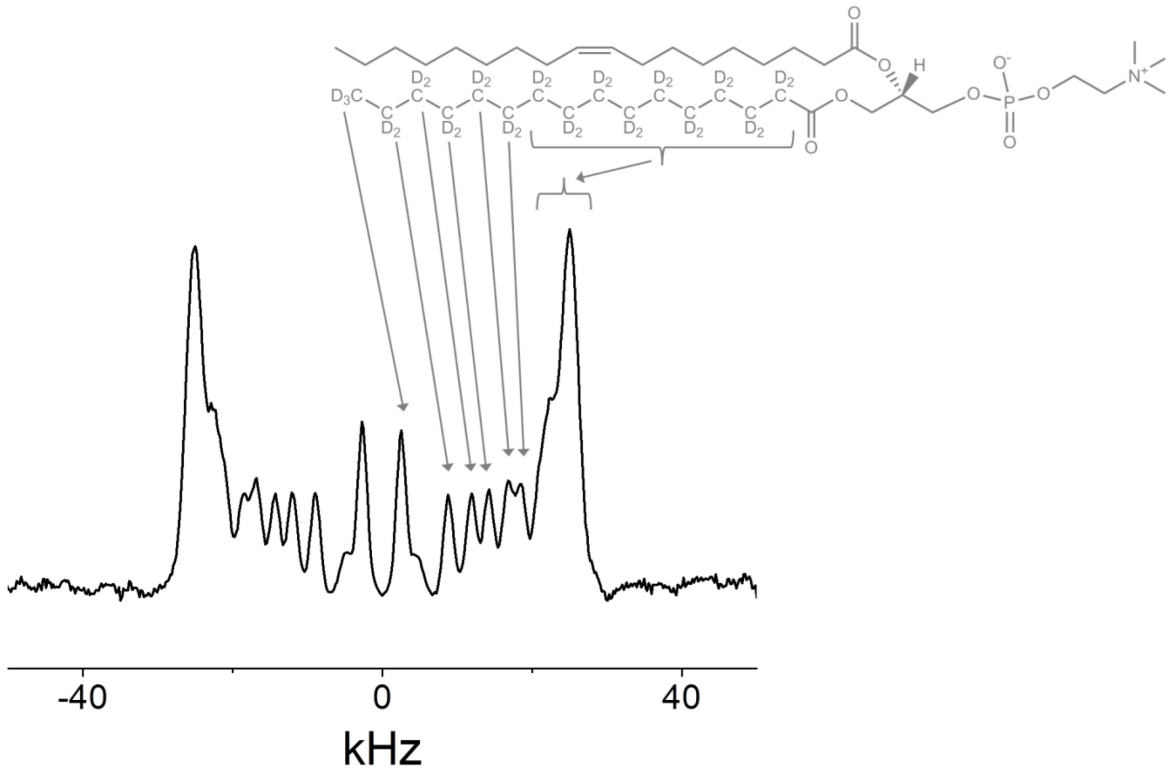

Figure 2.13 DePaked spectrum of POPC-d_{31} at 30°C. DePaked spectra are produced by a numerical inversion that extracts the $\theta = 0°$ bilayer orientation from the FT spectrum. The increase in resolution facilitates the assignment of peak frequencies to carbon positions, as illustrated for the perdeuterated saturated chain of POPC.

The splittings of dePaked spectra are twice as wide as those of powder pattern spectra, as they belong to bilayers with θ = 0° and the dominant peaks of the powder pattern correspond to the 90° orientation. Peaks are representative of motionally and orientationally equivalent deuterated positions in the sample. Carbon deuterium positions are assigned quadrupolar splitting values on the assumption that order and concomitant splittings monotomically increase moving up the chain towards the carbonyl. The large composite outer peak is created by an overlap of multiple positions experiencing similar order at the top of the chain. The terminal methyl is represented by the central pair of peaks.

The spectral line shape is temperature dependent. Decreasing temperature slows motion within the bilayer resulting in less motional averaging and an increase in spectral width. As the temperature drops, T_2 also decreases and individual peaks spread. These changes are gradual, but there comes a point where a sudden dramatic transformation of line shape is observed

corresponding to a phase transition in which acyl chains lose a degree of motional freedom as rapid rotational isomerization about bonds is restricted and segments take on predominately all trans configurations.

Figure 2.14 shows an example of a gel phase (L_β) spectrum for POPC-d_{31} at -15°C. Gel spectra appear broader and have fewer features than L_α spectra. Methylene peaks run together in gel spectra due to slow rotational diffusion to the point where they are no longer discernible. Only the terminal methyl peaks remain apparent.

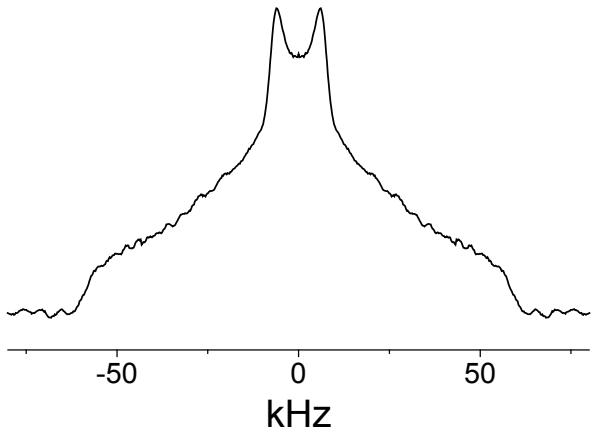

Figure 2.14 Gel spectrum of POPC-d_{31} at -15 °C. Below the L_β-L_α phase transition, linewidth of resonance peaks increases from 100's of Hz in the L_α phase to linewidth on the order of kHz and individual methylene peaks can no longer be distinguished. The spectrum is broad and almost featureless aside from the prominent terminal methyl peaks. The increased width of gel spectra corresponds to the restriction of chain isomerization and reorientation.

There is a static limit to the width of gel spectrum of 126 kHz. While $\eta = 0$ for the C-D bond, $\bar{\eta}$ is not necessarily zero for all types of motion. In the gel phase lipid molecular axes may not line up with the bilayer normal, but instead can be tilted and motion is no longer axially symmetric. The lack of spectral features prevents analysis of gel spectra beyond calculation of the first moment (M_1), where

$$M_1 = \frac{\int_{-\infty}^{\infty} |\omega| f(\omega) d\omega}{\int_{-\infty}^{\infty} f(\omega) d\omega}, \tag{37}$$

with $f(\omega)$ being the spectral line shape as a function of angular frequency and all angular frequencies are measured from the Larmor frequency at the spectrum center. Calculation of M_1 yields information about phase behavior and provides a measure of average order within the

hydrophobic region of the bilayer. For L_α spectra, M_1 is related to the average carbon-deuterium order parameter of the entire chain ($\overline{S_{CD}}$) through

$$M_1 = \frac{\pi}{\sqrt{3}} \frac{e^2 qQ}{h} \overline{S_{CD}} \,. \tag{38}$$

Decreased orientational mobility of the C-D bond results in a broader spectrum which is quantified by the order parameter. Figure 2.15 is of a M_1 vs. temperature plot for POPC-d_{31}. There is a steady increase in M_1 for decreasing temperature reflecting the growing spectral width. The discontinuity observed between -6 and -5°C identifies the chain melting temperature (T_m) and the transition between L_β and L_α phases (Morrow et al. 1992). As measured by DSC, the T_m of protiated lipid tends to be ~3.5°C higher than lipids with perdeuterated acyl chains (e.g. Davis 1979). This transition can be broadened and suppressed by addition of other molecules to membrane; the observation of such effects indicate the interaction between labeled lipid and the additive and the modification of membrane properties.

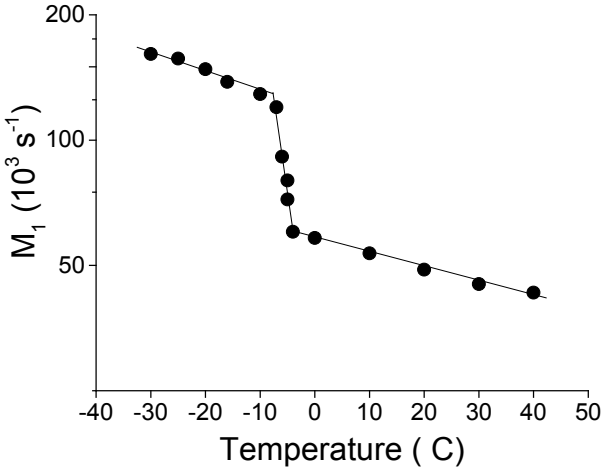

Figure 2.15 First moment (M_1) temperature plot for POPC perdeuterated on the sn-1 chain. M_1 of the spectrum is an experimental observable that is related to the average order parameter of the deuterated acyl chain segments. Order decreases as a function of increasing temperature. An abrupt drop in M_1 signifies a phase transition, in this example POPC transitions from gel phase for temperatures below -7℃ to the liquid crystalline phase above -4℃. Three lowest temperature data points are taken from McCabe (2000).

Increasing temperature leads to a rise in the number of gauche conformations present in acyl chains, which causes a greater degree of angular motion relative to the bilayer normal along with increased disorder in the chain below. An order parameter profile, as shown in Figure 2.16,

captures this variation in order along the chain; displaying C-D bond order parameters as a function of acyl chain carbon position.

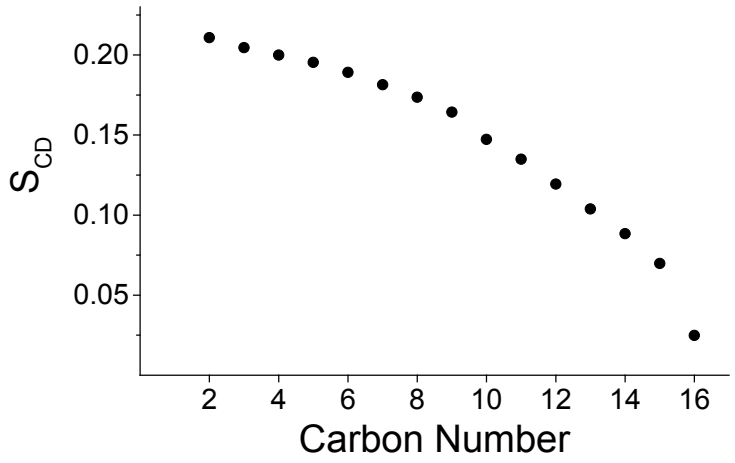

Figure 2.16 Smoothed order parameter profile for the deuterated sn-1 chain of POPC at 30°C. The terminal methyl, carbon number 16, is the most disordered of the acyl chain segments (an S_{CD} of zero would reflect completely isotropic motion). Order increases moving from the center of the bilayer towards the lipid head group. This variation in order reflects the flexibility gradient in the bilayer.

The order parameter profile displayed here was calculated from the dePaked spectrum in Fig. 2.13. The dePaking process extracts a single bilayer orientation, $\theta = 0°$, from the powder pattern spectrum. This makes it so Eqn. 19 can be directly applied in analysis of the spectrum and carbon-deuterium bond order parameters can effectively be read off the quadrupolar splittings. The carbon number index begins with the nondeuterated carbonyl at 1 and ends with the terminal methyl at 16. Lipid head groups are mostly confined to the aqueous interface of the membrane and methylene segments closest to the carbonyl will experience more restriction to motion than segments further down the flexible chain in the fluid interior. With less motional averaging, the quadrupolar splitting for deuterons in the upper portion of the chain will be the greatest and will decrease rapidly approaching the terminal methyl in the bilayer center. Methylene segments 2-8 experience the greatest restriction to motion and are attributed to the plateau region of the chain, named so for having near-constant order. The spectral peaks from this portion of the chain overlap in frequency making differentiation impossible. The order corresponding to these frequencies is calculated by dividing the composite peak evenly by area and assigning carbon numbers assuming a monotonic increase in order resulting in a smoothed

order profile for the upper chain (Lafleur et al. 1989). As temperature decreases, more methylenes will contribute to the plateau.

As we will see in Chapter 3, the spectral width for lipids with a perdeuterated *sn*-1 chain and polyunsaturated *sn*-2 chain will be considerably reduced compared to that of saturated or monounsaturated species due to the increase in disorder caused by the rapidly isomerizing PUFA chain. Order parameter profiles of PUFA-containing lipids will have a steeper slope, accordingly, and less methylenes will contribute to the plateau region (Huber et al. 2002).

2.6 Concluding Remarks

The utility of solid state ^{2}H NMR is not limited to the order parameter and phase analysis presented here. Lipid dynamic relaxation rates, area per lipid, hydrophobic thickness, and elasticity or rigidty of the membrane can also be obtained from spectral data (Brown et al. 2008, Petrache et al. 2000). In addition to these properties that can be directly observed, ^{2}H NMR data is often used to inform results from complementary biophysical methods such as X-ray diffraction (e.g. Brzustowicz et al. 2002), MD simulation (e.g. Soni et al. 2009), and neutron scattering (e.g. Marquardt et al. 2013) experiments.

In Chapter 3, ^{2}H NMR will be applied to model membrane systems to uncover the ordering and disordering effects of cholesterol and polyunsaturated fatty acids, respectively, and to detect domain formation within the membrane.

Acknowledgement

I would like to thank Xiaoling Leng for production and use of the MD simulation snapshot contained in Figure 2.5.

2.6 References

Abragam A (1983) Principles of nuclear magnetism. Clarendon Press, Oxford

Auger M (2000) Biological membrane structure by solid-state NMR. Curr Issues Mol Biol 2:119-124

Barnaal DE, LoweIJ (1966) Correction of free induction decay distortions due to finite bandwidths of pickup coil and receiver. Rev Sci Instrum 37:428-430

Bloom M, Davis JH, MacKay AL (1981) Direct determination of the oriented sample NMR spectrum from the powder spectrum for systems with local axial symmetry. Chem Phys Lett 80:198-202

Bloom M, Morrison C, Sternin E, Thewalt JL (1992) Spin echoes and the dynamic properties of membranes, in Bagguley DMS (ed) Pulsed magnetic resonance : NMR, ESR, and Optics. Clarendon Press, Oxford

Boden N, Levine YK (1978) Calculation of NMR spin echo responses in solids. J Mag Res 30:327-342

Brown MF (1996) Membrane structure and dynamics studied with NMR spectroscopy, In: Merz KM, Roux B (ed) Biological membranes: a molecular perspective from computation and experiment. Birkhäuser, Boston

Brown MF, Lope-Piedrafita S, Martinez GV, Petrache HI (2008) Solid-state deuterium NMR spectroscopy of membranes, In: Webb GA (ed) Modern magnetic resonance. Springer, New York

Brzustowicz MR, Cherezov V, Caffrey M, Stillwell W, Wassall SR (2002) Molecular organization of cholesterol in polyunsaturated membranes: microdomain formation. Biophys J 82:285-298

Burnett LJ, Muller BH (1971) Deuteron quadrupole coupling constants in three solid deuterated paraffin hydrocarbons: C_2D_6, C_4D_{10}, C_6D_{14}. J Chem Phys 55:5829-5831

Caspary WJ, Millett F, Reichbach M, Dailey BJ (1969) NMR determination of deuterium quadrupole coupling constants in nematic solutions. J Chem Phys 51:623-627

Davis JH, Jeffrey KR, Bloom M, Valic MI, Higgs (1976) Quadrupolar echo deuteron magnetic resonance spectroscopy in ordered hydrocarbon chains. Chem Phys Lett 42:390-394

Davis JH (1979) Deuterium magnetic resonance study of the gel and liquid crystalline phases of dipalmitoyl phosphatidylcholine. Biophys J 27:339-358

Davis JH (1983) The description of lipid conformation, order and dynamics by ^{2}H NMR. Biochim Biophys Acta 737:117-171

Dietrich R, Trahms L (1987) The principal values of axial chemical-shift tensors in powder spectra. J Mag Res 71:337-341

Haeberlen U (1976) High resolution NMR in solids: selective averaging. Academic Press, New York

Hahn EL (1950) Spin echoes. Phys Rev 10:580-594

Huber T, Rajamoorthi K, Kurze V, Beyer K, Brown MF (2002) Structure of docosahexaenoic acid-containing phospholipid bilayers as studied by ^{2}H NMR and molecular simulations. J Am Chem Soc 124:288-309

Jackson JD (1999) Classical electrodynamics, 3rd ed. J Wiley, Hoboken, NJ

Lafleur M, Fine B, Sternin E, Cullis PR, Bloom M (1989) Smoothed orientational order profile of lipid bilayers by ^{2}H-nuclear magnetic resonance. Biophys J 56:1037-1041

Katsaras J (1997) Highly aligned lipid membrane systems in the physiologically relavent “excess water” condition. Biophys J 73:2924-2929

Marcotte I, Auger M (2005) Bicelles as model membranes for solid- and solution-state NMR studies of membrane peptides and proteins. Concept Magn Reson A 24A:17-37

McCabe MA, Wassall SR (1995) Fast-Fourier-transformation dePaking. J Magn Reson Ser B 106:80-82

McCabe MA (2000) Solid state nuclear magnetic resonance of membranes. Dissertation, Purdue University

Morrow MR, Whitehead JP, Lu D (1992) Chain-length dependence of lipid bilayer properties near the liquid crystal to gel phase transition. Biophys J 63:18-27

Nagle JF, Tristram-Nagle S (2000) Structure of lipid bilayers. Biochim Biophys Acta 1469:159-195

Oldfield E, Chapman D, Derbyshire W (1971) Deuteron resonance: a novel approach to the study of hydrocarbon chain mobility in membrane systems. FEBS Lett 16:102-104

Pake GE (1948) Nuclear resonance absorption in hydrated crystals: fine structure if the proton line. J Chem Phys 16:327-336

Petrache HI, Dodd SW, Brown MF (2000) Area per lipid and acyl length distributions in fluid phosphatidylcholines determined by ^{2}H NMR spectroscopy. Biophys J 79:3172-3192

Pochapsky TC, Pochapsky SS (2007) NMR for physical and biological scientists. Garland Science, New York

Polozov IV, Gawrisch K (2007) NMR detection of lipid domains, In: McIntosh TJ (ed) Lipid rafts. Humana Press, Totowa, NJ

Powles JG, Strange JH (1963) Zero time resolution nuclear magnetic resonance transients in solids. Proc Phys Soc 82:6-15

Seelig J, Niederberger W (1974) Deuterium-labeled lipids as structural probes in liquid crystalline bilayers. A deuterium magnetic resonance study. J Am Chem Soc 96:2069-2072

Seelig J (1977) Deuterium magnetic resonance: theory and application to lipid membranes. Q Rev Biophys 10:353-418

Seelig J, Seelig A (1980) Lipid conformation in model membranes and biological membranes. Q Rev Biophys 13:19-61

Slichter CP (1990) Principles of magnetic resonance, 3rd edn. Springer, New York

Solomon I (1958) Multiple echoes in solids. Phys Rev 110:61-65

Soni SP, Ward JA, Sen SE, Feller SE, Wassall SR (2009) Effect of trans unsaturation on molecular organization in a phospholipid membrane. Biochem 48:11097-11107

Spiess HW (1983) Molecular dynamics of solid polymers as revealed by deuteron NMR. Colloid Polym Sci 261:193-209

Stockton GW, Johnson KG, et al. (1977) Deuterium NMR study of lipid organization in *Acholeplasma laidlawii* membranes. Nature 269:267-268

Veatch SL, Polozov IV, Gawrisch K, Keller SL (2004) Liquid domains in vesicles investigated by NMR and fluorescence microscopy. 86:2910-2922

Vega AJ, Luz Z (1987) Quadrupole echo distortion as a tool for dynamic NMR: Application to molecular reorientation in solid trimethylamine. J Chem Phys 86:1803-1813

Vermeer LS, de Groot BL, Réat V, Milon A, Czaplicki J (2007) Acyl chain order parameter profiles in phospholipid bilayers: computation from molecular dynamics simulations and comparison with ^{2}H NMR experiments. Eur Biophys J 36:919-931

CHAPTER 3: DOCOSAHEXAENOIC AND EICOSAPENTAENOIC ACIDS SEGREGATE DIFFERENTLY BETWEEN RAFT AND NONRAFT DOMAINS

3.1 Introduction

Fish oil supplements are increasingly recognized in clinical studies to have utility in treating a variety of important human afflictions (Calder and Yaqoob 2009, Chapkin et al. 2009, Fetterman and Zdanowicz 2009, Harris et al. 2009). However, the molecular mode of action of fish oil remains unclear. The major bioactive components of fish oil are the long chain ω-3 polyunsaturated fatty acids (n-3 PUFA) eicosapentaenoic (EPA, $20{:}5\Delta^{5,8,11,14,17}$) and docosahexaenoic (DHA, $22{:}6\Delta^{4,7,10,13,16,19}$) acids. Omega-3 fatty acids are characterized by having their last double bond three carbons from the terminal methyl (n or ω) end of the chain. One emerging mechanism of action for n-3 PUFA is modification of membrane organization in response to uptake of EPA and/or DHA into phospholipids of the cellular plasma membrane (Stillwell and Wassall 2003, Wassall and Stillwell 2008, Yaqoob and Shaikh 2010).

It is now generally accepted that lipids are not randomly distributed within a membrane. They are laterally arranged in patches or domains of specific composition that provide the environment necessary for the function of resident proteins (Levental et al. 2010). Differential lipid-lipid and lipid-protein affinity drives the formation of the domains. The best known example is the lipid raft (Pike 2006, Lingwood and Simons 2010). Lipid rafts are liquid ordered (l_o) domains enriched in saturated sphingolipids and cholesterol (chol) that serve as the platform for characteristic signaling proteins. The extended conformation adopted by the saturated acyl chains of sphingolipids is compatible with close proximity to the four rigid cycloalkane rings of the sterol, while hydrogen bonding of the amide on the sphingosine backbone of a sphingolipid molecule to the hydroxyl of adjacent sphingolipid and chol molecules glues the raft together (Bartels et al. 2008). By contrast, the shallow energy barrier to rotation about C-C bonds in the repeating =C-C-C= unit in a PUFA chain produces a multitude of rapidly changing conformations

(Feller 2008, Soubias and Gawrisch 2007) that push chol away, as evinced by reduced solubility (Shaikh et al. 2006) and binding coefficients (Nui and Litman 2002) measured for the sterol in polyunsaturated phospholipids.

We have hypothesized from work on model membranes that poor affinity of chol for PUFA promotes formation of membrane (nonraft) domains rich in PUFA-containing phospholipids but poor in chol (Shaikh et al. 2002, Shaikh et al. 2004, Soni et al. 2008, Kučerka et al. 2010). According to our hypothesis, highly disordered PUFA-rich domains coexist in a sea of bulk lipid with highly ordered lipid rafts that are enriched in sphingolipids and chol (Wassall and Stillwell 2008, Wassall and Stillwell 2009). A recent refinement to this view, based on detergent extraction (Fan et al. 2003, Shaikh et al. 2009) and microscopy studies of living cells (Shaikh et al. 2009, Kim et al. 2008), has polyunsaturated phospholipids infiltrating rafts as well as forming (nonraft) domains (Yaqoob and Shaikh 2010, Shaikh 2010). In either case, the basic model is that n-3 PUFA modulate membrane organization to diminish intracellular or extracellular signaling events.

Mixtures of polyunsaturated phospholipids with sphingomyelin (SM) and chol are the model membrane system that we have developed to investigate the sorting of lipids into SM-rich/chol-rich raftlike domains and PUFA-rich/chol-poor nonraft domains (Wassall and Stillwell 2008, Wassall and Stillwell 2009). DHA, the most unsaturated fatty acid commonly found in nature (Salem et al. 1986), was the focus of our earlier work. In a series of studies we employed solid-state ^{2}H NMR spectroscopy, together with a battery of complementary biophysical techniques, to characterize 1-palmitoyl-2-docosahexaenoylphosphatidylethanolamine (PDPE)/SM/chol (1:1:1 mol) membranes (Shaikh et al. 2002, Shaikh et al. 2004, Soni et al. 2008). The NMR spectra established the presence of motionally distinct DHA-rich/chol-poor (less-ordered) and SM-rich/chol-rich (more-ordered) domains that are nanoscale in size. Here we turn our attention to EPA, which is typically more abundant than DHA in fish oil capsules (Kris-Etherton et al. 2003) and differs in its efficacy in treating certain ailments (Mori et al. 1999, Park and Harris 2002, Vemuri et al. 2007).

We specifically address whether EPA and DHA interact differentially with SM and chol. Utilizing solid-state ^2H NMR the molecular organization of 1-[$^2H_{31}$]palmitoyl-2-eicosapentaenoylphosphatidylcholine (PEPC-d_{31}), 1-[$^2H_{31}$]palmitoyl-2-docosahexaenoylphosphatidylcholine (PDPC-d_{31}) and, as a control, 1-[$^2H_{31}$]palmitoyl-2-oleoylphosphatidylcholine (POPC-d_{31}), were compared in mixtures with SM (1:1 mol) and with SM and chol (1:1:1 mol). Figure 3.1 depicts the molecular structure of the phospholipids and sphingolipid studied.

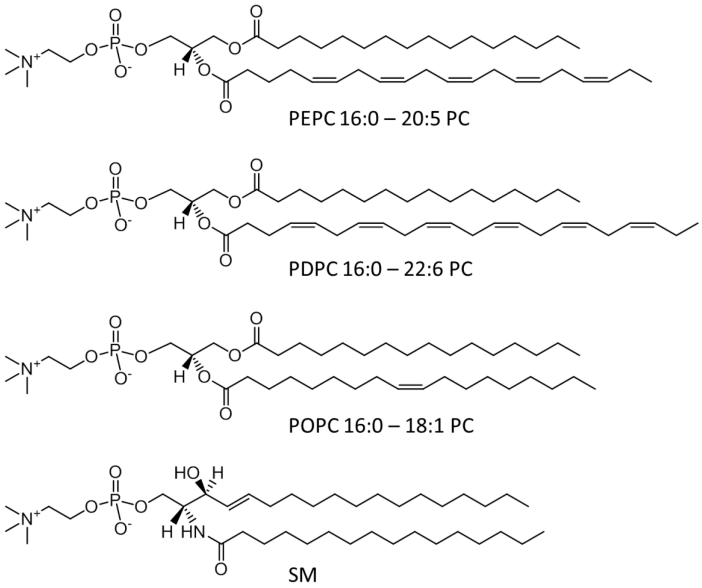

Figure 3.1 Molecular structure of PEPC, PDPC, POPC, and SM.

The ^2H NMR data establish that the two major bioactive components of fish oil do not exert the same effect on membrane organization. EPA segregates into PUFA-rich/chol-poor (nonraft) domains more than DHA. Strikingly, contrary to our earlier model, our experiments reveal that a substantial amount of the DHA-containing phospholipid incorporates into SM-rich/chol-rich (raft) domains. The observation that n-3 PUFA can infiltrate raftlike domains in a lipid mixture is consistent with recent studies in vitro and in vivo showing n-3 PUFA can incorporate into detergent resistant membranes (DRM) (Yaqoob and Shaikh 2010).

3.2 Materials and Methods, Solid-State ^{2}H NMR of Model Membranes

3.2.1 Materials

Avanti Polar Lipids (Alabaster, AL) was the source for POPC-d_{31}, PEPC-d_{31}, PDPC-d_{31} and egg SM as either a stock item or custom synthesis. Chol was purchased from Sigma Chemical (St. Louis, MO). All lipids were used without further purification. Deuterium depleted water was obtained from Cambridge Isotope Laboratories (Andover, MA).

3.2.2 Sample Preparation

Lipids mixtures containing ~50 mg total lipid were co-dissolved in chloroform in molar ratio 1:1 and 1:1:1, respectively, for deuterated PC/SM and deuterated PC/SM/chol samples (concentrations that will be assumed henceforth unless otherwise specified). The chloroform was evaporated under a steady stream of argon, and the samples were placed in vacuum overnight to remove any remaining solvent. After adding 50 wt % degassed 50 mM Tris buffer to the dried lipids, the samples were vortex-mixed and pH was adjusted to 7.5 in the presence of additional water. Three lyophilizations with deuterium-depleted water were then performed to remove trace amounts of natural abundance ^{2}HHO, and finally the lipids were hydrated at 50 wt %. In each instance hydration was performed above 45°C, which exceeds the gel-to-liquid-crystalline temperature for SM that has the highest chain-melting temperature (39°C) (Shaikh et al. 2009), to ensure proper mixing. Samples were packed and sealed in 5-mm glass NMR tubes, stored at -80°C and equilibrated at room temperature prior to experiments. Precautions were taken throughout the procedure to minimize oxidation (Shaikh et al. 2002), including limiting exposure to light and using a glove box purged with argon during manipulations.

3.2.3 Spectroscopy

Solid-state ^{2}H NMR spectra were acquired on a home built spectrometer (Soni et al. 2009) operating at 46.0 MHz with a 7.05 T super-conducting magnet (Oxford Instruments, Osney Mead, UK). Pulse programming was accomplished with an in-house assembled programmable pulse generator, while signals were obtained in quadrature using a dual-channel digital oscilloscope (R1200 M; Rapid Systems, Seattle, WA). Sample temperature was regulated to ±0.5°C by a temperature controller (1600 Series; Love Controls, Michigan City, IN). To eliminate spectral distortion due to receiver recovery time, a phase-alternated quadrupolar echo

sequence $(90^{\circ}_{x}$-τ-90°_{y}-acquire-delay)$_n$ was implemented (Davis et al. 1976). Parameters were 90° pulse width ≈3 μs; separation between pulses τ = 50 μs; delay between pulse sequences = 1.0 s (gel phase) or 1.5 s (liquid-crystalline phase); sweep width = ±250 kHz (gel phase) or ±100 kHz (liquid-crystalline phase); dataset = 2 K; and number of transients = 2048 (gel phase) or 1536 (liquid-crystalline phase).

3.2.4 Spectral Analysis

First moments M_1 were calculated from ^{2}H-NMR spectra according to

$$M_1 = \frac{\int_{-\infty}^{\infty} |\omega| f(\omega) d\omega}{\int_{-\infty}^{\infty} f(\omega) d\omega}, \quad (1)$$

where ω is the frequency with respect to the central Larmor frequency and $f(\omega)$ is the lineshape (Davis 1983). In practice, the integral was a summation over the digitized data. The expression

$$M_1 = \frac{\pi}{\sqrt{3}} \left(\frac{e^2 qQ}{h} \right) \left| \overline{S}_{CD} \right| \quad (2)$$

was employed in the lamellar liquid-crystalline phase to relate the first moment M_1 to the average order parameter $\overline{S}_{CD}$ for the perdeuterated palmitoyl *sn*-1 chain via the static quadrupolar coupling constant $(e^2 qQ/h)$ = 167 kHz. A reproducibility of ±2% typically applies to the M_1 values measured.

Spectra were also fast-Fourier-transform (FFT) dePaked to enhance resolution in the liquid-crystalline phase (McCabe and Wassall 1997). This numerical procedure generates a spectrum representative of a planar membrane of single alignment from the powder pattern signal. In processing the intrinsically noisy dePaked data, the out-of-phase channel was zeroed prior to Fourier transformation. The resultant spectra were reflected about the central frequency and possess an improvement in signal/noise by a factor of$\sqrt{2}$.

3.3 Results

3.3.1 Solid-State ^{2}H NMR of Model Membranes

Solid-state ^{2}H NMR spectra were obtained for 50 wt % aqueous multilamellar suspensions of PEPC-d_{31}, PDPC-d_{31} and POPC-d_{31} in mixtures with SM, and with SM and chol. The perdeuterated palmitoyl (16:0) *sn*-1 chain of the PC molecules constitutes an essentially noninvasive probe and

the spectra compared the molecular organization of EPA-containing PC versus DHA-containing PC in the mixed membranes. Oleic acid (OA)-containing PC acted as a monounsaturated control. The experiments were conducted from high-to-low temperature over a range from 40 to -32°C that encompasses the gel-to-liquid-crystalline phase transition for each lipid. Representative spectra can be seen in Figure 3.2.

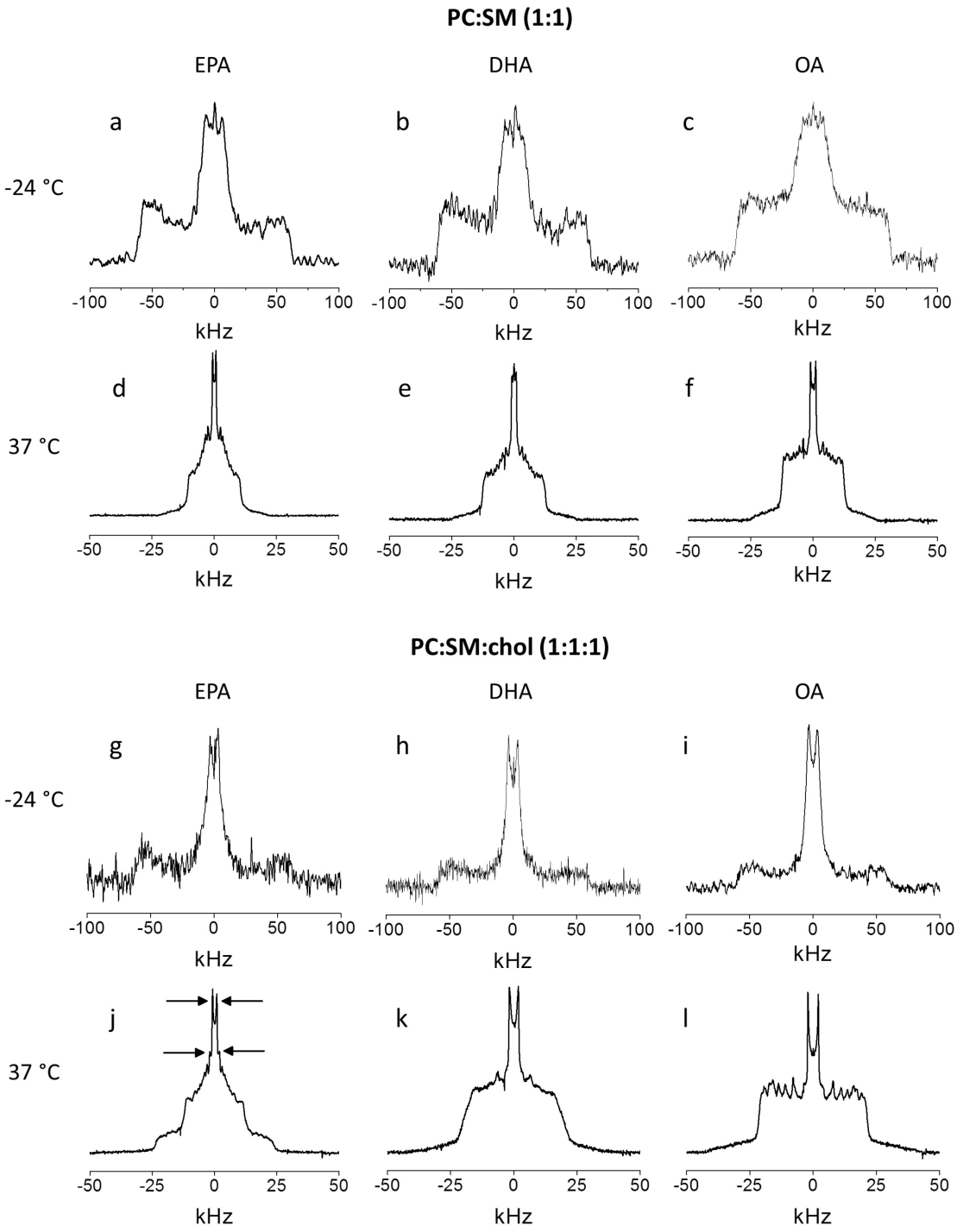

Figure 3.2 ^{2}H NMR spectra for 50 wt % aqueous dispersions in 50 mM Tris buffer (pH 7.5) of PEPC-d_{31}/SM (1:1 mol) (*a* and *d*), PDPC-d_{31}/SM (1:1 mol) (*b* and *e*) and POPC-d_{31}/SM (1:1 mol) (*c* and *f*) (*upper panel*), and PEPC-d_{31}/SM/chol (1:1:1 mol) (*g* and *j*), PDPC-d_{31}/SM/chol (1:1:1 mol) (*h* and *k*) and POPC-d_{31}/SM/chol (1:1:1 mol) (*i* and *l*) (*lower panel*). Spectra were recorded at -24 (*upper row*) and 37°C (*lower row*). (*Arrows, j*) Signals assigned to the terminal methyl group on PEPC-d_{31} in PC-rich (inner splitting) and SM-rich (outer splitting) domains (see Fig. A1.2 in Appendix A1).

3.3.1.1 PC/SM Mixtures

At low temperature, -24°C, the spectra for PEPC-d_{31}, PDPC-d_{31} and POPC-d_{31} in the mixtures with SM are symptomatic of the gel phase (Fig. 3.2, *a-c*). They appear broad and relatively featureless with edges at ±63 kHz reflecting the slow rotational diffusion of the all-*trans* palmitic acid chain that renders the lineshape nonaxially symmetric (asymmetry parameter $\eta \neq 0$) (Davis 1983). By contrast at high temperature, 37°C, the lineshape in each case is characteristic of phospholipids in the lamellar liquid-crystalline phase (Fig. 3.2, *d-f*). A superposition of powder patterns from all of the individual deuterated positions along the perdeuterated palmitoyl *sn*-1 chain produces a spectrum with well-defined edges at $\pm \sim 12$ kHz corresponding to the plateau region of nearly constant order in the upper portion of the chain and a series of pairs of peaks within the spectrum associated with less-ordered methylenes and the terminal methyl in the lower portion of the chain (Davis 1983). Greater disorder and a shorter plateau region are indicated for the PUFA-containing phospholipids by the slightly narrower width and lower intensity of the edges seen for PEPC-d_{31} (Fig. 3.2 *d*) and PDPC-d_{31} (Fig. 3.2 *e*) relative to POPC-d_{31} (Fig. 3.2 *f*).

The spectra presented in Figure 3.2 illustrate the tremendous change in lineshape that accompanies the melting of lipid chains at the gel-to-liquid-crystalline phase transition. The first moment (M_1), defined in Eq. 1, offers a way to quantify lineshape and provides a means to investigate phase behavior when plotted as a function of temperature. Figure 3.3 shows the dependence on temperature for the values of M_1 calculated from the spectra collected for PEPC-d_{31}, PDPC-d_{31} and POPC-d_{31} in the mixtures with SM between -32 and 40°C.

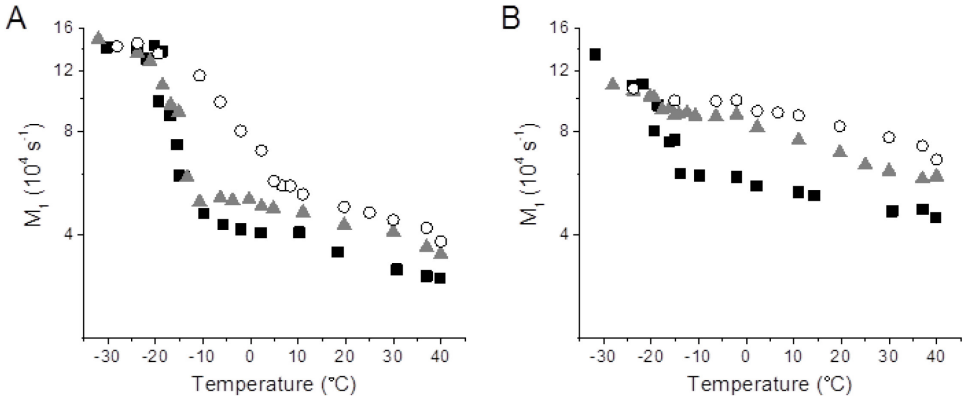

Figure 3.3 Variation of the first moment M_1 derived from ^{2}H NMR spectra as a function of temperature for PEPC-d_{31}/SM (1:1 mol) (■), PDPC-d_{31}/SM (1:1 mol) (▲) and POPC-d_{31}/SM (1:1 mol) (○) in the absence (*A*) and presence (*B*) of chol (1:1:1 mol).

An abrupt drop signifying the transition from gel ($M_1 > 1.3 \times 10^5$ s^{-1}) to liquid-crystalline ($M_1 < 0.6 \times 10^5$ s^{-1}) state is seen with each mixture (Fig. 3.3 *A*). The midpoint temperature (designated as the transition temperature T_m) and width of this drop in value for the moment are, respectively, -16 and 5°C for PEPC-d_{31} and -14 and 6°C for PDPC-d_{31}, as opposed to -3 and 18°C for POPC-d_{31}.

An appraisal of data obtained with the corresponding pure PC membranes establishes that the transition observed in the mixed membranes with SM is broadened but hardly shifted in temperature, and that the broadening is much smaller with polyunsaturated than monounsaturated phospholipid. For PDPC-d_{31} T_m = -12.7°C (Barry et al. 1991) and for POPC-d_{31} T_m = -6°C (Wassall et al. 2010), and in both cases the transition is relatively narrow (2-3°C in width). Although to the best of our knowledge details of the phase behavior have not been published for PEPC, DSC measurements on pure PC bilayers with stearic (18:0) acid at the *sn*-1 position and a series of unsaturated fatty acids at the *sn*-2 position indicate T_m is slightly lower (3-4°C) with EPA than DHA (Niebylski and Salem 1994).

The modest impact upon the temperature of the phase transition seen here for PEPC-d_{31}, PDPC-d_{31} and POPC-d_{31} in the presence of SM indicates that the mixing of PC and SM is inhomogeneous, which we attribute to segregation into PC-rich and SM-rich domains. A similar interpretation has previously been applied to ^{2}H NMR spectra recorded for POPC/SM mixtures (Bartels et al. 2008, Bunge et al. 2008, Ausili et al. 2008). Other studies on PEPC/SM or PDPC/SM mixtures have not been published. The appreciably smaller SM-associated effect on the width of the phase transition for PEPC-d_{31} and PDPC-d_{31} in relation to POPC-d_{31} (Fig. 3.3A) we ascribe to enhanced separation between the PUFA-containing phospholipids and sphingolipid compared to the OA-containing phospholipid and sphingolipid.

3.3.1.2 PC/SM/Chol Mixtures

In Figure 3.2 (*lower panel*) spectra for PEPC-d_{31}, PDPC-d_{31} and POPC-d_{31} in mixtures with SM and chol are plotted. All three systems exhibit a spectrum that is gel-like in appearance at -24°C (Fig. 3.2, *g-i*). There is a reduction in intensity in the wings compared to the spectra collected under identical conditions in the absence of chol (Fig. 3.2, *a-c*). The implication is that the sterol

disrupts the regular packing of the chains of PEPC-d_{31}, PDPC-d_{31} and POPC-d_{31} in the mixed membranes in the gel state. The spectra observed in the liquid-crystalline state at 37°C reveal a remarkable differential in the response of each PC to the introduction of chol into the mixed PC/SM systems (Fig. 3.2, *j-l*). A spectrum that is similar in shape to POPC-d_{31}/SM (Fig. 3.2 *f*), but appreciably broader with edges at ±20 kHz, is seen with POPC-d_{31}/SM/chol (Fig. 3.2 *l*). This broadening reflects the restriction to chain motion caused by the rigid steroid ring moiety.

The addition of chol to the mixtures containing PUFA and SM elicits a more profound alteration in spectral shape. In the spectrum for PEPC-d_{31}/SM/chol (Fig. 3.2 *j*), a narrow component with edges at ±12 kHz closely resembling that seen in the absence of sterol (Fig. 3.2 *d*) appears superposed upon a wider second spectral component with edges at ±23 kHz. The distinction is less dramatic in the case of the system containing DHA where a second spectral component is not discernible (Fig. 3.2 *k*). Instead the spectrum for PDPC-d_{31}/SM/chol is smeared-out with less sharply defined edges at ±19 kHz and barely resolved peaks, except for the central pair due to the terminal methyl group. Interpretation of the spectra collected at 37°C in terms of the sorting of lipids into PC-rich and SM-rich domains that is amplified when chol is present to different extent by EPA and DHA will be given later in the Discussion.

Figure 3.3 *B* shows the variation with temperature of the first moment evaluated for PEPC-d_{31}, PDPC-d_{31} and POPC-d_{31} in the mixtures with SM and chol. A clear distinction is apparent in the effect that the sterol has on the phase behavior of EPA- versus DHA- and OA-containing phospholipid in the mixtures with SM. The value of M_1 for POPC-d_{31}/SM/chol slowly decreases with increasing temperature and a discontinuity is no longer observed. The introduction of chol into the POPC-d_{31}/SM membrane broadens the phase transition for POPC-d_{31} beyond detection, indicating extensive mixing of chol and POPC-d_{31}. PDPC-d_{31} responds comparably. The moments that were measured for PDPC-d_{31}/SM/chol similarly decline gradually and without break as temperature rises. In dramatic contrast, much less thorough mixing of chol with PEPC-d_{31} is indicated in PEPC-d_{31}/SM/chol. A sharp fall in first moment (from $M_1 \sim 1.4 \times 10^5$ to $\sim 0.6 \times 10^5$ s^{-1}) still occurs, but is somewhat reduced in magnitude and (with midpoint ~-18°C and width ~12°C) less precipitous compared to PEPC-d_{31}/SM (Fig. 3.3 *A*). Unlike not only POPC-d_{31}, but also

PDPC-d_{31}, adding chol does not totally obliterate the phase transition for PEPC-d_{31} in the mixed membrane.

We surmise from the temperature variation of the spectra seen here for PEPC-d_{31}, PDPC-d_{31} and POPC-d_{31} in 1:1 mol mixtures with SM and in 1:1:1 mol mixtures with SM and chol that the lipids incompletely mix to form PC-rich and SM-rich domains. Notably, a lower affinity of sterol for EPA than DHA and thereby a greater propensity for DHA-containing PC than EPA-containing PC to incorporate into SM-rich/chol-rich raftlike domains are implied. It should be noted that the two-domain model invoked does not rule out more complex phase behavior.

3.3.2 Detergent Extraction of Cells

To complement our experiments on model membranes, we explored the incorporation of EPA and DHA into biological membranes. Details of the methods are provided in Appendix A1. The uptake of EPA versus DHA, relative to a bovine serum control, into DRM (raft) and detergent-soluble membranes (DSM) (nonraft) fractions isolated from EL4 cells by detergent extraction is compared in Figure A1.1 in Appendix A1. EPA constituted ~2% (not statistically significant, p = 0.05) and ~11% of the total fatty acid, respectively, found in DRM (*upper panel*) and DSM (*lower panel*) after treatment with EPA, whereas DHA constituted ~6% and ~33% of the total fatty acid found in DRM and DSM, respectively, after treatment with DHA. It is important to note that elevated levels of docosapentaenoic (DPA, 22:5n-3) acid, the elongation product of EPA (Kaur et al. 2011), were detected in DRM (~6%) and DSM (~23%) when the cells were treated with EPA. The combined concentration of EPA+DPA approximately matches the uptake measured for DHA in each fraction (i.e. the total level of n-3 PUFA is roughly the same after treatment with EPA and DHA).

3.4 Discussion

The n-3 PUFA found in fish oils alleviate the symptoms associated with a multitude of inflammatory, autoimmune and metabolic diseases (Calder and Yaqoob 2009, Chapkin et al. 2009, Fetterman and Zdanowicz 2009, Harris et al. 2009). The diversity of the health benefits suggests an underlying general mechanism. We (Stillwell and Wassall 2003, Wassall and Stillwell 2008, Yaqoob and Shaikh 2010), and other research groups (Fan et al. 2003, Kim et al. 2008,

Zech et al. 2009), have hypothesized that changes in molecular organization within the plasma membrane due to the incorporation of n-3 PUFA into phospholipids modulate the conformation, and thereby the activity, of signaling proteins. The formation of highly disordered domains that are enriched in DHA-containing phospholipids but depleted in chol is a model that we developed based on studies on lipid bilayers (Wassall and Stillwell 2008, Wassall and Stillwell 2009). These nonraft domains form because the rapidly varying conformers adopted by PUFA are averse to near approach to the rigid steroid moiety of the sterol. An alternative model in which, paradoxically, PUFA-containing phospholipids invade and disrupt the highly ordered environment existing within lipid rafts that are enriched in predominantly saturated chain sphingolipids and chol has recently been developed based on in-vitro and in-vivo studies (Yaqoob and Shaikh 2010, Shaikh 2010). Central to the formulation of this model was the significant amount of DHA detected in DRM isolated from cells treated with PUFA.

In this investigation we employed solid-state ^{2}H NMR to compare the molecular organization of an EPA- and DHA-containing phospholipid in mixtures with the lipid raft molecules SM and chol. EPA, with 20 carbons and 5 double bonds, and DHA, with 22 carbons and 6 double bonds, are the n-3 PUFA present in fish oils. Our experiments on model membranes demonstrate a significant difference in the partitioning of EPA and DHA between raft and nonraft domains, and reveal that n-3 PUFA can accumulate in raftlike domains.

3.4.1 Segregation into PC-Rich (Nonraft) and SM-Rich (Raft) Domains

We interpret the ^{2}H NMR spectra for PEPC-d_{31}, PDPC-d_{31} and POPC-d_{31} mixed with SM (Fig. 3.2, *upper panel*) in terms of segregation into PC-rich and SM-rich domains. The precipitous drop in value of the first moment derived from the spectra as a function of temperature that accompanies chain melting indicates in each instance that the transition from gel to liquid-crystalline state is broadened and only minimally shifted in temperature due to the presence of SM (Fig. 3.3 *A*). Inhomogeneous mixing of PC and SM is implied.

A marked differential in the response of EPA and DHA to the addition of chol is revealed by the ^{2}H NMR spectra for PEPC-d_{31}, PDPC-d_{31} and POPC-d_{31} in the mixtures with SM and chol (Fig. 3.2, *lower panel*). Substantial exposure to chol is inferred for PDPC-d_{31} from the absence of a

discontinuity in the temperature dependence of the moments derived from spectra (Fig. 3.3 *B*). A phase transition from gel to liquid-crystalline state for PDPC-d_{31} is no longer discernible in PDPC-d_{31}/SM/chol because chol disturbs the packing and obstructs reorientation of the DHA-containing phospholipid in the gel and liquid-crystalline states, respectively. This behavior resembles that observed with POPC-d_{31} in our POPC-d_{31}/SM/chol control (Fig. 3.3 *B*) and POPC-d_{31}/SM/chol mixtures of similar composition (Bartels et al. 2008, Levental et al. 2010, Ausili et al. 2008). There is, on the contrary, still an abrupt drop in the plot of moment against temperature for PEPC-d_{31} in PEPC-d_{31}/SM/chol (Fig. 3.3 *B*). Less interaction with the sterol, so that a phase transition remains, is implied for the EPA-containing phospholipid compared to its DHA-containing counterpart when mixed with SM and chol.

Further insight is gleaned from the average order parameter $\overline{S}_{CD}$, the correspondence of which to bilayer thickness underscores the physical significance (Petrache et al. 2000), calculated via Eq. 2 from the first moment M_1 for spectra at 37°C (see Table A1.1 in Appendix A1). The values of $\overline{S}_{CD}$ in PC/SM mixtures where chol was absent are lower for PEPC-d_{31} ($\overline{S}_{CD} = 0.100$) and PDPC-$d_{31}$ ($\overline{S}_{CD} = 0.122$) than POPC-$d_{31}$ ($\overline{S}_{CD} = 0.137$), confirming our qualitative assessment of the spectra. They show, moreover, that EPA-containing PC is more disordered than DHA-containing PC in combination with SM. Consistent with demixing into PC-rich and SM-rich domains that produces a population-weighted average value for $\overline{S}_{CD}$ from the two domains, comparison with previously published data on POPC-d_{31} (Wassall et al. 2010) and PDPC-d_{31} (Salmon et al. 1987) indicates there is only a small (little more than experimental uncertainty) increase in order due to SM. No data for PEPC-d_{31} were found in a search of the literature.

After the addition of chol to the PC/SM mixed membranes, $\overline{S}_{CD}$ is increased in every case. The increase is greatest with POPC-d_{31} ($\Delta\overline{S}_{CD} = 0.094$) and, reflecting the poor affinity chol has for highly disordered PUFA (Wassall and Stillwell 2009), is more modest with PEPC-d_{31} ($\Delta\overline{S}_{CD} = 0.056$) and PDPC-$d_{31}$ ($\Delta\overline{S}_{CD} = 0.070$). Based on the hierarchy of the changes in $\overline{S}_{CD}$ measured, we infer that the sterol is pushed out of PC-rich domains into SM-rich domains by EPA > DHA > OA. Here it is assumed that a given concentration of chol exerts an equivalent ordering effect upon PEPC-d_{31}, PDPC-d_{31} and POPC-d_{31} individually. This assumption is supported by spectra

published for [$^2H_{35}$]stearoyl-2-oleoylphosphatidylcholine (SOPC-d_{35}) (Polozov and Gawrisch 2007) and [$^2H_{35}$]stearoyl-2-docosahexaenoylphosphatidylcholine (SDPC-d_{35}) (Mihailescu et al. 2011) and by spectral moments reported for POPC-d_{31} (Hsueh et al. 2007) and [$^2H_{31}$]palmitoyl-2-arachidonoylphosphatidylcholine (PAPC-d_{31}) (Jackman et al. 1999) that suggest the *sn*-1 chain in the monounsaturated and polyunsaturated systems responds comparably to chol.

3.4.2 Domain Size is Increased with PUFA

The variation in appearance of the spectra for PEPC-d_{31}/SM/chol, PDPC-d_{31}/SM/chol and POPC-d_{31}/SM/chol at 37°C (Fig. 3.2, *lower panel*) implies that the size of domains is enlarged by EPA and DHA with respect to OA. That only a single spectral component was observed in the spectrum for POPC-d_{31}/SM/chol (Fig. 3.2 *l*), we ascribe to incomplete demixing into PC-rich (less-ordered) and SM-rich (more-ordered) domains between which there is fast exchange (Bloom and Thewalt 1994). A time-averaged spectrum, rather than a superposition of spectral components, is produced because POPC-d_{31} moves among domains at a rate that exceeds the difference in splitting for spectra from the two domains. Invoking the difference in splitting ($\Delta\nu = 1600$ Hz) previously reported for the terminal methyl groups on POPC-d_{31} and [$^2H_{31}$]-N-palmitoylsphingomyelin (PSM-d_{31}) in a PC/SM/chol (3:3:2 mol) mixture of similar composition (Bunge et al. 2008) as representative of PC-rich and SM-rich domains, the lifetime for the residency of lipid molecules in a domain must be less than $\tau = (2\pi\Delta\upsilon)^{-1} = 9.9 \times 10^{-5}$ s. The exchange of lipids between domains is presumed to be mediated by lateral diffusion with D ~ $5\text{x}10^{-12}$ m^2s^{-1} (Filippov et al. 2006) so that the root mean displacement $r = (4D\tau)^{1/2}$ associated with the lifetime places an upper limit of <45 nm upon the radius of domains.

Slow exchange at a rate less than the difference in splitting for spectra due to PEPC-d_{31} in PC-rich and SM-rich domains, in contrast, applies to PEPC-d_{31}/SM/chol (Fig. 3.2 *j*). The result is observation of a superposition of individual spectral components from the two domains. There is a narrow spectral component with edges at ±12 kHz (less-ordered PC-rich/chol-poor domains) superposed upon a wider second component with edges at ±23 kHz (more-ordered SM-rich/chol-poor domains). The difference in splitting ($\Delta\nu = 2800$ Hz) for the terminal methyl groups on PEPC-d_{31} in the two domains (highlighted by *arrows* and see Fig. A1.2) then, by an

analogous calculation to that outlined above, corresponds to a lifetime for residency in a domain that must exceed $\tau = 5.7 \times 10^{-5}$ s and places a lower limit of >35 nm on the size.

A second spectral component is not discernible in the spectrum for PDPC-d_{31}/SM/chol (Fig. 3.2 *k*). Instead, a broadened spectrum in which individual peaks are smeared out was observed. We attribute this blurring of spectral features to exchange between domains on an intermediate timescale that is comparable to the difference in splitting for PDPC-d_{31} in PC-rich and SM-rich domains. A domain size that falls between the ballpark estimates determined based on the extremes for fast and slow exchange in the OA- and EPA-containing systems is the likely explanation. Thus, we deduce that domains are larger with EPA and DHA relative to OA in PC/SM/chol-mixed membranes. The effect is also more marked for EPA than DHA. We emphasize that the splitting for the terminal methyl group employed in our calculations is sensitive to exchange on the timescale of the residual quadrupolar coupling associated with a rapidly rotating methyl group and that the estimates for domain size constitute upper or lower limits.

A PUFA-induced increase in the size of domains was not evident in our earlier work comparing PDPE with POPE (Shaikh et al. 2004, Soni et al. 2008). ^{2}H NMR spectra recorded for 1-[$^2H_{31}$]palmitoyl-2-oleoylphosphatidylethanolamine (POPE-d_{31}), 1-[$^2H_{31}$]palmitoyl-2-docosahexaenoylphosphatidylethanolamine (PDPE-d_{31}) and PSM-d_{31} in PE/SM (1:1 mol) and PE/SM/chol (1:1:1 mol) mixtures were consistent with the DHA-containing phospholipid, as well as the OA-containing phospholipid, undergoing fast exchange between PE-rich and SM-rich domains. The spectra for not only POPE-d_{31}, but also PDPE-d_{31}, remained well resolved upon the addition of chol. There was neither a smearing-out of spectral features nor the appearance of a second spectral component. An upper limit of < 20 nm, moreover, was placed upon domain size (Soni et al. 2008). That, unlike PDPC-rich domains, an increase in size is not implied for PDPE-rich domains in the presence of the sterol we attribute to headgroup structure. The smaller PE headgroup and hydrogen bonding to adjacent polar groups produce negative stress curvature that drives a tendency to adopt inverted hexagonal H_{II} phase that is enhanced with increasing level of unsaturation (Shaikh et al. 2003). Liquid-crystalline PDPE becomes inverted hexagonal at ~13°C and is lamellar over only a very narrow temperature range (6 - 10°C). This inherent

instability of the PDPE bilayer may serve to restrict the area of PDPE-rich domains relative to PDPC-rich domains.

3.4.3 PUFA Infiltrate Rafts

An estimate of the amount of EPA- and DHA-containing phospholipids that incorporates into SM-rich/chol-rich raftlike domains can be made from the spectra for PEPC-d_{31}/SM/chol and PDPC-d_{31}/SM/chol at 30°C displayed in Figure 3.4.

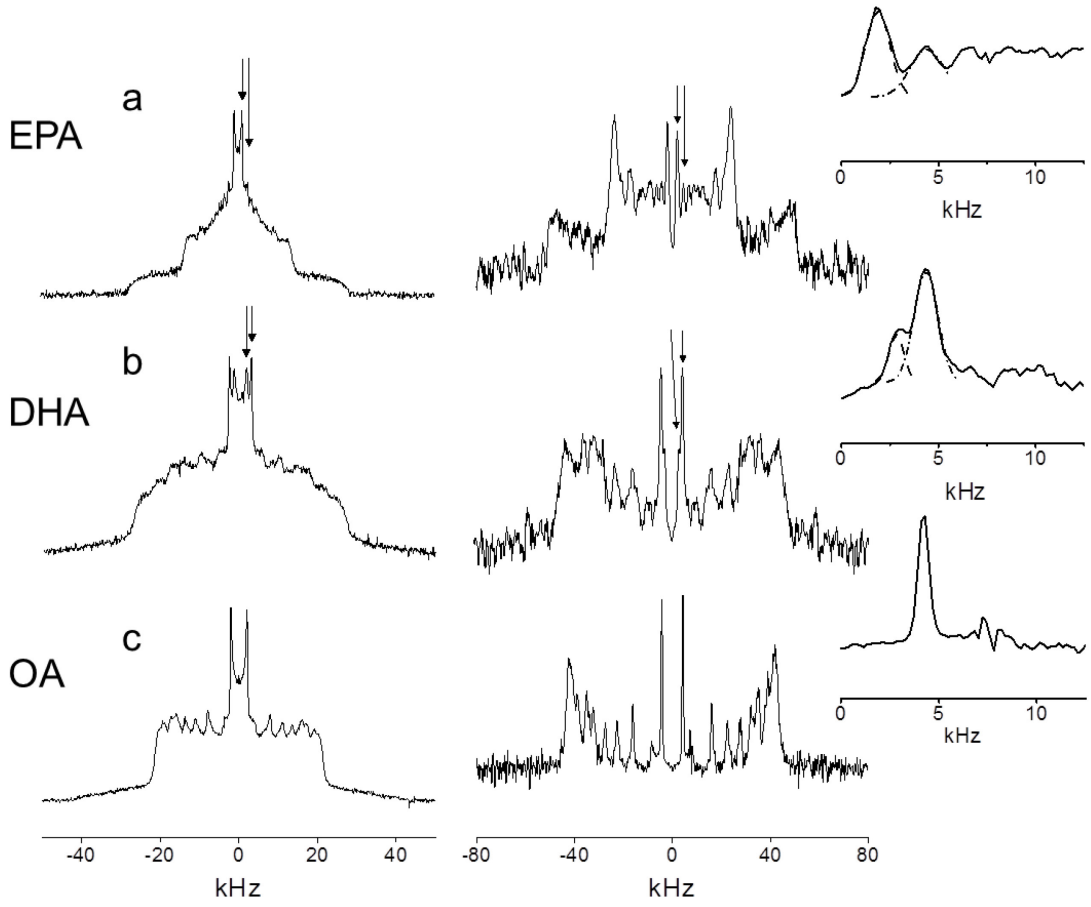

Figure 3.4 ^{2}H NMR spectra for PEPC-d_{31}/SM/chol (1:1:1 mol) (*a*), PDPC-d_{31}/SM/chol (1:1:1 mol) (*b*) and POPC-d_{31}/SM/chol (1:1:1 mol) (*c*) at 30°C. Standard FFT (powder pattern) spectra are plotted (*left column*); FFT dePaked (aligned) spectra are also plotted (*right column*). Peaks from signals assigned to the terminal methyl group on PEPC-d_{31} (*a*) and PDPC-d_{31} (*b*) in PC-rich (inner splitting) and SM-rich (outer splitting) domains are designated (*arrows*), whereas there is only a single peak for the terminal methyl group on POPC-d_{31} (*c*) (see Fig. A1.3 and A1.4 in Appendix A1). (*Insets*) Blow-up of these peaks (*dashed lines* are a Lorentzian fit). The signals are symmetric in frequency about the center of the spectra and only the peaks to the right of center with positive frequency are labeled.

The spectrum for PEPC-d_{31}/SM/chol (Fig. 3.4 *a, left*) closely resembles the spectrum at 37°C (Fig. 3.2 *j*). It is a superposition of narrow and broad components that, as at the higher temperature, we attribute to PEPC-d_{31} in PC-rich and SM-rich domains, respectively. However, the spectra for PDPC-d_{31}/SM/chol at 30 (Fig 3.4 *b, left*) and 37°C (Fig. 3.2 *k*) differ. A pair of peaks (indicated by *arrows* and see Fig. A1.3) that coalesces into a single peak on going up in temperature is visible in the spectrum acquired at the lower temperature. We assign them to the terminal methyl groups of PDPC-d_{31} in less-ordered PC-rich (*inner peak*) and more-ordered SM-rich (*outer peak*) domains. A reduction in the rate of exchange between domains due to slower diffusion with decreased temperature may be responsible. The observation of a separate NMR signal from each domain for PEPC-d_{31} in PEPC-d_{31}/SM/chol and for PDPC-d_{31} in PDPC-d_{31}/SM/chol means that the relative concentration of PUFA-containing phospholipids in the two domains can be evaluated. A similar calculation for POPC-d_{31} in POPC-d_{31}/SM/chol was precluded. The spectrum at 30°C (Fig. 3.4 *c, left* and see Fig. A1.3) was of the same form as at 37°C (Fig. 3.2 *l*) and, consistent with fast exchange between domains remaining at lower temperature, a second spectral component did not appear.

We applied the FFT dePaking algorithm (McCabe and Wassall 1997) to determine the ratio of the quantity of PEPC-d_{31} and PDPC-d_{31} in PC-rich and SM-rich domains. By this numerical procedure, spectra characteristic of a membrane of single alignment were obtained. Figure 3.4 (and see Fig. A1.4) illustrates that the powder patterns producing the two methyl peaks in the conventional spectra for PEPC-d_{31}/SM/chol (Fig. 3.4 *a*, *left*) become resolved as a pair of doublets (identified by *arrows*) in the dePaked spectra (Fig 3.4 *a*, *right*). The ratio of the integrated intensity of inner and outer peaks, corresponding to the ratio of the amount of PEPC-d_{31} in the less ordered PC-rich and more ordered SM rich domains, was then estimated to be 3:2 assuming a Lorentzian fit that is shown in the inset. Most of the EPA-containing PC forms a more-disordered domain, whereas a smaller fraction (40%) incorporates into the SM-rich domain. By contrast, a ratio of 1:3 for the integrated intensity of the inner and outer peaks was determined when the pair of overlapping doublets (identified by *arrows* and also see Fig. A1.4) in the dePaked spectrum for PDPC-d_{31}/SM/chol (Fig 3.4 *b, right*) was analyzed. Although a more-disordered DHA-rich domain is formed, the majority (75%) of the DHA-containing PC is found to infiltrate into the more-ordered SM-rich (raftlike) domain. This remarkable finding is contrary to

the propensity to segregate into DHA-rich/chol-poor (nonraft) domains identified in our previously published experiments on PDPE/SM/chol mixtures (Shaikh et al. 2002, Shaikh et al. 2004, Soni et al. 2008).

It should be understood that our estimate for the relative amount of PUFA-containing PC in each domain is approximate. The complexity of spectra meant that an analysis of the entire lineshape, which would be ideal, was not feasible. Instead, we focused upon the comparatively well-resolved signals attributed to terminal methyl groups. A potential problem with this approach is the possibility that a methylene group, rather than the terminal methyl group in a more-ordered domain, is responsible for the second innermost doublet in the dePaked spectrum for either PEPC-d_{31}/SM/chol (Fig. 3.4 *a*) or PDPC-d_{31}/SM/chol (Fig. 3.4 *b*). This possibility is discounted because a substantially greater differential in spitting with respect to the innermost doublet would be expected for a methylene group in the lower portion of a chain where order rapidly decreases towards the terminal methyl end.

The appearance of a minor spectral artifact at twice the frequency of the true signal following application of the FFT dePaking procedure (McCabe and Wassall 1997) is another potential problem. A pair of small satellite peaks either side of the innermost doublet is an example of the artifact (Fig. 3.4 *c*) that, dependent upon the disposition of signals, can affect the analysis made here. The dePaked spectrum for PEPC-d_{31}/SM/chol (Fig. 3.4 *a*) is a worst case. There the artifact associated with the innermost doublet that we attribute to the terminal methyl group on PEPC-d_{31} in a less-ordered PC-rich domain lies buried underneath the second innermost doublet that we assign to the terminal methyl group on PEPC-d_{31} in a more-ordered SM-rich domain. A slight overestimation of PEPC-d_{31} found in the raftlike domain results. The situation is less severe with the dePaked spectrum for PDPC-d_{31}/SM/chol (Fig. 3.4 *b*). In this case the artifact accompanying the innermost doublet assigned to PDPC-d_{31} in a less-ordered PC-rich domain falls just outside the second innermost doublet attributed to PDPC-d_{31} in a more-ordered SM-rich domain and is too small to be discerned.

How PDPE-d_{31} distributes between PE-rich and SM-rich domains in a PDPE-d_{31}/SM/chol (1:1:1 mol) membrane could not be quantified in our earlier NMR work because, as discussed above,

only a single component spectrum was observed (Shaikh et al. 2004). Preferential segregation of PDPE-d_{31} into PE-rich/chol-poor domains was inferred from the relatively small increase in average order parameter registered by PDPE-d_{31} when chol was added to the PDPE-d_{31}/SM 1:1 mol mixture. In support of this interpretation, detergent extraction experiments conducted on PDPE/SM/chol (1:1:1 mol) showed that <30% PDPE was present in DRM where >90% SM and chol was found (Shaikh et al. 2004). A reduction in the amount of DHA-containing phospholipid that incorporates into SM-rich/chol-rich domains is implied, therefore, for PDPE compared to PDPC. The reduced affinity that PE has for chol compared to PC offers an explanation for this difference (Shaikh et al. 2006, Nui and Litman 2002). We speculate that the uptake of DHA into lipid rafts within biological membranes may be dependent upon the lipid species into which the PUFA incorporates.

Because our ^{2}H-NMR experiments demonstrate that PDPC incorporates into SM/chol-rich (raft) domains to a greater extent than PEPC, we tested whether there is a difference in the incorporation of EPA and DHA in cells. DRM (rafts) and DSM (nonrafts) were isolated from EL4 cells in the presence of cold Triton X-100. It is acknowledged that the detergent produces artifacts (Heerklotz 2002). Nevertheless, this widely used method is a valuable screen with accepted utility as a predictive tool (Lingwood and Simons 2010, Edidin 2003). Figure A1.1 compares the uptake of EPA versus DHA, relative to a bovine serum albumin control, into EL4 cells. The data substantiate n-3 PUFA can be taken up into the DRM (raft) (see Fig. A1.1, *top panel*) as well as the DSM (non raft) (Fig. A1.1, *bottom panel*) fraction of a biological membrane. Indeed, ~30% of the uptake of EPA or DHA into EL4 cells was seen to be into DRM in earlier work (Shaikh et al. 2009). The complexity of cellular metabolism should be borne in mind here, because significant changes were detected in the levels of other fatty acids. Although the amount of DHA substantially exceeds the amount of EPA measured in both fractions, preferential incorporation of DHA cannot be inferred because the lower level of EPA comes at the expense of conversion to its elongation product DPA (Kaur et al. 2011).

3.4.4 Biological Implications

The data presented here agree with several cell culture and animal studies that show n-3 PUFA can directly infiltrate DRM, potentially impacting downstream cell

signaling (Fan et al. 2003, Shaikh et al. 2009, Kim et al. 2008, Zech et al. 2009, Rockett et al. 2011). In whole animals, we and others have established by a combination of imaging and lipidomic methods that n-3 PUFA disrupt lipid raft clustering in EL4 and primary B and T cells (Fan et al. 2003, Kim et al. 2008, Rockett et al. 2011). By showing that DHA incorporates into raftlike domains more than EPA, the results obtained on model membranes in this work advance the field by providing evidence that DHA will be more effective than EPA in modifying lipid raft organization. This observation is highly consistent with our recent studies in which treatment of EL4 cells with DHA, but not EPA, was found to perturb the clustering and size of cholera-toxin induced lipid raft clusters (Fan et al. 2003).

Considerable controversy remains on how n-3 PUFA affect the spatial organization of lipid rafts. A primary issue is whether n-3 PUFA disrupt lipid rafts or make them more ordered. On the one hand, Kim et al. (2008) proposed that n-3 PUFA can make raft domains more ordered. Using generalized polarization microscopy, these investigators reported that synapse lipid rafts of $CD4^+$ T cells from *fat-1* transgenic mice, which have high endogenous levels of n-3 PUFA, demonstrate increased order. Zech et al. (2009), on the other hand, found that n-3 PUFA treatment of Jurkat T cells significantly disrupted raft organization as determined with lipidomics and polarization imaging. The difference between systems (in vitro versus ex vivo) was offered as an explanation (Kim et al. 2010).

Our work has the potential to explain the apparent discrepancy at a molecular level. The differential in segregation between raft and nonraft domains revealed for EPA and DHA suggest that the levels of these n-3 PUFA could determine impact on lipid raft organization. For instance, it is possible that EPA-containing phospholipids upon forming nonraft domains may redistribute chol molecules toward rafts to make them more ordered within the synapse. In contrast, DHA-containing phospholipids may make rafts more disordered and could have the opposite effect on rafts by forcing chol molecules out of rafts into nonraft regions. Clearly, more data are needed on the model membrane and cellular systems to establish a complete understanding of how EPA and DHA serve to modify membrane domain organization.

Supplemental Material

Appendix A1 contains additional experimental methods, one table, four figures, and references.

Acknowledgements

This work is reprinted from Biophysical Journal, 103(2), Justin A. Williams, Shawn E. Batten, Mitchell Harris, Benjamin Drew Rockett, Saame Raza Shaikh, William Stillwell, and Stephen R. Wassall, Docosahexaenoic and Eicosapentaenoic Acids Segregate Differently between Raft and Nonraft Domains, 228-237, Copyright (2012), with permission from Elsevier.

This work was supported in part by a grant from the National Institutes of Health (No. R15AT006122 to S.R.S.).

3.5 References

Ausili A, Torrecillas A, et al. (2008) Edelfosine is incorporated into rafts and alters their organization. J Phys Chem B 112:11643–11654

Barry JA, Trouard TP, Salmon A, Brown MF (1991) Low-temperature ^{2}H NMR spectroscopy of phospholipid bilayers containing docosahexaenoyl (22:6ω3) chains. Biochemistry 30:8386-8394

Bartels T, Lankalapalli RS, Bittman R, Beyer K, Brown MF (2008) Raftlike mixtures of sphingomyelin and cholesterol investigated by solid-state ^{2}H NMR spectroscopy. J Amer Chem Soc 130:14521-14532

Bloom M, Thewalt J (1994) Spectroscopic determination of lipid dynamics in membranes. Chem Phys.Lipids 73:27-38

Bunge A, Müller P, Stöckl M, Herrmann A, Huster D (2008) Characterization of the ternary mixture of sphingomyelin, POPC, and cholesterol: support for an inhomogeneous lipid distribution at high temperature. Biophys J 94:2680-2690

Calder PC, Yaqoob P (2009) Omega-3 polyunsaturated fatty acids and human health outcomes. Biofactors 35:266-272

Chapkin RS, Kim W, Lupton JR, McMurray DN (2009) Dietary docosahexaenoic and eicosapentaenoic acid: emerging mediators of inflammation. Prost Leuk Essent Fatty Acids 81:187-91

Davis JH, Jeffrey KR, Bloom M, Valic MI, Higgs TP (1976) Quadrupolar echo deuteron magnetic resonance spectroscopy in ordered hydrocarbon chains. Chem Phys Lett 42:390-394

Davis JH (1983) The description of membrane lipid conformation, order and dynamics by ^{2}H NMR. Biochim Biophys Acta 737:117-171

Edidin M (2003) The state of lipid rafts: from model membranes to cells. Annu Rev Biophys Biomol Struct 32:257-283

Fan Y, McMurray DN, Ly LH, Chapkin RS (2003) Dietary (n-3) polyunsaturated fatty acids remodel mouse T-cell lipid rafts. J Nutr 133:1913-1920

Feller SE (2008) Acyl chain conformations in phospholipid bilayers: a comparative study of docosahexaenoic acid and saturated fatty acids. Chem Phys Lipids 153:76-80

Fetterman JW, Zdanowicz MM (2009) Therapeutic potential of n-3 polyunsaturated fatty acids in disease. Am J Health Syst Pharm 66:1169-1179

Filippov A, Orädd G, Lindblom G (2006) Sphingomyelin structure influences the lateral diffusion and raft formation in lipid bilayers. Biophys J 83:3408-3415

Harris WS, Mozaffarian D, et al. (2009) Towards establishing dietary reference intakes for eicosapentaenoic and docosahexaenoic acid. J Nutr 139:804S-819S

Heerklotz H (2002) Triton promotes domain formation in lipid raft mixtures. Biophys J 83:2693-2701

Hsueh YW, Chen MT, et al. (2007) Ergosterol in POPC membranes: physical properties and comparison with structurally similar sterols. Biophys J 92:1606-1615

Jackman CS, Davis PJ, Morrow MR, Keough KMW (1999) Effect of cholesterol on the chain-ordering transition of 1-palmitoyl-2-arachidonoyl phosphatidylcholine. J Phys Chem B 103:8830-8836

Kaur G, Sinclair AJ, Cameron-Smith D, Barr DP, Molero-Navajas JC, Konstantopoulos N (2011) Docosahexaenoic acid (22:5n-3) down-regulates the expression of genes involved in fat synthesis in liver cells. Prost Leuk Essent Fatty Acids 85:155-161

Kim W, Fan Y, Barhoumi R, Smith R, McMurray DN, Chapkin RS (2008) n-3 polyunsaturated fatty acids suppress the localization and activation of signaling proteins at the immunological synapse in murine CD4+ T cells by affecting lipid raft formation. J Immunol 181:6236-6243

Kim W, Khan NA, McMurray DN, Prior IA, Wang N, Chapkin RS (2010) Regulatory activity of polyunsaturated fatty acids in T cell signaling. Prog Lipid Res 49:250-261

Kris-Etherton PM, Harris WS, Appel LJ (2003) Fish consumption, fish oil, omega-3 fatty acids, and cardiovascular disease. Arterioscler Thromb Vasc Biol 23:e20-e30

Kučerka N, Marquardt D, et al. (2010) Cholesterol in bilayers with PUFA chains: Doping with DMPC or POPC results in sterol reorientation and membrane-domain formation. Biochemistry 49:7485-7493

Levental I, Grzybek M, Simons K (2010) Greasing their way: lipid modifications determine protein association with lipid rafts. Biochemistry 49:6305–6316

Lingwood D, Simons K (2010) Lipid rafts as a membrane-organizing principle. Science 327:46-50

McCabe MA, Wassall SR (1997) Rapid deconvolution of NMR powder spectra by weighted fast Fourier transformation. Solid State Nucl Magn Reson 10:53-61

Mihailescu M, Soubias O, Worcester D, White SH, Gawrisch K (2011) Structure and dynamics of cholesterol-containing polyunsaturated lipid membranes studied by neutron diffraction and NMR. J Membrane Biol 239:63-71

Mori TA, Bao DQ, Burke V, Puddey IB, Beilin LJ (1999) Docosahexaenoic acid but not eicosapentaenoic acid lowers ambulatory blood pressure and heart rate in humans. Hypertension 34:253-260

Niebylski CD, Salem N (1994) A calorimetric investigation of a series of mixed-chain polyunsaturated phosphatidylcholines: effect of sn-2 chain length and degree of unsaturation. Biophys J 67:2387-2393

Nui SL, Litman BJ (2002) Determination of membrane partition coefficient using a lipid vesicle-cyclodextrin binary system: effect of phospholipid acyl chain unsaturation and headgroup composition. Biophys J 83:3408-3415

Park Y, Harris W (2002) EPA, but not DHA, decreases mean platelet volume in normal subjects. Lipids 37:941-946

Petrache HI, Dodd SW, Brown MF (2000) Area per lipid and acyl chain length distributions in fluid phosphatidylcholines determined by ^{2}H NMR spectroscopy. Biophys J 78:3172-3192

Pike LJ (2006) Rafts defined: a report on the Keystone symposium on lipid rafts and cell function. J Lipid Res 17:1597-1598

Polozov I, Gawrisch K (2007) NMR detection of lipid domains. Methods Mol Biol 398:107-126

Rockett BD, Franklin A, Harris M, Teague H, Rockett A, Shaikh SR (2011) Membrane raft organization is more sensitive to disruption by (n-3) PUFA than nonraft organization in EL4 and B Cells. J Nutr 141: 1041-1048

Salem N, Kim HY, Yergey JA (1986) Docosahexaenoic acid: membrane function and metabolism. In Simopoulos AP, Kifer RR, Martin R (ed) The health effects of polyunsaturated fatty acids in seafoods. Academic Press, New York. 317-363

Salmon A, Dodd SW, Williams GD, Beach JM, Brown MF (1987) Configurational statistics of acyl chains in polyunsaturated lipid bilayers from ^{2}H NMR. J Amer Chem Soc 109:2600-2609

Shaikh SR, Brzustowicz MR, Gustafson N, Stillwell W, Wassall SR (2002) Monounsaturated PE does not phase separate from the lipid raft molecules sphingomyelin and cholesterol: role for polyunsaturation? Biochemistry 41:10593-10602

Shaikh SR, Cherezov V, Caffrey M, Stillwell W, Wassall SR (2003) Interaction of cholesterol with a docosahexaenoic acid-containing phosphatidylethanolamine. Trigger for microdomain formation? Biochemistry 42:12038-12037

Shaikh SR, Dumaual AC, et al. (2004) Oleic and docosahexaenoic acid differentially phase separate from lipid raft molecules: a comparative NMR, DSC, AFM, and detergent extraction study. Biophys J 87:1752-1766

Shaikh SR, Cherezov V, et al. (2006) Molecular organization of cholesterol in unsaturated phosphatidylethanolamines: x-ray diffraction and solid state ^{2}H NMR reveal differences with phosphatidylcholines. J Amer Chem Soc 128:5375-5383

Shaikh SR, Rockett BD, Salameh M, Carraway K (2009) Docosahexaenoic acid modifies the clustering and size of lipid rafts and the lateral organization and surface expression of MHC class I of EL4 cells. J Nutr 139:1632-1639

Shaikh SR, LoCascio DS, Soni SP, Wassall SR, Stillwell W (2009) Oleic- and docosahexaenoic acid-containing phosphatidylethanolamines differentially phase separate from sphingomyelin. Biochim Biophys Acta 1788:2421-2426

Shaikh SR (2010) Diet-induced docosahexaenoic acid nonraft domains and lymphocyte function. Prost Leuk Essent Fatty Acids 28:159-164

Soni SP, LoCascio DS, et al. (2008) Docosahexaenoic acid enhances segregation of lipids between raft and nonraft domains: ^{2}H NMR study. Biophys J 95:203-214

Soni SP, Ward JA, Sen SE, Feller SE, Wassall SR (2009) Effect of trans unsaturation on molecular organization in a phospholipid membrane. Biochemistry 48:11097-11107

Soubias O, Gawrisch K (2007) Docosahexaenoyl chains isomerize on the sub-nanosecond time scale. J Amer Chem Soc 129:6678-6679

Stillwell W, Wassall SR (2003) Docosahexaenoic acid: membrane properties of a unique fatty acid. Chem Phys Lipids 126:1-27

Vemuri M, Kelley DS, Mackey BE, Rasooly R, Bartolini G (2007) Docosahexaenoic acid (DHA) but not eicosapentaenoic acid (EPA) prevents trans-10, cis-12 conjugated linoleic acid (CLA)-induced insulin resistance in mice. Metab Syndr Relat Disord 5:315–322

Wassall SR, Stillwell W (2008) Docosahexaenoic acid domains: the ultimate non raft membrane domain. Chem Phys Lipids 153:57-63

Wassall SR, Stillwell W (2009) Polyunsaturated fatty acid-cholesterol interactions: domain formation. Biochim Biophys Acta 1788:24-32

Wassall SR, McCabe MA, Wassall CD, Adlof RO, Feller SE (2010) Solid state ^{2}H NMR and MD simulations of positional isomers of a monounsaturated phospholipid membrane: structural implications of double bond location. J Phys Chem B 114:11474-11483

Yaqoob P, Shaikh SR (2010) The nutritional and clinical significance of lipid rafts. Curr Opin Clin Nutr Metab 13:156-166

Zech T, Ejsing C, et al. (2009) Accumulation of raft lipids in T-cell plasma membrane domain engaged in TCR signaling. EMBO J 28:466-476

CHAPTER 4: AN EPR METHOD FOR MEASURING THE AFFINITY OF A SPIN LABELED ANALOG OF CHOLESTEROL FOR PHOSPHOLIPIDS

4.1 Introduction

The concentration of cholesterol (chol) in cellular membranes, which may be as much as 45 mol% of total lipid in mammalian membranes (Yeagle 1993), plays a crucial role in controlling the physical properties and biological function of the membrane (Ohvo-Rekilä et al. 2002; Silvius 2003). Alteration of membrane features and events is primarily a consequence of the sterol's interaction with neighboring lipids and proteins. Unequal affinity of chol for different lipids is potentially a driving factor in promoting the sorting of membrane lipids into patches or domains of specific composition (Lingwood and Simons 2009). The purpose of the domains is to provide a local environment necessary for the function of resident proteins (Leventhal et al. 2010). Here we describe a novel electron paramagnetic resonance (EPR) method for measuring the affinity of a spin labeled analog of chol for lipids and present results obtained on phospholipids with increasing levels of acyl chain unsaturation to illustrate the utility of the method.

Chol is a mostly nonpolar molecule that consists of a tetracyclic ring structure with a hydroxyl group at one end and a short hydrocarbon tail at the other (Fig. 4.1). It usually resides in membranes so that the hydroxyl group sits just below the aqueous interface while the short chain extends towards the center of the bilayer, the long molecular axis lining-up approximately parallel to the fatty acyl chains of lipid molecules (Khelashvili and Harries 2013). This arrangement places the rigid planar ring system of the steroid moiety at the same depth as the upper portion of adjacent lipid acyl chains and impedes isomerization between trans and gauche conformations of C-C bonds. The restriction to chain motion leads to an increase in molecular packing, thickness and mechanical rigidity for the membrane (McMullen et al. 2004). Preferential affinity for chol is conferred upon saturated lipids because the extended conformation adopted by saturated chains is compatible with close proximity to the rigid steroid

moiety and allows for strong van der Waals interactions (Brown 1998). A tendency for saturated lipids to segregate into domains with chol is a consequence. The tendency is enhanced in the case of sphingolipids by hydrogen bonding between the hydroxyl group on the sterol and the amide on the sphingosine backbone. Lipid rafts, domains 10-200 nm in size enriched in sphingolipids "glued" together by chol (Pike 2006), are purported to serve as the platform for signaling proteins in the outer leaflet of plasma membranes (Simons and Ikonen 1997, Brown and London 2000). Phospholipids containing polyunsaturated fatty acids (PUFA) represent the opposite extreme to sphingolipids with predominantly saturated chains. The shallow energy barrier to rotation about C-C bonds in the repeating =C-C-C= unit in a PUFA chain produces a multitude of rapidly changing conformations that push chol away and drive the formation of membrane domains rich in PUFA-containing phospholipids but depleted in the sterol (Wassall and Stillwell 2009). These (non-raft) domains are organizationally the antithesis of rafts and, we have hypothesized, are responsible in part for the diverse range of health benefits attributed to dietary consumption of PUFA in fish oils.

There is an immense diversity of natural lipids (Yeagle 1993). The charge, size and ability to hydrogen bond of the head groups vary while the chains vary in length and degree of unsaturation. These variations produce differing affinities for chol that are potentially significant enough to generate lateral membrane segregation in biological systems (Silvius 2003). Chol's affinity for different membrane compositions has been investigated by a variety of techniques. An early approach was to measure the partitioning of chol between large (LUV) and small (SUV) unilamellar vesicles prepared from different lipids (Yeagle and Young 1986). LUV containing chol were incubated with SUV or LUV were incubated with SUV containing chol and then separated on the basis of size. The relative affinity of the two lipids for the sterol was determined from the equilibrium distribution of chol between the two sizes of vesicle. Subsequent work used methyl-β-cyclodextrin (mβCD) to facilitate the exchange of chol between donor and acceptor LUV that were separable due to the charge on phosphatidylgylcerol (PG) included in the donor vesicles (Leventis and Silvius 2001). MβCD is a ring-shaped molecule consisting of 7 glucose units that is soluble in water but possesses a hydrophobic cavity capable of reversibly binding small hydrophobic molecules such as chol. By extracting membrane-bound chol from donor vesicles and forming a water-soluble complex that transfers the sterol to acceptor vesicles, the time

taken to reach equilibrium was reduced (López et al. 2011). A later refinement was to measure the partitioning of chol solely between mβCD and LUV, thereby avoiding the mixing of donor and acceptor lipid species, and affinity among differing lipids could then be compared indirectly using mβCD as a reference (Nui and Litman 2002; Halling et al. 2008). MβCD (~1 nm in size) and LUV (100 nm in diameter) were separated after equilibration by centrifugation across a filter and the concentration of chol was assayed enzymatically or with a radiolabeled tracer. The necessity to physically separate vesicles and mβCD, which has the potential to introduce artifacts, was eliminated by an application of isothermal titration calorimetry (ITC) (Tsamaloukas et al. 2005). In this method an estimate of the partitioning of chol between LUV and mβCD was obtained from an analysis of power compensation due to the heat of reaction recorded after each of a series of injections of LUV containing chol into an aqueous solution of mβCD (release protocol) and of LUV into an aqueous solution containing mβCD-chol complexes (uptake protocol). The same advantage was shared by another method that directly determined the distribution of cholestatrienol (CTL), a fluorescent analog of chol, between mβCD and LUV from measurements of the steady state anisotropy (Nyholm et al. 2010). This fluorescence experiment is the inspiration for the current study.

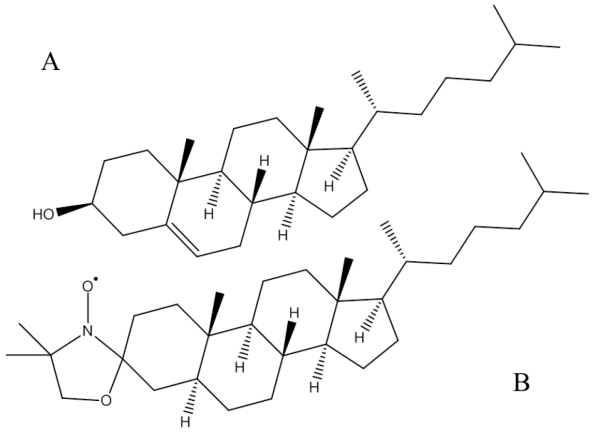

Figure 4.1 Molecular structure of cholesterol (chol) (A) and 3β-doxyl-5α-cholestane (chlstn) (B).

We introduce an EPR method to add to the arsenal of techniques for investigating the partitioning of chol among lipids. EPR spectra for 3β-doxyl-5α-cholestane (chlstn), a spin labeled analog of chol (Fig. 4.1) that is commercially available, incorporated into LUV are distinguished from the EPR spectrum for chlstn complexed with mβCD due to the motional inequivalence of the two environments. Exploiting this property it is straightforward to calculate the ratio of the

population of chlstn partitioned between LUV and mβCD at equilibrium by spectral simulation without separating the fractions. Partition coefficients measured for chlstn in this work are compared with results obtained by other methods to demonstrate that the relative affinity of the spin labeled analog for different lipids matches chol. Measurements made on phosphatidylcholine (PC) LUV are then reported that support the hypothesis of a decreased sterol affinity with increasing acyl chain unsaturation that could influence lateral organization within a membrane.

4.2 Materials and Methods

4.2.1 Materials

3β-doxyl-5α-cholestane (chlstn), cholesterol (chol) and methyl-β-cyclodextrin (mβCD) were purchased from Sigma-Aldrich (St. Louis, MO). Fisher Scientific (Pittsburgh, PA) was the source for butylated hydroxyl toluene (BHT). The phospholipids 1-palmitoyl-2-oleoyl-*sn*-glycero-3-phosphocholine (16:0-18:1PC, POPC), 1-palmitoyl-2-linoleoyl-*sn*-glycero-3-phosphocholine (16:0-18:2PC, PLPC), 1-palmitoyl-2-docosahexaenoyl-*sn*-glycero-3-phosphocholine (16:0-22:6PC, PDPC) and 1,2-dioleoyl-*sn*-glycero-3-phosphocholine (18:1-18:1PC, DOPC) were obtained from Avanti Polar Lipids (Alabaster, AL) and were used without further purification.

4.2.2 Sample Preparation

4.2.2.1 LUV

Stock solutions of PC lipid and chlstn in chloroform were mixed in appropriate volumes. The lipid was dried under a gentle stream of argon and the film produced was placed under vacuum overnight to evaporate remaining traces of solvent. Sample mass was then checked. After hydration with buffer (100 mM NaCl/10 mM Tris, pH 7.4), four freeze-thaw cycles were completed and LUV were created by extrusion: 25 passes across a 100 nm nucleopore Whatman track-etched filter performed with an Avanti mini-extruder. Samples were protected from oxidation by the addition of BHT (1 BHT: 250 PC lipids) and manipulations were performed in an argon atmosphere.

4.2.2.2 MβCD-Chlstn Complex

To produce a mβCD-chlstn complex, chlstn was dried upon the bottom of a test tube and a mβCD PBS solution was added. The solution was subsequently sonicated at 65°C until the chlstn film was visibly removed from the glass.

4.2.3 Partitioning Experiments

4.2.3.1 EPR

We have performed partitioning experiments between LUV and mβCD using both uptake and release protocols. For release experiments, chlstn originates with and partitions from LUV to mβCD initially free of sterol. For uptake experiments, LUV free of sterol were introduced into a solution containing mβCD-chlstn complex. Fig. 4.2 shows a cartoon representation of the two types of experiment.

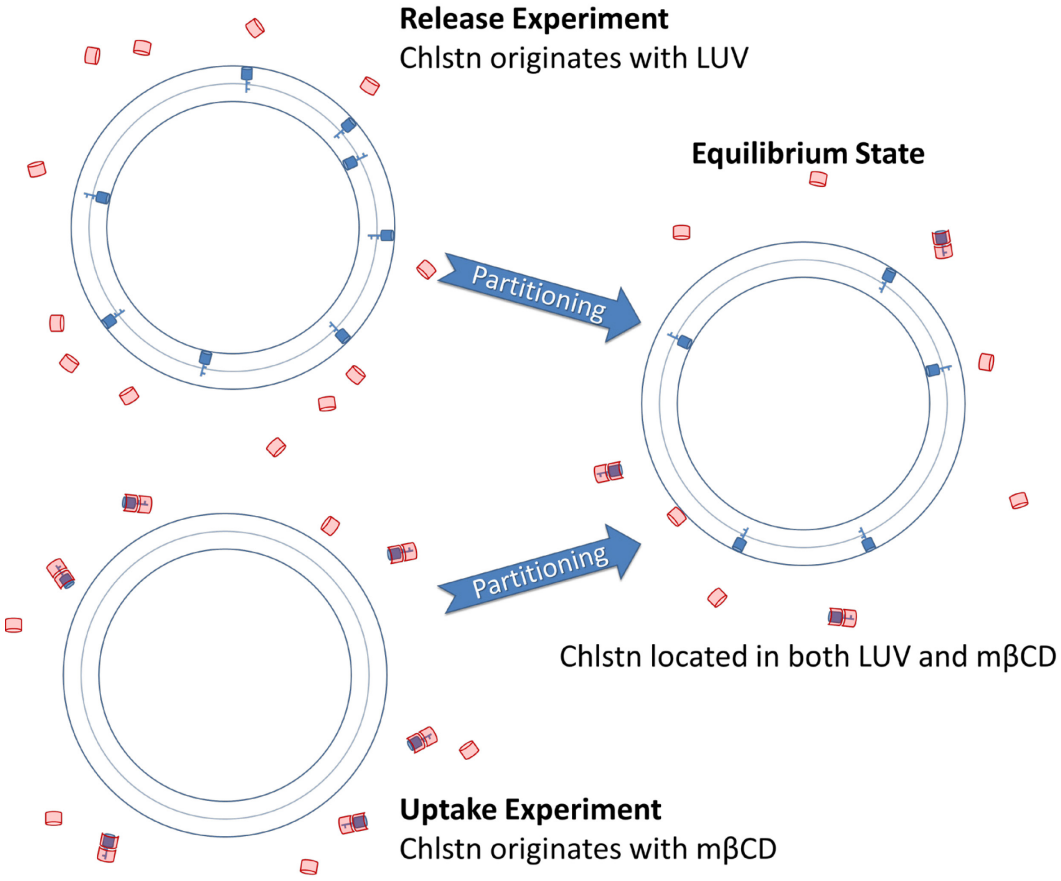

Figure 4.2 Cartoon of uptake and release experiments. A single LUV and multiple mβCD are depicted.

The partitioning of chlstn between LUV and mβCD is characterized by partition coefficients calculated according to the model derived by Tsamaloukas et al. (2005)

$$K_x = \frac{C_{chlstn}^{LUV}\left(C_{m\beta CD} - 2C_{chlstn}^{m\beta CD}\right)^2}{\left(C_{LUV} - C_{chlstn}^{LUV}\right)C_{chlstn}^{m\beta CD}}. \quad (1)$$

In this expression, K_x is the hybrid mole partition coefficient, where the molar concentration at equilibrium for chlstn in LUV, chlstn bound by mβCD, total mβCD, and total PC are denoted as C_{chlstn}^{LUV}, $C_{chlstn}^{m\beta CD}$, $C_{m\beta CD}$, and C_{LUV} respectively. The model assumes a stoichiometry of 2:1 for the mβCD-chlstn complex and accounts for the decrease in free mβCD due to binding with chlstn. A maximum uncertainty less than ±20% applies to the values derived for K_x.

Release experiments, in which mβCD was added to a suspension of LUV containing chlstn, were designed to achieve a partitioning solution composition of 15 mM PC, 0.152 mM chlstn and a variable amount of mβCD. The concentration of chlstn, which corresponds to 1 mol% relative to phospholipid, was chosen to minimize magnetic (dipole-dipole and spin exchange) interactions between spin labels (Sackmann and Traüble 1972). Four trials were performed for each phospholipid with mβCD concentrations of 4, 5, 6, and 7 mM. Partitioning solutions were incubated at 37°C on a shaker for one hour to reach an equilibrium distribution. In uptake experiments, where mβCD-chlstn complex was added to LUV free of chlstn, the partition solution consisted of 15 mM PC, 0.152 mM chlstn, and 5 mM mβCD. This solution was then incubated in the same manner as in the release experiment.

To measure the partitioning of chlstn between LUV and mβCD by EPR, equilibrated samples were transferred to 25 µL fused silica capillaries that were sealed with Critoseal clay and inserted into the temperature controlled (37 °C) rectangular TE_{102} cavity of a Bruker (Billerica, MA) X-band ESP 300 EPR spectrometer operating at 9.29 GHz. Experimental EPR parameters were microwave power, 12.6 mW; field center, 3300 G; sweep width, 100 G; sweep time, 83.89 s; time constant, 655.4 ms; modulation amplitude, 1 G; and dataset, 1000 points. The signal detected was the first derivative of the absorption spectrum composed of three resonances characteristic of the hyperfine coupling between the unpaired electron and ^{14}N nuclear spin of the doxyl label (Marsh 1981). Four scans were taken per sample and averaged. The spectra were normalized according to the double integral, which is proportional to concentration of chlstn.

Reference spectra for each lipid at 15 mM PC with 0.152 mM (1 mol%) chlstn and for 5 mM mβCD with 0.152 mM chlstn were recorded. The percentages of chlstn located in LUV and mβCD at equilibrium were then determined with a spectral fitting procedure that will be explained in the Results.

4.3.3.2 ITC

For purposes of comparison, ITC measurements of the partitioning of chol between LUV and mβCD were performed. A brief description of the experimental method can be found in Appendix A2.

4.4 Results

4.4.1 Measurement of K_x by EPR

The basis of our approach to measuring the partition coefficient K_x of chlstn between LUV and mβCD may be understood by inspecting the EPR spectra presented in Fig. 4.3. Representative EPR spectra obtained for chlstn incorporated within POPC LUV (Fig. 4.3A) and bound to mβCD (Fig. 4.3B) demonstrate that the spectral shape depends upon whether the spin label is located within LUV or in complex with mβCD.

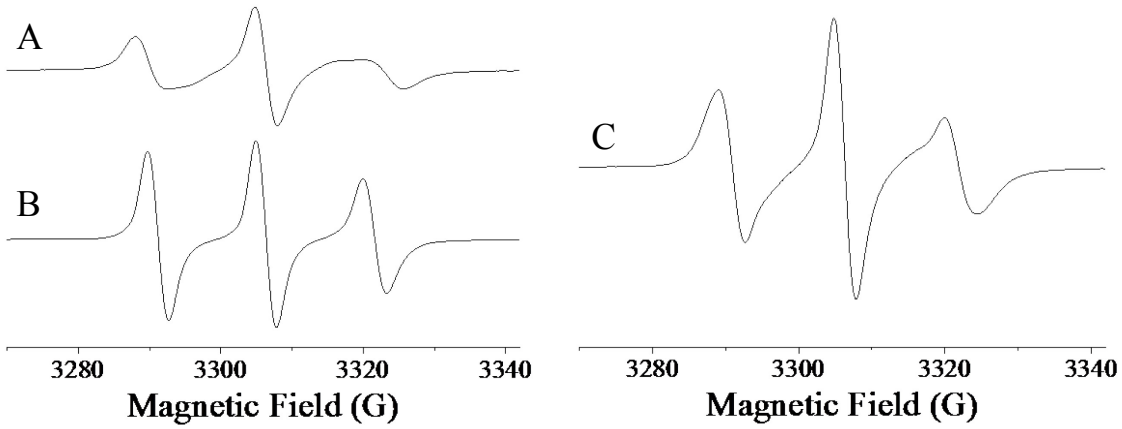

Figure 4.3 Representative reference EPR spectra for chlstn within POPC LUV (A) and in complex with mβCD (B); and an experimental spectrum from a partition (uptake) experiment where chlstn is present both in complex with mβCD and incorporated into POPC LUV (C). A fit of spectrum C that was obtained from a combination of spectra A and B scaled in relative intensity is shown in Fig. A2.1 in Appendix A2. Spectra were recorded at 37 °C. Composition of samples were 15 mM POPC with 0.152 mM (1 mol%) chlstn (A), 5 mM mβCD with 0.152 mM chlstn (B) and 15 mM POPC, 0.152 mM chlstn with 5 mM mβCD (C).

On the timescale to which EPR of a nitroxide group is sensitive (10^{-11} - 10^{-7} s), the tumbling of LUV is too slow to produce motional narrowing so that the spectrum for a spin labeled lipid in LUV is a powder pattern comprised of a superposition of spectra from membranes in a spherically symmetric distribution of orientations (Schreier et al. 1978). The resultant spectrum has broad high and low field absorption peaks that are characteristic of the fast anisotropic motion undergone by chlstn within a membrane (Fig. 4.3A). While bound to mβCD, in contrast, chlstn experiences isotropic motion because the MβCD-chlstn complex is very much smaller than LUV and tumbles rapidly in solution. The resulting spectrum (Fig. 4.3B) has high and low field peaks that are substantially narrower compared to the LUV-chlstn spectrum. In a partitioning experiment chlstn resides in both mβCD and LUV. The spectrum obtained is then a superposition of spectra from both environments that are population-weighted in intensity, as illustrated by the spectrum that was recorded in an uptake experiment when POPC LUV were equilibrated with mβCD-chlstn complex (Fig. 4.3C). There the presence of two spectral components is most evident in the appearance of the high field peak that is comprised of a sharp signal due to chlstn bound to mβCD superposed upon a broad component due to chlstn incorporated into LUV.

Our procedure for determining K_x entails simulating a spectrum that reproduces the EPR spectrum observed in a partitioning experiment. Spectra recorded for chlstn in LUV prepared from the same lipid as the partitioning experiment and in the mβCD complex separately were combined for the full range of relative intensity between a fractional intensity of 1 for LUV and 0 for mβCD to 0 for LUV and 1 for mβCD in 0.0001 increments. The combination that most accurately reproduces the mixed spectrum of the partitioning experiment was next assessed according to a least squares criterion. Specifically, the difference between the simulation and experiment for each data point was squared and summed over the entire spectrum and the combination with the smallest sum was deemed to be the best fit. The relative intensity of spectra leading to the best fit is equivalent to the ratio of the concentration of chlstn in LUV and mβCD in the mixed sample, from which a value for K_x was calculated via Eq. 1. Figure A2.1 in Appendix A2 provides an example of the quality of fit achieved for the spectrum shown in Figure 4.3C that was obtained in an uptake experiment where chlstn (0.152 mM) originally bound to mβCD (5mM) was incubated with POPC LUV (15 mM). Based on this best fit 73% of the total

chlstn was found to be taken up into the LUV, which coincides with a value of K_x = 4.3 mM for POPC.

4.4.2 Acyl Chain Unsaturation

To illustrate the utility of our EPR method, we report K_x values measured for chlstn in PC membranes with differing amounts of acyl chain unsaturation. Reference spectra for chlstn in LUV prepared from all of the lipids under consideration are plotted in Fig. 4.4, arranged from most unsaturated lipid (PDPC–with 6 double bonds, top) to least (POPC with 1 double bond, bottom).

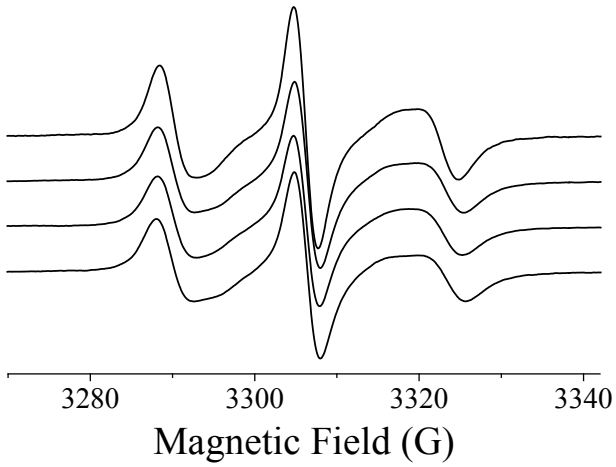

Figure 4.4 LUV reference spectra of 15 mM PC with 1 mol% chlstn at 37 °C, arranged from bottom to top: POPC, DOPC, PLPC and PDPC.

The spectral shape in DOPC, PLPC and PDPC is very similar to in POPC. A slight narrowing of resonances at higher levels of unsaturation is apparent on close inspection that corresponds to a reduction in the degree of anisotropy for the motion of chlstn in a more disordered membrane interior. These LUV reference spectra were used in the same manner as described for POPC to fit spectra recorded in partition experiments conducted on their respective lipid species. The values of K_x determined for chlstn are given in Table 4.1. They are an average from uptake experiments, where mβCD was the donor and LUV were the acceptor, and release experiments, where LUV were the donor and mβCD was the acceptor. Results from the two types of experiment, which agree within experimental uncertainty, can be found in Table A2.1 in Appendix A2.

Table 4.1 Partition coefficients K_x and partition coefficients K_B^A relative to POPC measured by EPR for chlstn at 37 °C. The K_x values and uncertainties in K_x are an average of the results from release and uptake experiments found in Table A2.1 of Appendix A2. The error in K_B^A includes the uncertainty in K_x for POPC as well as for PLPC, PDPC or DOPC.

Lipid	K_x (mM)	K_B^A
POPC	4.4 ± 0.4	1
PLPC	3.4 ± 0.3	0.77 ± 0.14
PDPC	2.2 ± 0.4	0.50 ± 0.14
DOPC	2.6 ± 0.4	0.59 ± 0.14

Comparing POPC, PLPC and PDPC, all having saturated palmitoyl sn-1 chains, a trend towards reduced affinity for chlstn is seen to accompany an increasing level of unsaturation in the sn-2 chain. POPC (K_x = 4.4 ± 0.4 mM) with one carbon-carbon double bond has a K_x value twice as large as PDPC (K_x = 2.2 ± 0.4 mM) with six double bonds. Comparing POPC and DOPC (K_x = 2.6 ± 0.4 mM), furthermore, less favorable interaction with chlstn is seen to follow the introduction of an unsaturation into the sn-1 chain.

4.5 Discussion

There has been considerable interest in chol's ability to affect lateral organization within cellular membranes and in the molecule's non-uniform distribution among membranes. One mechanism thought to be influential is variation in the molecular interaction of the sterol with different lipid species. This view has been the motivation behind numerous studies of the affinity of chol for lipids by a range of experimental techniques. The best approach that has been developed so far is to measure the equilibrium partitioning of chol between LUV and mβCD, from which a determination of relative affinity between lipids may be made. Various methods, each with a set of pros and cons, have been used to estimate the concentration of sterol in the two environments. A problem with the methods involving physical separation of mβCD from LUV prior to measurement by enzymatic assay (Nui and Litman 2002) or quantitation with a radiotracer (Halling et al. 2008) is that the equilibrium partitioning may be altered during centrifugation. The ITC method that monitors the heat of reaction due to the exchange of chol between LUV and mβCD (Tsamaloukas et al. 2006) eliminates this step and arguably has the potential to set the "gold standard" for measurement. However, care has to be taken in

choosing a concentration window where large amounts of phospholipid are not extracted by mβCD and in our experience can be extremely time consuming to achieve. The reliance on a probe that is not commercially available is a drawback of the much quicker technique based upon measurement of the steady state polarization of CTL (Nyholm et al. 2010) that also avoids the need to centrifuge.

We have devised a new EPR method that measures the equilibrium distribution of chlstn between LUV and mβCD. This spin labeled analog of chol has been extensively employed in studies of molecular organization and dynamics in membranes (Raguz et al 2011). Other analogs should work equally well. 25-doxyl-cholesterol that better mimics chol (Scheidt et al 2003), for instance, is an appealing alternative but unavailable commercially. The distinction in the shape of EPR spectra for chlstn incorporated in LUV (Fig. 4.3A) vs. bound to mβCD (Fig. 4.3B), which is depicted in Fig. 4.3 for POPC, is at the heart of our method. Our procedure entails incubating chlstn in mβCD as the donor with LUV as the acceptor (uptake experiment) or, vice-versa, chlstn in LUV as the donor with mβCD as the acceptor (release experiment). An estimate of the equilibrium distribution of chlstn between donor and acceptor is then ascertained from the resultant spectrum by adding the spectra recorded for chlstn individually in the two environments and scaling their relative intensity to provide a best fit as judged by a least squares analysis. The fit to the spectrum obtained for POPC in an uptake experiment (Fig. 4.3C) by this process, which identified 0.73 vs. 0.27 as the ratio of chlstn in LUV and mβCD (corresponding to K_x = 4.3 mM), may be found in Appendix A2 (Fig. A2.1).

Partition coefficients K_x measured for POPC by EPR and other methods are compiled in Table 4.2. It is immediately apparent that the partition coefficient determined for chlstn (K_x = 4.4 ± 0.4 mM) is an order of magnitude less than the range of values (K_x = 32 - 49 mM) obtained for chol. The smaller value of K_x is predominantly ascribed to differential interaction of the spin labeled molecule with mβCD. Greater affinity for mβCD, together with the more polar nature of the fluorescently labeled analog, was invoked to account for the comparably small partition coefficient that was reported for CTL ($K_x = 5.0 \pm 0.9$ mM) (Nyholm et al. 2010).

Table 4.2 Equilibrium partition coefficients (K_x) measured for chol and analogs of chol between POPC LUV and mβCD at 37°C. Values taken from [1]Nui and Litman (2002), [2]Halling et al. (2008), [3] Tsamaloukas et al. (2005), [4]Ekholm et al. (2011) and [5]this study (Table 4.1). The value quoted for Nui and Litman was recalculated from their data assuming a 1:2 ratio for the stoichiometry of the chol/mβCD complex.

Method	K_x (mM)
Physical Separation, chol (enzyme assay)[1]	49 ± 4
Physical Separation, chol (^{3}H radiolabel)[2]	32 ± 2
ITC, chol[3]	37 ± 7
Fluorescence, CTL[4]	5.9 ± 0.9
EPR, chlstn[5]	4.4 ± 0.4

We suggest that in the case of chlstn, which unlike CTL is less polar than chol, greater exposure to mβCD contributes to the reduction in value for K_x. Specifically, the bulky doxyl group in the spin labeled analog that replaces the OH group in chol (Fig. 4.1) protrudes into the lipid-water interface (Scheidt et al. 2003), making extraction by mβCD at the membrane surface easier.

A relative partition coefficient K_B^A (lipid A relative to lipid B) that is independent of mβCD can be calculated by taking the ratio

$$K_B^A = \frac{K_x^A}{K_x^B} \quad (2)$$

of partition coefficients K_X^A and K_X^B measured in individual assays with LUV prepared from the two lipids (A and B, respectively) (Nui and Litman 2002). The associated change in free energy of chol partitioning between the two types of vesicle is then given by

$$\Delta G = -RTlnK_B^A \quad (3)$$

where R is the universal gas constant and T is temperature. Fig. 4.5 compares partition coefficients derived according to Eq. 2 for chlstn and chol from EPR and ITC experiments, respectively, on DOPC and PDPC relative to POPC.

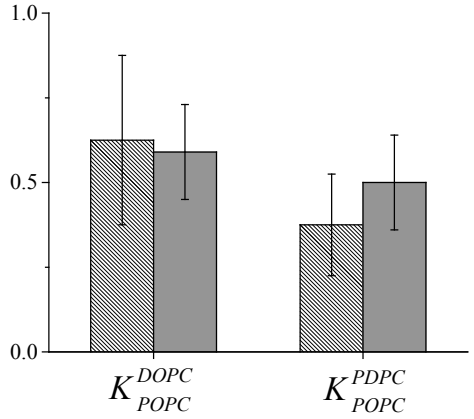

Figure 4.5 Comparison of relative partition coefficients (K_B^A) obtained for chlstn ▭ by EPR and chol ▨ by ITC. Experiments conducted at 37°C. The values for K_B^A for chlstn are taken from Table 4.1 and for chol are taken from Table A2.2 in Appendix A2. The error in K_B^A includes the uncertainty in K_x for POPC as well as for PDPC or DOPC.

They agree within experimental uncertainty (K_{POPC}^{DOPC} = 0.59 ± 0.14 vs. 0.63 ± 0.25 and K_{POPC}^{PDPC} = 0.50 ± 0.14 vs. 0.38 ± 0.15 for chlstn vs. chol), indicating that chlstn and chol share the same relative affinity for different lipids and validating the EPR method. It would be interesting in subsequent work to compare measurements involving more ordered, saturated lipids such as sphingomyelin as a further test.

The results obtained in experiments performed on phospholipids possessing different levels of acyl chain unsaturation to demonstrate the applicability of the EPR method are consistent with unfavorable interaction between chol's tetracyclic ring and acyl chain double bonds. The partition coefficients (K_x and K_B^A relative to POPC calculated via Eq. 2) listed in Table 4.1 confirm that affinity for chlstn is reduced when the number of double bonds in the sn-2 chain increases (POPC > PLPC > PDPC) and when the saturated sn-1 chain is replaced with an unsaturated chain (POPC > DOPC) (Nui and Litman 2002). Invoking Eq. 3, the respective reductions in partition coefficient for PDPC and DOPC correspond to an energy barrier $\Delta G = 1.8$ kJ/mol for the exchange of chlstn between POPC and PDPC and $\Delta G = 1.4$ kJ/mol for the exchange of chlstn between POPC and DOPC. That the free energy barrier for DOPC with just a single extra double bond in the sn-1 chain is only slightly less than PDPC with an extra 5 double bonds in the sn-2 chain implies chol preferentially associates with the saturated sn-1 chain in mixed-chain

phospholipids with PUFA at the sn-2 position. This finding corroborates experimental and computer-modeling studies on saturated-polyunsaturated PC membranes. A tendency to locate next to the saturated stearoyl sn-1 chain was inferred from solid state ^{2}H NMR spectra for [3α-$^{2}H_1$]cholesterol revealing that the tilt angle of the sterol is insensitive to the presence of polyunsaturation at the sn-2 position (Brzustowicz et al. 1999), a view supported by a higher rate of chain-to-cholesterol nuclear Overhauser enhancement cross-relaxation that was detected in ^{1}H MAS NMR experiments on 1-stearoyl-2-docosahexaenoylphosphatidylcholine (SDPC)/[25,26,26,26,27,27,27-$^{2}H_7$]cholesterol membranes (Huster et al. 1998) and by molecular dynamics (MD) simulations on a SDPC/cholesterol bilayer in which the sterol prefers solvation by saturated over polyunsaturated chains (Pitman et al. 2004).

In summary, we have established a new method for measuring the relative affinity of chol for different lipids. The method is quick and straightforward. K_x values describing the partitioning of chlstn between LUV and mβCD are directly determined from EPR spectra without the potentially artifact inducing step of physically separating LUV and mβCD fractions. The partitioning coefficient K_B^A between two lipids derived from the ratio of K_x obtained with the spin label analog reliably reflects the relative affinity of chol for the lipids. Measurements made on phospholipids with differing degrees of acyl chain unsaturation demonstrate chlstn prefers to associate with saturated chains and to avoid increasingly unsaturated chains, which is consistent with a propensity for lipids to be driven into membranes domains enriched or depleted in chol according to the compatibility of their molecular structure. Future work is planned to explore how affinity for chol is affected by other facets of the structure of phospholipid molecules such as the location and type of double bond.

Supplemental Material

Appendix A2 contains a brief description of ITC method, an example of the fit of an EPR spectrum, and uptake and release results from EPR and ITC experiments.

Acknowledgement

This work is a reprint of published material. Springer and The Journal of Membrane Biology, 246(9), 2013, 689-696, An Electron Paramagnetic Resonance Method for Measuring the Affinity of a Spin-Labeled Analog of Cholesterol for Phospholipids, Justin A. Williams, Cynthia D. Wassall, Marvin D. Kemple, and Stephen R. Wassall; with kind permission from Springer Science and Business Media. The final publication is available at http://link.springer.com, DOI: 10.1007/s00232-013-9586-z.

4.6 References

Brown RE (1998) Sphingolipid organization in biomembranes: what physical studies of model membranes reveal. J. Cell Sci 111:1-9

Brown DA, London E (2000) Structure and function of sphingolipid and cholesterol-rich membrane rafts. J Biol Chem 275:17221-17224

Brzustowicz MR, Stillwell W, Wassall, SR (1999) Molecular organization of cholesterol in polyunsaturated phospholipid membranes: a solid state ^{2}H NMR investigation FEBS Lett 451:197-202

Ekholm O, Jaikishan S, Lönnfors M, Nyholm TKM, Slotte JP (2011) Membrane bilayer properties of sphingomyelins with amide-linked 2- or 3-hydroxylated fatty acids. Biochim Biophys Acta 1808: 727-732

Halling KK, Ramstedt B, Nyström JH, Slotte JP, Nyholm TKM (2008) Cholesterol interactions with fluid-phase phospholipids: effect on the lateral organization of the bilayer. Biophys J 95:3861-3871

Huster D, Arnold K, Gawrisch, K (1998) Influence of docosahexaenoic acid and cholesterol on lateral lipid organization in phospholipid mixtures. Biochemistry 37:17299–17308

Khelashvilia G, Harries D (2013) How sterol tilt regulates properties and organization of lipid membranes and membrane insertions. Chem Phys Lipids 169:113-123

Levental I, Grzybek M, Simons K (2010) Greasing their way: lipid modifications determine protein association with membrane rafts. Biochemistry 49:6305–6316

Leventis R, Silvius JR (2001) Use of cyclodextrins to monitor transbilayer movement and differential lipid affinities. Biophys J 81:2257-2267

Lingwood D, Simons K (2009) Lipid rafts as a membrane organizing principle. Science 327:46-50

López CA, de Vries AH, Marrink SJ (2011) Molecular mechanism of cyclodextrin mediated cholesterol extraction. PLoS Comput Biol 7:e1002020

Marsh D (1981) Electron spin resonance: spin labels. In: Grell E (ed) Membrane spectroscopy, Springer-Verlag, Berlin, pp 51-142

McMullen TPW, Lewis RNAH, McElhaney RN (2004) Cholesterol-phospholipid interactions, the liquid-ordered phase and lipid rafts in model and biological membranes. Curr Opin Collioid Int Sci 8:459-468

Nui SL, Litman BJ (2002) Determination of membrane cholesterol partition coefficient using a lipid vesicle-cyclodextrin binary system: effect of phospholipid acyl chain unsaturation and headgroup composition. Biophys J 83: 3408-3415

Nyholm TKM, Grandell PM, Westerlund B, Slotte JP (2010) Sterol affinity for bilayer membranes is affected by their ceramide content and ceramide chain length. Biochim Biophys Acta 1798:1008-1013

Ohvo-Rekilä H, Ramstedt B, Leppimäki P, Slotte JP (2002) Cholesterol interactions with phospholipids in membranes. Prog Lipid Res 41:66-97

Pike LJ (2006) Rafts defined: a report on the Keystone symposium on lipid rafts and cell function. J. Lipid Res. 17:1597-1598

Pitman MC, Suits F, MacKerell Jr AD, Feller SE (2004) Molecular-level organization of saturated and polyunsaturated fatty acids in a phosphatidylcholine bilayer containing cholesterol. Biochemistry *43*:15318–15328

Raguz M, Mainali L, Widomska J, Subczynski K (2011) Using spin-label electron paramagnetic resonance (EPR) to discriminate and characterize the cholesterol bilayer domain. Chem Phys Lipids 164:819-829

Sackmann E, Traüble H (1972) Studies of the crystalline-liquid crystalline phase transition of lipid model membranes. I. Use of spin labels and optical probes as indicators of the phase transition. J Amer Chem Soc 94:4482-4491

Scheidt HA, Muller P, Herrmann A, Huster D (2003) The potential of fluorescent and spin-labeled steroid analogs to mimic natural cholesterol. J Biol Chem 46:45563-45569

Schreier S, Polnaszek CF, Smith ICP (1978) Spin labels in membranes: Problems in practice. Biochim Biophys Acata 515:375-436

Silvius J (2003) Role of cholesterol in lipid raft formation: lessons from lipid model systems. Biochim Biophys Acta 1610:174-183

Simons K, Ikonen E (1997) Functional rafts in cell membranes. Nature 387:569-572

Tsamaloukas A, Szadkowska H, Slotte PJ, Heerklotz H (2005) Interactions of cholesterol with lipid membranes and cyclodextrin characterized by calorimetry. Biophys J 89:1109-1119

Wassall SR, Stillwell W (2009) Polyunsaturated fatty acid–cholesterol interactions: Domain formation in membranes. Biochim Biophys Acta 1788:24-32

Yeagle PL, Young JE (1986) Factors contributing to the distribution of cholesterol among phospholipid vesicles. J Biol Chem 261:8175-8181

Yeagle PL (1993) The membranes of cells, 2nd edition. Academic Press, Orlando

CHAPTER 5: CONCLUSIONS

The focus of this work has concerned how PUFA-containing lipids, through interaction with chol, can potentially influence membrane structure. Solid state ^{2}H NMR was used to identify differences in the nature of domain formation between PC containing ω-3 PUFA, EPA or DHA, within PC/SM/chol mixtures in reference to a monounsaturated-PC control mixture (Williams et al. 2012). Additionally, a new technique was developed for measuring chol-lipid affinity utilizing EPR and a spin labeled analog of chol (3β-doxyl-5α-cholestane); from which a hierarchy, supported by ITC data, of chol-lipid affinity was established among PC lipids with varying degrees of unsaturation (Williams et al. 2013). This final chapter will summarize findings from these experiments and suggest directions for future research.

Central to this work is the hypothesis, that chol's incompatibility with close proximity to PUFA could incite lateral segregation within biomembranes and the formation of highly disordered domains which are rich in PUFA-containing lipids but depleted in chol (Wassall and Stillwell 2009). Chol is thought to be enriched in lipid rafts with high SM content (Simons and Ikonen 1997), driven there by its well-documented affinity for SM over PC or PE lipids (Demel et al. 1977). Chol affinity for varying levels of lipid unsaturation has been less extensively studied. PUFA chains are weakly interacting; thus, accumulation of polyunsaturated lipids into liquid-disordered domains would be motivated, not by self-attraction, but primarily by PUFA-chol aversion.

In Chapter 4, as an extension of the many chol-lipid affinity investigative schemes that have come before (Yeagle and Young 1986, Leventis and Silvius 2001, Nui and Litman 2002, Nyholm et al. 2010), we described a novel method that utilizes EPR to quantify the partitioning of a spin-labeled chol analog (chlstn) between LUVs and mβCD. MβCD acts as a chol binding reference to

compare LUV of different composition against (Williams et al. 2013). Through spectral simulation of experimental equilibrium partitioning spectra (Fig. A2.1), partition coefficients (K_x) were calculated and used to determine relative chol-lipid affinity (Table 4.1). We found a trend of lower K_x for increasing unsaturation (the value for POPC reduced by half for PDPC) and a substantial decrease in K_x for lipids lacking a saturated sn-1 chain (the value for PDPC comparable to that of DOPC). Absolute K_x magnitudes for chlstn did not match previous reports for chol (Table 4.2), but relative K_B^A values (lipid A relative to lipid B) agreed within experimental uncertainty with corresponding ITC measurements on chol (Fig. 4.5). The EPR method has the benefit of being fast and that measurements are made on an equilibrated sample, avoiding the potentially artifact inducing step of physically separating mβCD and LUV fractions. Furthermore, because only trace amounts of the spin-label were used, extraction or absorption of chlstn was unlikely to appreciably affect membrane order or induce phase separation in LUV.

As with other approaches, our method is not without its limitations. Chlstn does not fully mimic the condensing effect of chol (Scheidt et al. 2003). We have plans of repeating these measurements using 25-doxyl-cholesterol, an alternative spin-labeled analog of chol whose hydroxyl and planar steroid nucleus is consistent with that of chol and more faithfully mimics its behavior. The catalog of lipids surveyed may also expand so that a more systematic appraisal of the differences in and among n-3 and n-6 PUFA-chol interactions may be made. We plan to verify these measurements by yet another new method: solution state NMR of analogs of chol labeled with ^{2}H or ^{13}C in the LUV-mβCD system. This approach would have the positive attributes of requiring no physical separation prior to an assessment of partitioning and use of a minimally invasive probe.

In Chapter 3, the effect of n-3 PUFA on membrane organization in model membranes containing the lipid raft forming molecules SM and chol was reported. Solid state ^{2}H NMR was used to contrast 1-[$^{2}H_{31}$]palmitoyl-2-eicosapentaenoylphosphatidylcholine (PEPC-d_{31}) and 1-[$^{2}H_{31}$]palmitoyl-2-docosahexaenoylphosphatidylcholine (PDPC-d_{31}) with, as a control, 1-[$^{2}H_{31}$]palmitoyl-2-oleoylphosphatidylcholine (POPC-d_{31}) in 1:1:1 mol mixtures with SM and chol (Williams et al. 2012). By interpretation of ^{2}H NMR spectral lineshape (Fig. 3.2) and first moment analysis as a function of temperature (Fig. 3.3), we determined there was segregation of PC

between SM-rich (more-ordered) and PC-rich (less-ordered) domains in all three PC/SM/chol mixtures. The size of domains was estimated to be largest with PEPC-d_{31} (>35 nm) and smallest with POPC-d_{31} (<45 nm), while PDPC-d_{31} (~40 nm) fell in between. There was evidence of substantial infiltration of both PEPC-d_{31} and PDPC-d_{31} into the more-ordered SM-rich domain which in the case of PDPC-d_{31} consituted a surprising majority (75%) of the PUFA-containing phospholipid present. This finding is in contrast with studies of similar mixtures of PE/SM/chol, where only minimal incorporation of the equivalent DHA-containing PE into the more-ordered domain was observed (Shaikh et al. 2004, Soni et al. 2008). The difference can likely be attributed to the greater hydrophobic-shielding afforded by the larger head group of PC (Huang et al. 1999) and therefore enhanced sterol affinity over PE (Demel et al. 1977).

The biological implications are that, depending upon the type of phospholipid, PUFA-containing phospholipids can infiltrate ordered raft domains and disrupt signaling of resident protein through modulation of membrane properties. Evidence of this type of activity was reported in a biological study by Rockett et al. (2012) in which the lipid content of DRM (raft-like) and DSM (nonraft-like) fractions from the B cell membranes of mice fed a fish oil (the two main components of which are the ω-3 PUFAs EPA and DHA) enriched diet were analyzed. Mirroring our model results, a significant portion of PC-esterified DHA and EPA were found in DRM fractions, DHA to a greater extent than EPA. The opposite held true for PE-esterified DHA and EPA, where, for both PUFA, the majority were located in the DSM fraction. Alteration of raft organization and signaling could be the mechanism that explains some of the many health benefits associated with fish oil consumption.

As a continuation of this work, our group is currently conducting solid state ^{2}H NMR experiments that examine how PUFA affects the organization of the more-ordered SM-rich domains in PDPC/SM/chol and PEPC/SM/chol mixtures. In these mixtures, a deuterated SM analog (N-palmitoyl[$^2H_{31}$]-D-*erythro*-sphingosylphosphorylcholine) will be observed to directly assess the potential disordering of raft domains due to PUFA-incorporation.

5.1 References

Demel RA, Jansen JWCM, van Dijck PWM, van Deenen LLM (1977) The preferential interaction of cholesterol with different classes of phospholipids. Biochim Biophys Acta 465:1-10

Leventis R, Silvius JR (2001) Use of cyclodextrins to monitor transbilayer movement and differential lipid affinities. Biophys J 81:2257–2267

Nui SL, Litman BJ (2002) Determination of membrane cholesterol partition coefficient using a lipid vesicle–cyclodextrin binary system: effect of phospholipid acyl chain unsaturation and headgroup composition. Biophys J 83:3408–3415

Nyholm TKM, Grandell PM, Westerlund B, Slotte JP (2010) Sterol affinity for bilayer membranes is affected by their ceramide content and ceramide chain length. Biochim Biophys Acta 1798:1008–1013

Rockett BD, Teague H, Harris M, Melton M, Williams J, Wassall SR, Shaikh SR (2012) Fish oil increases raft size and membrane order of B cells accompanied by differential effects on function. J Lipid Res 53:674-685

Scheidt HA, Muller P, Herrmann A, Huster D (2003) The potential of fluorescent and spin-labeled steroid analogs to mimic natural cholesterol. J Biol Chem 46:45563–45569

Shaikh SR, Dumaual AC, et al. (2004) Oleic and docosahexaenoic acid differentially phase separate from lipid raft molecules: a comparative NMR, DSC, AFM, and detergent extraction study. Biophys J 87:1752-1766

Simons K, Ikonen E (1997) Functional rafts in cell membranes. Nature 387:569-572

Soni SP, LoCascio DS, et al. (2008) Docosahexaenoic acid enhances segregation of lipids between raft and nonraft domains: ^{2}H NMR study. Biophys J 95:203-214

Wassall SR, Stillwell W (2009) Polyunsaturated fatty acid–cholesterol interactions: domain formation in membranes. Biochim Biophys Acta 1788:24–32

Williams JA, Batten SE, et al. (2012) Docosahexaenoic and eicosapentaenoic acids segregate differently between raft and nonraft domains. Biophys J 103:228-237

Williams JA, Wassall CD, Kemple MD, Wassall SR (2013) An EPR method for measuring the affinity of a spin labeled analog of cholesterol for phospholipids. J Mem Biol 246:689-696

Yeagle PL, Young JE (1986) Factors contributing to the distribution of cholesterol among phospholipid vesicles. J Biol Chem 261:8175-8181

APPENDIX

A1: Supplemental Material for Docosahexaenoic and Eicosahexaenoic Acids Segregate Differently between Raft and Nonraft Domains

A1.1 Detergent Extraction of Cells

A1.1.1 Cells

EL4 cells were maintained at 37 °C in a 5% CO_2 incubator. The cells were grown in RPMI 1640 1X with 10% heat inactivated fetal bovine serum (HyClone, Logan, UT) supplemented with 2 mM L-glutamine and 1% penicillin/streptomycin. 10-20 x 10^6 cells were treated with fatty acids complexed to BSA as previously described (Rockett et al. 2010). Briefly, EPA and DHA (Nu-Chek Prep, Elysian, MN) free fatty acid stocks were stored with BHT (Sigma) in amber vials to prevent oxidation and were complexed to fatty acid free BSA (Roche, Indianapolis, IN) at a 1.5:1 ratio. Cells were incubated with 25 µM fatty acids in serum-free RPMI overnight (~15.5 hours) to maximize uptake of fatty acids. BSA treatment in the absence of EPA or DHA served as control (Rockett et al. 2010). We have previously reported that treatment of cells under these conditions results in uptake of the fatty acids into polar lipids (~80-85%) (1,2).

A1.1.2 Biochemical Analysis of DRM

Fatty acid-treated cells were washed with cold PBS and dissolved in cold MBS buffer (150 mM NaCl, 2 mM EDTA, 25 mM Mes at pH 6.5) containing 1% Triton X-100 and a protease inhibitor cocktail (Sigma). Cells were broken with a 23g needle and placed on ice for 30 minutes. Broken cells (2.5 mL) were then mixed with an equal volume of 90% sucrose in MBS. This solution (4 mL) was overlaid with 4 mL of 35% sucrose followed by 4mL of 5% sucrose. The three component solution was centrifuged at 40,000 rpm in a SW41Ti Beckman rotor (Brea, CA) for 20 hours at 4 °C. Sucrose gradient fractions were then collected from the top to bottom of the tubes on ice. Radiolabeled cholesterol (^{14}C or ^{3}H labeled, Perkin Elmer, Waltham, MA) controls were acquired to determine DRM (raft) and detergent soluble membrane (DSM, non-raft) fractions. Generally, DRM and DSM were defined as fractions 3-6 and 9-12, respectively.

Lipids were extracted from DRM and DSM fractions using methods previously described (Rockett et al. 2010). Extracted fatty acids from DRM and DSM were methylated using boron trifluoride (Sigma) and analyzed using a Shimadzu gas chromatograph (GC-2010, Columbia, MD). Identified peaks were based on standards (Nu-Chek Prep). DRM and DSM data were obtained

from 3-4 independent experiments. Statistical significance was established with a one-way ANOVA followed by a Bonferroni multiple comparison t test using GraphPad Prism.

Table A1.1 Average order parameters $\overline{S}_{CD}$ derived from ^{2}H NMR spectra for PEPC-d_{31}, PDPC-d_{31} and POPC-d_{31} in 1:1 mol mixtures with SM, and in 1:1:1 mol mixtures with SM and cholesterol at 37 ºC. There is a correspondence of the average order parameter to the bilayer thickness (Petrache et al. 2000).

Membrane composition	$\overline{S}_{CD}$		$\Delta\overline{S}_{CD}$
	No cholesterol	With cholesterol	
PEPC-d_{31}/SM	0.100	0.156	0.056
PDPC-d_{31}/SM	0.122	0.192	0.070
POPC-d_{31}/SM	0.137	0.231	0.094

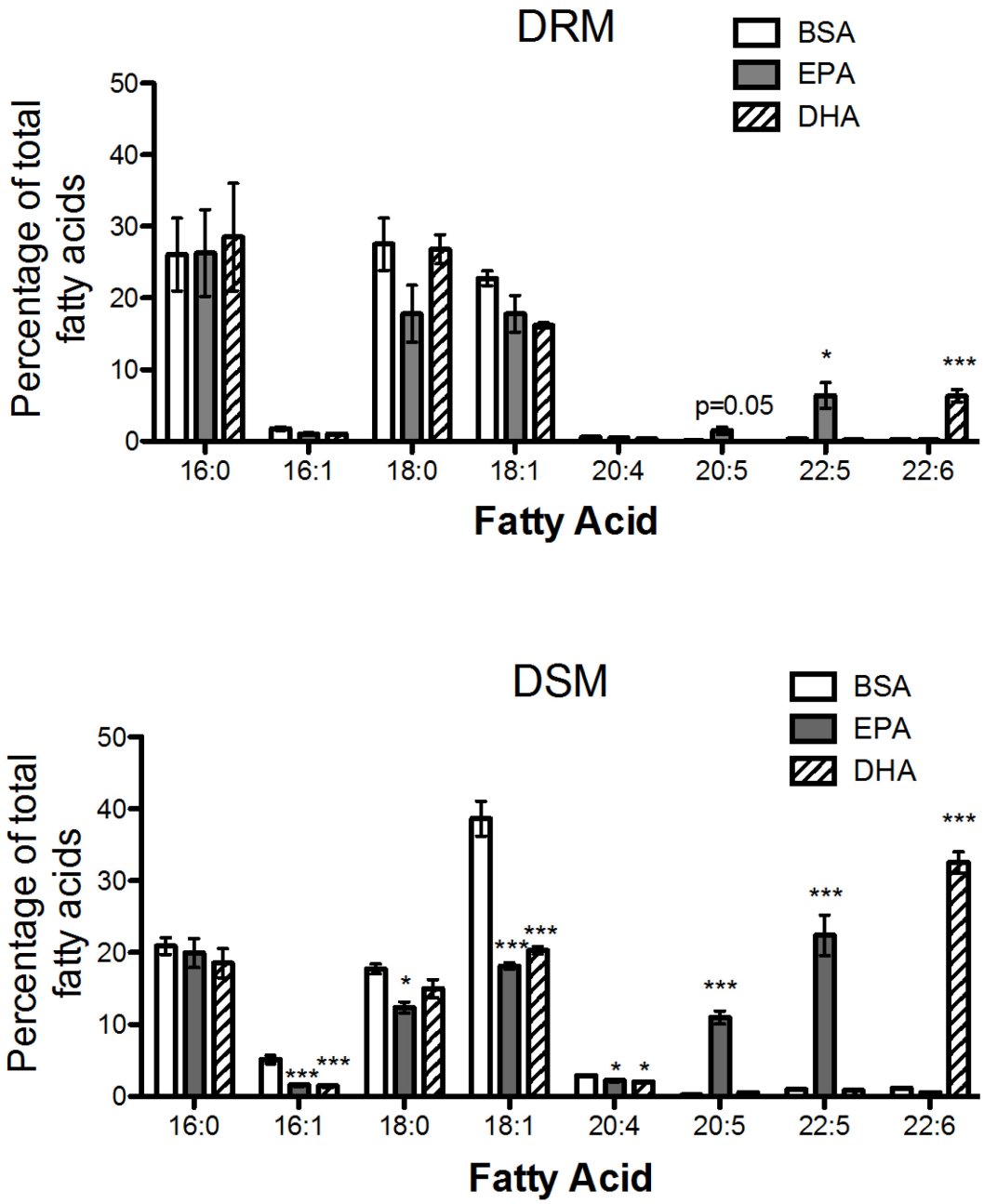

Figure A1.1 Fatty acid analysis of the DRM (upper panel) and DSM (lower panel) fractions of EL4 T cells. EL4 T cells were treated overnight with 25μM BSA (control), EPA or DHA in serum free conditions and subjected to cold detergent extraction. Fatty acids were then extracted from DRM and DSM, methylated and analyzed with gas chromatography. Asterisks denote significance from BSA (*$p<0.05$ and ***$p<0.001$).

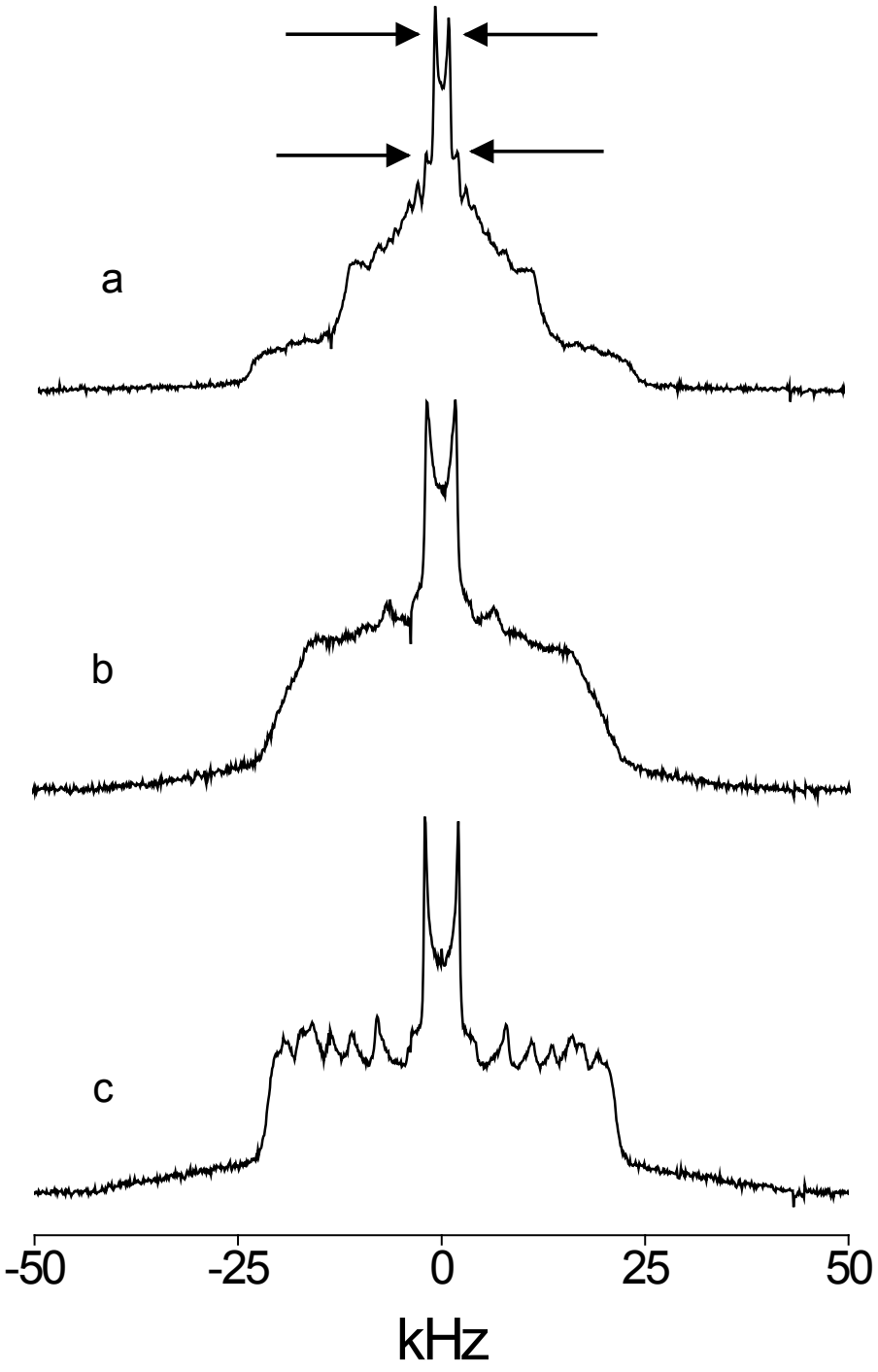

Figure A1.2 ^{2}H NMR spectra for 50 wt% aqueous dispersions in 50 mM Tris buffer (pH 7.5) of PEPC-d_{31} (a), PDPC-d_{31} (b), and POPC-d_{31} (c) in 1:1:1 mol mixtures with SM and chol at 37 °C. Arrows highlight that the signal for the terminal methyl group is split in two in the spectrum for PEPC-d_{31} but not in the spectra for PDPC-d_{31} and POPC-d_{31}.

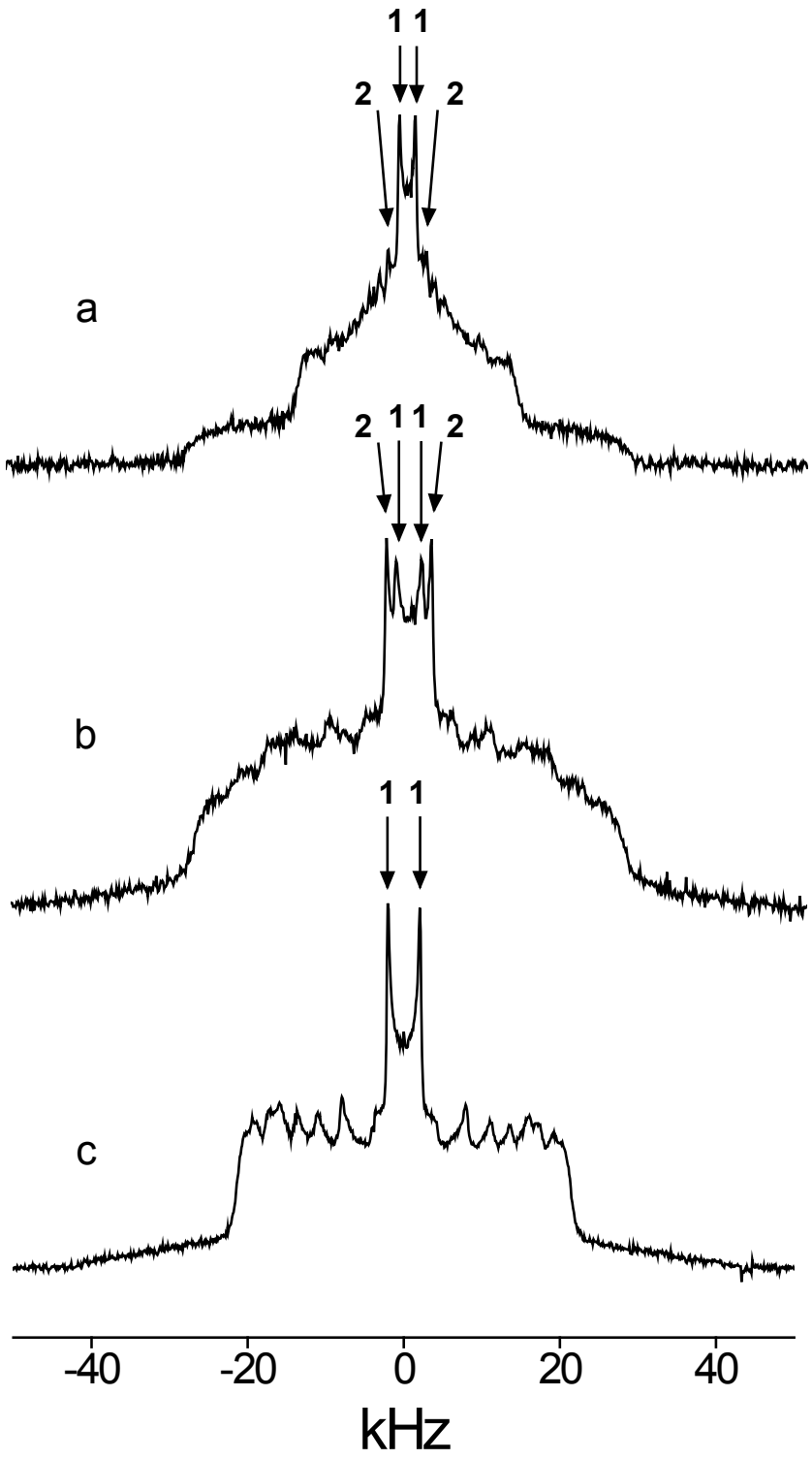

Figure A1.3 ^{2}H NMR spectra for 50 wt% aqueous dispersions in 50 mM Tris buffer (pH 7.5) of PEPC-d_{31} (a), PDPC-d_{31} (b) and POPC-d_{31} (c) in 1:1:1 mol mixtures with SM and chol at 30 °C. Arrows highlight that the signal for the terminal methyl is split into a pair of inner (1) and outer (2) peaks in the spectra for PEPC-d_{31} (a) and PDPC-d_{31} (b), whereas in the spectrum for POPC-d_{31} (c) there is only a single pair (1) of peaks.

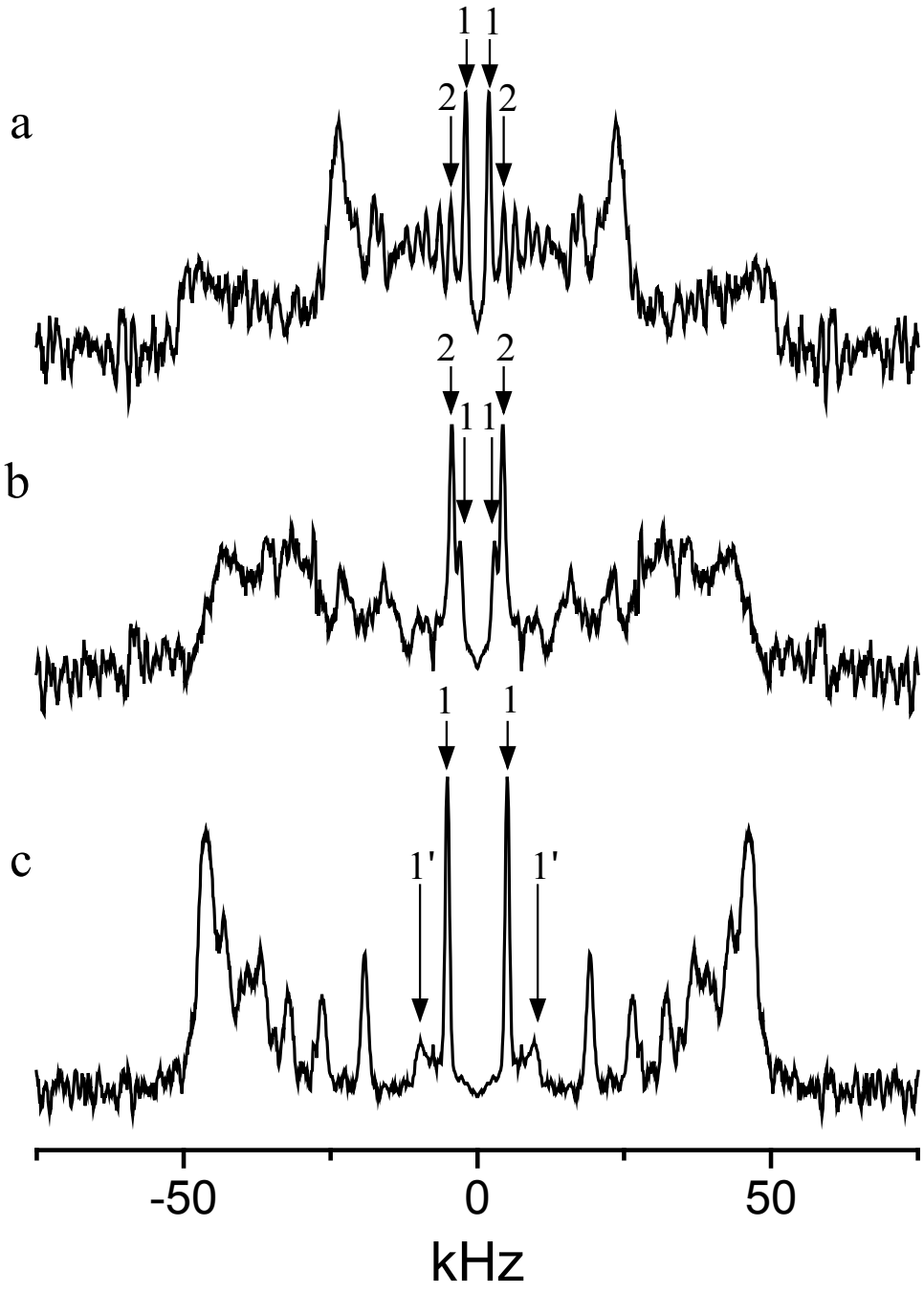

Figure A1.4 FFT depaked ^{2}H NMR spectra for 50 wt% aqueous dispersions in 50 mM Tris buffer (pH 7.5) of PEPC-d_{31} (a), PDPC-d_{31} (b) and POPC-d_{31} (c) in 1:1:1 mol mixtures with SM and chol at 30 °C. Arrows highlight that the signal for the terminal methyl is split into a pair of inner (1) and outer (2) peaks in the spectra for PEPC-d_{31} (a) and PDPC-d_{31} (b), whereas in the spectrum for POPC-d_{31} (c) there is only a single pair of peaks (1) with a pair of satellite peaks (1′) that are artifacts produced by the FFT depaking algorithm.

A1.2 References

Rockett BD, Salameh M, Carraway K, Morrison K, Shaikh SR (2010) n-3 PUFA improves fatty acid composition, prevents palmitate-induced apoptosis, and differentially modifies B cell cytokine secretion in vitro and ex vivo. J Lipid Res 51:1284–1297

Petrache HI, Dodd, Brown MF (2000) Area per lipid and acyl chain length distributions in fluid phosphatidylcholines determined by ^{2}H NMR spectroscopy. Biophys J 78:3172-3192.

A2: Supplemental Material for An EPR Method for Measuring the Affinity of a Spin Labeled Analog of Cholesterol for Phospholipids

A2.1 Partition coefficient measurement by ITC

Sample preparation, substituting chol for chlstn, was as outlined for the EPR work in Methods. Because mβCD was in great excess compared to chol in these experiments, the approximation

$$C_{m\beta CD} - 2C_{chol}^{m\beta CD} \approx C_{m\beta CD} \tag{S1}$$

applies and Eq 1 becomes

$$K_x = \frac{C_{chol}^{LUV}(C_{m\beta CD})^2}{(C_{LUV}+C_{chol}^{LUV})C_{chol}^{m\beta CD}}. \tag{S2}$$

ITC experiments were carried out on a VP-ITC microcalorimeter (MicroCal, Piscataway, NJ). The procedure follows that of Tsamaloukas et al. (2005). Briefly, a series of injections were made of a 10 mM LUV suspension into a calorimeter cell (1.38 mL) filled with a solution of 5 or 10 mM mβCD while the power necessary to maintain a constant temperature of 37 °C was recorded as chol partitioned between LUV and mβCD. Both lipid and mβCD solutions were thoroughly degassed before being loaded in the calorimeter. Uptake experiments having 90 μM chol initially bound to mβCD in the calorimeter cell and release experiments incorporating between 1 and 3 mM chol in LUV loaded in the injector were performed. The typical injection sequence was 1×1 μL, 3×5 μL and 10×10 μL with 40 min between injections. The observed power integrated over time and normalized with respect to the number of lipid moles injected was used to calculate K_x. Specifically, the heat observed during an injection indicates the transfer of chol and is described by

$$Q_i = \frac{[\Delta C_{chol}^{LUV}]_i^{trans}}{C_{LUV}(i)-C_{LUV}(i-1)}\Delta H + Q_{dil}. \tag{S3}$$

In this equation, Q_i is the observed integrated compensation power normalized with respect to lipid moles injected, $C_{LUV}(i) - C_{LUV}(i-1)$ is the change in concentration of lipid in the sample cell due to the *i*th injection, ΔH is the change in molar enthalpy associated with the transfer of chol from mβCD to LUV, Q_{dil} is the molar heat of dilution and $\left[\Delta C_{chol}^{LUV}\right]_i^{trans}$ is the change in concentration of chol in the bilayer upon the *i*th injection. The Excel solver tool was used to calculate K_x by adjusting the parameters ΔH and Q_{dil}, and consequently C_{chol}^{LUV}, to minimize the

sum of squared deviations between the experimental Q_i for each injection and the value derived with Eq S3.

In addition to chol, mβCD binds phospholipid. To account for the endothermic extraction of phospholipids from LUV, blank experiments were run with the same injection parameters as uptake and release experiments, but without chol. The heat observed in blank experiments was subtracted from the corresponding uptake and release experimental data prior to analysis. The estimated maximum error for K_x is ±20%.

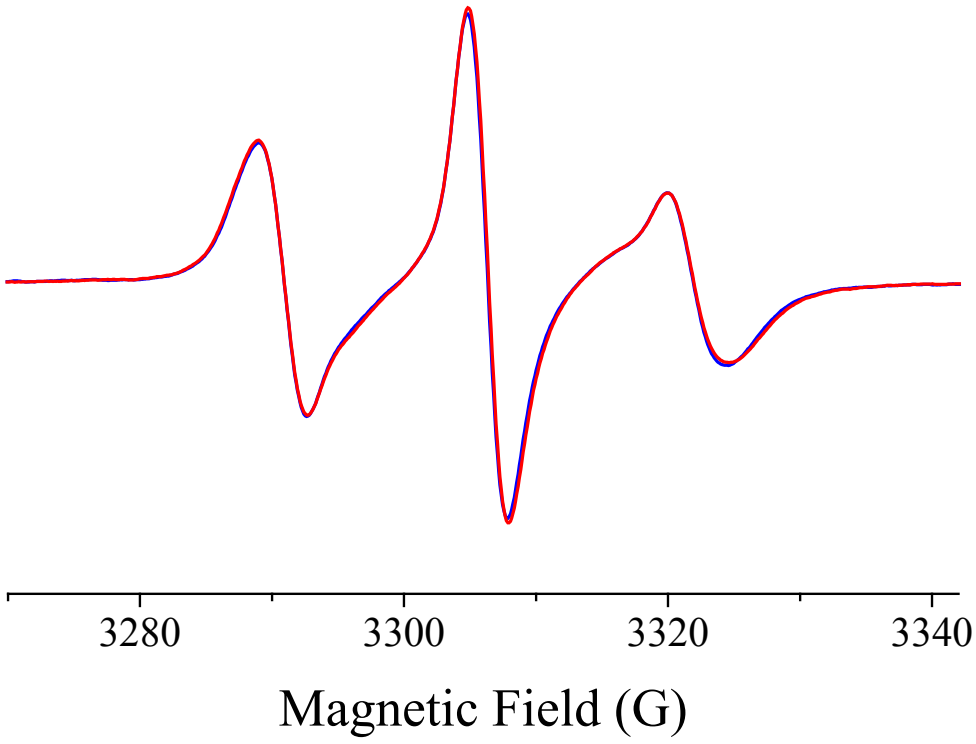

Figure A2.1 Simulated fit of experimental partition spectrum by scaled combination of LUV and mβCD reference spectra. Relative populations of chlstn in the mβCD and LUV environments of an equilibrated partition sample can be determined by finding the ratio of normalized reference spectra whose combination yields the best fit (—) of the mixed sample spectra (—). The ratio corresponds to the relative population of chlstn in LUV and mβCD and is used to calculate chlstn LUV-mβCD partition coefficient K_x. Experimental spectrum is for an uptake experiment in which 15 mM POPC was equilibrated with 0.152 mM chlstn, 5 mM mβCD at 37 °C. Best fit was achieved with normalized reference spectra for POPC (Fig. 4.2A) and mβCD (Fig 4.2B) combined in a ratio of 0.73:0.27.

Table A2.1 Partition coefficients K_x measured by EPR for chlstn in release and uptake experiments at 37 °C. Release value is average of four trials and error is standard deviation of experiments. Uptake value is from a single trial and uncertainty is an estimate of maximum error based upon reproducibility.

Lipid	K_x (mM)	
	Release	Uptake
POPC	4.4 ± 0.3	4.3 ± 0.4
PLPC	3.3 ± 0.2	3.5 ± 0.3
PDPC	2.4 ± 0.4	1.9 ± 0.4
DOPC	2.9 ± 0.3	2.3 ± 0.4

Table A2.2 Partition coefficients K_x and partition coefficients K_B^A relative to POPC measured by ITC for chol at 37 °C. The K_x values are an average of the results obtained in uptake and release experiments and the uncertainty in K_x is an estimate of maximum error based upon reproducibility. The error in K_B^A includes the uncertainty in K_x for POPC as well as for PDPC or DOPC. Representative ITC data are shown in Fig. A2.2.

Lipid	$\boldsymbol{K_x}$ **(mM)**	$\boldsymbol{K_B^A}$
POPC	40 ± 8	1
PDPC	15 ± 3	0.38 ± 0.15
DOPC	25 ± 5	0.63 ± 0.25

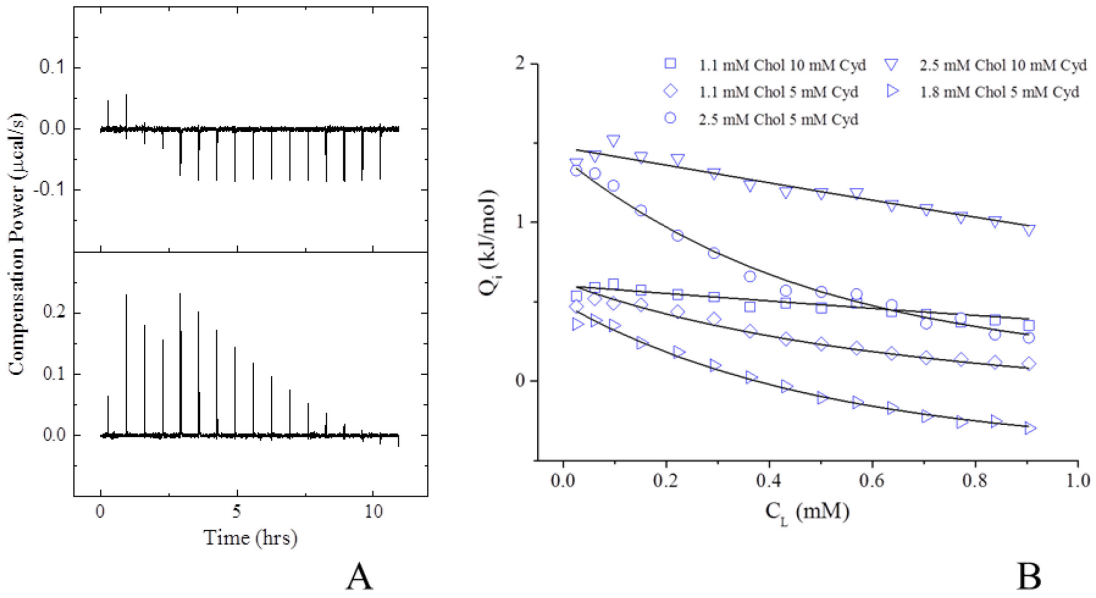

Figure A2.2 Representative chol release experiment, ITC data. (A) Blank and release titration power response curves after baseline subtraction. The blank experiment (upper panel) is used to account for endothermic heat of PC extraction by mβCD and exothermic dilution of mβCD. For this procedure 10 mM DOPC was injected into 5 mM mβCD. The release experiment (lower panel) entailed injecting 10 mM DOPC LUV with 1.11 mM chol into a 5mM mβCD solution. The compensation peaks are positive indicating that transfer of chol from LUV to mβCD is an endothermic event. Both experiments were conducted at 37 °C with an injection schedule of 1×1μL, 3×5μL, 12×10 μL with 40 min between injections. (B) Fitting of ITC partitioning data with the K_x model. Q_i is the normalized observed heat after blank subtraction and is plotted against PC concentration in calorimeter cell. The parameters of the fit ($K_x = 25 \pm 5$ mM, $\Delta H = -5.4 \pm 0.2$ kJ/mol, and Q_{dil}) are determined by the Excel solver tool; single values of K_x and ΔH are found to globally fit all trials while Q_{dil} varies among experiments. DOPC experiments were performed with 10 mM PC and the amounts of mβCD and chol indicated in the caption for individual release assays.

A2.2 Reference

Tsamaloukas A, Szadkowska H, Slotte PJ, Heerklotz (2005) Interactions of cholesterol with lipid membranes and cyclodextrin characterized by calorimetry. Biophys J 89:1109-1119

VITA

VITA

Justin A. Williams

EDUCATION

Doctor of Philosophy in Physics - Purdue University, Indianapolis, IN anticipated **12/2013**
Dissertation Title: Biophysical Studies of Cholesterol in Unsaturated Phospholipid Model Membranes

Master of Science in Physics - Purdue University, Indianapolis, IN **2009**
Thesis Title: Affinity of α-Tocopherol for Polyunsaturated Phospholipids Characterized by Isothermal Titration Calorimetry and UV Absorption

Bachelor of Science in Physics - Purdue University, Indianapolis, IN **2006**
Minors: Mathematics and Biology

RESEARCH EXPERIENCE

Member of Dr. Stephen Wassall's Biophysics Research Group, IUPUI 2006 - 2013

Research focused on measurement of membrane molecular organization and development of methods to measure interaction energies of membrane components with a special interest in polyunsaturated fatty acid containing lipids, cholesterol, and Vitamin E. Solid State ^{2}H NMR Spectroscopy was the primary experimental technique implemented, along with complementary techniques of Isothermal Titration Calorimetry (ITC), Electron Paramagnetic Resonance Spectroscopy, and UV Spectroscopy. General responsibilities included preparation of membrane samples, calibrating and making improvement on NMR probes, optimizing experimental protocols, and analysis of data with Excel and Origin programs.

ITC Training Received at University of Toronto, Leslie Dan School of Pharmacy 2008

AWARDS

GK-12 Fellowship, National Science Foundation	2009 - 2011
Student Travel Grant, IUPUI Center for Membrane Biosciences	2011
Travel Fellowship, IUPUI Graduate Student Office	2009
Educational Enhancement Grant, IUPUI Graduate Student Office	2009
Outstanding Teaching Assistant Award, American Association of Physics Teachers	2007
Dean's List, IUPUI University College	2005

PUBLICATIONS

Williams JA, Wassall CD, Kemple MD, Wassall SR (2013) An electron paramagnetic resonance method for measuring the affinity of a spin-labeled analog of cholesterol for phospholipids. J Membrane Biol 246:689-696 doi: 10.1007/s00232-013-9586-z

Marquardt D, **Williams JA**, Kucerka N, Atkinson J, Wassall SR, Katsaras J, Harroun T (2013) Tocopherol activity correlates with its location in a membrane: A new perspective on the antioxidant Vitamin E. J Am Chem Soc 135:7523-7533 doi: 10.1021/ja312665r

Williams JA, Batten SE, Harris M, Rockett BD, Shaikh SR, Stillwell W, Wassall SR (2012) Docosahexaenoic and eicosapentaenoic acids segregate differently between raft and nonraft domains. Biophys J 103:228-237 doi: 10.1016/j.bpj.2012.06.016

Rockett BD, Teague H, Harris M, Melton M, **Williams JA**, Wassall SR, Shaikh SR (2012) Fish oil increases raft size and membrane order of B cells accompanied by differential effects on function. J Lipid Res 53:674-685 doi: 10.1194/jlr.Mo21782

Soni SP, LoCascio DS, Liu Y, **Williams JA**, Bittman R, Stillwell W, Wassall SR (2008) Docosahexaenoic acid enhances segregation of lipids between raft and nonraft domains: ^{2}H-NMR study. Biophys J 95:203-214 doi: 10.1529/biophysj.107.123612

PRESENTATIONS

Biophysical Society (Poster)

2013 Williams JA, Wassall CD, Kemple MD, and Wassall SR*, Dependence of cholesterol-phospholipid affinity on degree of acyl chain unsaturation as determined by EPR.

Kinnun JJ*, Williams JA, Stillwell W, Bittman R, Shaikh SR, and Wassall SR, Disordering of raft domains by DHA and EPA observed with solid-state ^{2}H NMR spectroscopy.

Leng X*, Williams JA, Marquardt D, Kučerka N, Katsaras J, Atkinson J, Harroun TA, Feller SE, and Wassall SR, Interaction of α-tocopherol with a polyunsaturated lipid studied by MD simulations.

Marquardt D*, Kučerka N, Williams JA, Atkinson J, Wassall SR, Katsaras J, Harroun TA, The location of Vitamin E in model membranes and its effect on oxidation.

2012 Williams JA*, Wassall CD, Kagimbi MW, Eslinger CL, Kemple MD, and Wassall SR, Cholesterol-lipid affinity determined by EPR.

Leng X, Williams JA, Gorman JM, Feller SE, Atkinson J, and Wassall SR*, Molecular organization of Vitamin E in a polyunsaturated membrane.

Justice MJ*, Petrusca DN, Williams J, Schweitzer KS, Petrache I, Wassall SR, and Petrache HI, Engulfment of model membranes by alveolar macrophages.

Shaikh SR*, Rockett BD, Teague H, Williams J, and Wassall SR, Connecting model membrane experiments to in vivo studies: DHA acyl chains incorporate into raft-like membranes more than EPA in model membranes, in vitro, and in vivo.

2011 Williams JA*, Batten SE, McCabe MA, Stillwell W, Shaikh SR, and Wassall SR, EPA and DHA interact differentially with cholesterol: Solid State ^{2}H NMR of PUFA-containing phospholipids in mixtures with lipid raft molecules.

Williams JA*, Marquardt D, Stillwell W, Atkinson J, Harroun TA, and Wassall SR, Vitamin E responds to its lipid environment.

Rockett BD*, Franklin A, Harris M, Teague H, Williams JA, Wassall SR, Nguyen AH, Stottrup BL, and Shaikh SR, N-3 polyunsaturated fatty acids disrupt micron and nanometer scale non-raft organization by increasing cell size and minimizing molecular interactions with surrounding rafts.

2010 Williams JA, Shaikh SR, Locascio DS, Görgülü ST, Heerklotz H, Stillwell W, and Wassall SR*, α-Tocopherol and polyunsaturated fatty acid membrane domains.

Harroun TA*, Williams JA, Atkinson J, Salonen E, Katsaras J, Stillwell W, and Wassall SR, Membrane organization of Vitamin E is sensitive to lipid unsaturation.

2009 Williams JA*, LoCascio DS, Tsamaloukas A, Heerklotz H, Stillwell W, and Wassall SR, Preferential interaction of α-tocopherol with PUFA-containing lipids characterized by isothermal titration calorimetry.

IUPUI Physics Department Colloquium (Invited Speaker)

2012 Driven by disorder: Modification of membrane organization by polyunsaturated phospholipids.

Indiana Academy of Science (Platform)

2013 Kinnun JJ*, Williams JA, Stillwell W, Bittman R, Shaikh SR, and Wassall SR, DHA and EPA interaction with raft domains observed with solid state ^{2}H NMR spectroscopy.

Leng X*, Williams JA, Marquardt D, Harroun TA, Atkinson J, Feller SE, and Wassall SR, Interaction of α-Tocopherol with a polyunsaturated lipid studied by MD simulations.

2009 Williams JA*, LoCascio DS, Tsamaloukas A, Heerklotz H, Stillwell W, and Wassall SR, Affinity of Vitamin E for lipid membranes.

IUPUI Research Day

2012 Kagimbi M*, Williams JA, and Wassall SR, Affinity of cholesterol for polyunsaturated fatty-acid containing phospholipids. (Poster)

2010 Williams JA*, Harroun TA, Atkinson J, Salonen E, Katsaras J, Stillwell W, and Wassall SR, Membrane organization of Vitamin E is sensitive to lipid unsaturation. (Platform)

2009 Williams JA*, LoCascio DS, Tsamaloukas A, Heerklotz H, Stillwell W, and Wassall SR, Preferential interaction of α-Tocopherol with polyunsaturated lipids characterized by isothermal titration calorimetry. (Poster)

American Physical Society (Platform)

2013 Marquardt D*, Williams JA, Kucerka N, Atkinson J, Katsaras J, Wassall SR, and Harroun T, Tocopherol activity correlates with its location in a membrane: A new perspective on the anti-oxidant Vitamin E.

IUPUI Summer Research Project SEED (Poster)

2012 Zi V*, Williams JA, Ray B, and Wassall SR, Cholesterol binding to phospholipid.

(* indicates presenter)

TEACHING EXPERIENCE

IUPUI Physics Department, Indianapolis 2006-2013

Laboratory Instructor - Assisted in troubleshooting student's experiments and explaining relation between observed phenomena and course concepts.

Excerpts from most recent Student Satisfaction Survey

> Justin is very knowledgeable and helpful. I feel like I won the lottery with him as my lab instructor for this course. We would still be working on a few of those labs were he not there to offer assistance.
>
> Justin was well-prepared for every laboratory session and also made time for each and every student. He was an outstanding instructor!

Recitation Mentor – Sharpened students' problem solving skills in a group setting.

Supplemental Instruction Mentor – Created session plans and led discussions about course material.

Average performance approval rating of 95% from student evaluations.

Department Tutor - Communication skills used to clarify Physics concepts for students on different learning levels.

Research Group Member 2006-2013

Responsible for training new members on use of NMR spectrometer, ITC calorimeter, and sample preparation techniques. Mentored students participating in Project SEED and Undergraduate Research Program.

NSF GK-12 Fellow 2009-2011

Collaborated with local high school teacher to develop new classroom materials meant to stimulate student's interest in science and acted as a "scientist in the classroom."